

NASA Contractor Report 187623

11-083  
11-264  
p. 89

**Air-Breathing Hypersonic Vehicle Guidance  
and Control Studies; An Integrated  
Trajectory/Control Analysis Methodology:  
Phase I**

**Philip D. Hattis and Harvey L. Malchow**

**The Charles Stark Draper Laboratory, Inc.  
Cambridge, Massachusetts**

**Contract NAS1-18565  
September 1991**



National Aeronautics and  
Space Administration

**Langley Research Center**  
Hampton, Virginia 23665-5225

(NASA-CR-187623) AIR-BREATHING HYPERSONIC  
VEHICLE GUIDANCE AND CONTROL STUDIES; AN  
INTEGRATED TRAJECTORY/CONTROL ANALYSIS  
METHODOLOGY: PHASE I (Draper (Charles  
Stark) Lab.) 89 0

N92-17002

Unclass  
0048764

CSCL 01C 63/08



## Table of Contents

| <u>Section</u>   | <u>Page</u> |
|--|-------------|
| <u>I. Task Synopsis</u>  | 1           |
| <u>II. Introduction (Background on Task)</u>   | 2           |
| <u>A. Problem Overview</u>   | 2           |
| <u>B. Applicable Previous and Parallel Work</u>  | 2           |
| 1. Early HSV Integrated Design Studies   | 3           |
| 2. HSV Modeling and G&C Studies  | 3           |
| 3. Hypersonic Air Data System Studies  | 3           |
| <u>III. List of Symbols and Acronyms</u>   | 4           |
| <u>IV. Research Goals</u>  | 9           |
| <u>A. Initial Task Focus</u>   | 9           |
| 1. Development of Model Smoothing Techniques   | 9           |
| 2. Simplified Vehicle Model Development  | 9           |
| 3. Constrained Near-Fuel-Optimal Trajectory Development                                | 9           |
| <u>B. Longer Term Research Objectives</u>  | 10          |
| 1. Treatment of Vehicle Thrust Direction and Pitch Moment Changes with Angle of Attack | 10          |
| 2. Incorporation of Thermal Constraints into Trajectory Results                        | 10          |
| 3. HSV G&C Performance Robustness Studies  | 10          |
| <u>V. Progress for June 1990 - January 1991</u>  | 11          |
| <u>A. Formulation of an Integrated Trajectory/Control Analysis Methodology</u>         | 11          |
| 1. Overview  | 11          |
| 2. Data Smoothing Techniques   | 12          |
| 3. Mathematical Basis of Analysis Algorithm  | 13          |
| a. The Optimization Problem Formulation and Features                                   | 13          |
| b. A Technique to Construct an Initial Trajectory Guess                                | 15          |
| c. The Sequence of Computational Studies   | 16          |

| <u>Section</u>  | <u>Page</u> |
|---|-------------|
| <b><u>B. Demonstration Case Preliminaries</u></b>                     | 18          |
| <b>1. Vehicle/Environment Models</b>                                  | 18          |
| a. Available Database   | 18          |
| b. Simplifications  | 20          |
| <b>2. Strategy for Final Near-Fuel-Optimal Trajectory Development</b> | 21          |
| a. Trajectory Definition (Boundary Conditions)                        | 21          |
| b. Nine State Vehicle Dynamics Models                                 | 22          |
| c. Optimization Algorithm Formulation for the Example Application     | 24          |
| d. Relevant Partial Derivatives                                       | 28          |
| <b>3. Preliminary Near-Fuel-Optimal Trajectory Development</b>        | 29          |
| a. A Representative Trajectory Partition                              | 29          |
| b. Simpler Seven State Vehicle Dynamics Models                        | 29          |
| c. The Boundary Conditions  | 33          |
| d. Cost Function Specification  | 33          |
| e. Relevant Partial Derivatives                                       | 34          |
| f. Calculation of Elevon Trim Deflection                              | 36          |
| g. Initial Conditions   | 39          |
| <b><u>C. Analysis Demonstration Results</u></b>                       | 40          |
| <b>1. Cases Run</b>   | 40          |
| <b>2. Observations from Demonstration Case Results</b>                | 40          |
| a. Observations from Specific Variable Plots                          | 40          |
| b. Observed Acceleration and/or Mass Flow Discontinuities             | 41          |
| c. Analysis Observations Affecting G&C Design                         | 42          |
| d. The Mach 2 Transients  | 43          |
| e. Performance Sensitivity to Modelling Uncertainty                   | 43          |
| <b><u>D. Progress Toward AIPS Requirements Specification</u></b>      | 45          |
| <b><u>VI. Conclusions</u></b>   | 46          |

| <u>Section</u>   | <u>Page</u> |
|--|-------------|
| <b><u>VII. References</u></b>  | 48          |
| <b><u>Appendix A: Nine State Function Partial Derivatives for the Example Model</u></b>  | 49          |
| <b><u>1. Derivatives with Respect to States</u></b>                                      | 49          |
| <b><u>2. Derivatives with Respect to Controls</u></b>                                    | 55          |
| <b><u>Appendix B: Seven State Function Partial Derivatives for the Example Model</u></b> | 57          |
| <b><u>1. Derivatives with Respect to States</u></b>                                      | 57          |
| <b><u>2. Derivatives with Respect to Controls</u></b>                                    | 61          |

## Table of Figures

| <u>Figure</u> | <u>Description</u>   | <u>Page</u> |
|---------------|--|-------------|
| V-1           | Spline Construction for a Parameter with Two Independent Variables | 64          |
| V-2           | Vehicle Mass Model Curve Fit                                       | 65          |
| V-3           | Vehicle Pitch Inertia Model Curve Fit                              | 65          |
| V-4           | Coordinate Systems for Dynamics Equations                          | 66          |
| V-5           | Integrated Trajectory/Control Optimization Algorithm Structure     | 67          |
| V-6           | Demonstration Case - Angle of Attack vs Mach Number                | 68          |
| V-7           | Demonstration Case - Angle of Attack vs Time                       | 69          |
| V-8           | Demonstration Case - Equivalence Ratio vs Mach Number              | 70          |
| V-9           | Demonstration Case - Equivalence Ratio vs Time                     | 71          |
| V-10          | Demonstration Case - Elevon Deflection vs Mach Number              | 72          |
| V-11          | Demonstration Case - Elevon Deflection vs Time                     | 73          |
| V-12          | Demonstration Case - Dynamic Pressure vs Mach Number               | 74          |
| V-13          | Demonstration Case - Dynamic Pressure Derivative vs Mach Number    | 75          |
| V-14          | Demonstration Case - Flight Path Angle vs Mach Number              | 76          |
| V-15          | Demonstration Case - Flight Path Derivative vs Mach Number         | 77          |
| V-16          | Demonstration Case - Ground Relative Acceleration vs Mach Number   | 78          |
| V-17          | Demonstration Case - Inertial Acceleration vs Mach Number          | 79          |
| V-18          | Demonstration Case - Mass vs Mach Number                           | 80          |
| V-19          | Demonstration Case - Mass Flow vs Mach Number                      | 81          |
| V-20          | Demonstration Case - Altitude vs Mach Number                       | 82          |
| V-21          | Demonstration Case - Mach Number vs Time                           | 83          |

# I. Task Synopsis

Air-breathing hypersonic vehicles, with fully integrated airframe and propulsion systems, are expected to face the most complicated design, trajectory, and control coupling challenges of any class of flight vehicles ever considered. Assessment of appropriate trajectory management and control strategies must be accomplished during the conceptual phases of vehicle design to assure a high probability that the fully integrated system will accomplish mission objectives. Also, a valid mathematical basis is needed to rate the relative performance of alternative vehicle design concepts and/or subsystem technologies against a common mission goal. To address these concerns, a generically applicable methodology has been developed to construct trajectories and control strategies while accommodating physically derived constraints on vehicle operations.

This task has adapted a Draper Laboratory developed tool which generates optimal trajectory/control histories in an integrated manner to the treatment of single-stage-to-orbit air-breathing hypersonic vehicles. The mathematical basis for implementing the methodology as a two-point boundary value problem solution technique is documented. The tool formulation permits an assessment of the entire near-minimum-fuel trajectory and desired control strategy from takeoff to orbit while satisfying physically derived inequality constraints and while achieving efficient propulsive mode phasing. A strategy has also been formulated and is documented to construct preliminary trajectory and control history representations with less computational burden than required for the overall flight profile assessment (by a partitioning of the trajectory into boundary condition matched segments).

A tabulated data version of an example hypersonic vehicle model has been used in a demonstration of the integrated analysis methodology. To assure good numerical behavior of the algorithm (no discontinuities in the interpolated values or their first derivatives), it has been necessary to develop a smoothing routine for the tabulated data. A cubic spline curve smoothing routine that can function with any multidimensional tabulated vehicle model was developed, implemented, and documented.

A demonstration of the analysis methodology was accomplished using the example vehicle model and the data smoothing routine. A constrained near-fuel-optimal trajectory was developed from horizontal takeoff to 20,000 ft/sec relative air speed while aiming for a polar orbit. The inequality constraint imposed on the system was a dynamic pressure limit of 1000 psf.

The demonstration case provided examples of the kind of information that the analysis methodology can develop for a wide range of HSV designs and mission applications. A near-fuel-optimal trajectory that satisfies the applied constraints was determined. Previously unspecified propulsive discontinuities were located. Flight regimes demanding rapid attitude changes were identified, dictating control effector and closed-loop G&C design requirements based on the required control response. Available closed-loop controller authority was ascertained after evaluating effector use for vehicle trim. Also, inadequacies in vehicle model representations and specific subsystem models with insufficient fidelity were determined (as manifested by unusual control characteristics and/or excessive sensitivity to uncertainty).

After completion of analysis of the information resulting from use of the integrated trajectory/control methodology, closed-loop guidance and control design requirements can be established. This information must precede specification of on-board advanced information processing system design characteristics.

### III. List of Symbols and Acronyms

|           |  |
|-----------|--|
| $\alpha$  | the atmospheric speed of sound (a function of $r$ )  |
| AIPS      | advanced information processing system   |
| $B$       | a matrix term in the trajectory optimization variation equations   |
| $c$       | the vehicle longitudinal reference length  |
| $C$       | a vector term in the variation equations   |
| $C_D$     | the vehicle drag coefficient   |
| $C_{D_a}$ | the drag increment coefficient for the basic vehicle derived from the Langley data base (a function of $\alpha$ and $M_f$ )  |
| $C_{D_e}$ | the drag increment coefficient of the combined left and right elevons derived from the Langley data base (a function of $\alpha$ , $\delta_e$ , and $M_f$ ) - it has a value of zero after the rocket engine turn-on switch time   |
| $C_J$     | a coefficient to establish the desired weight given to cost improvement contributions to variation terms   |
| $C_{J_i}$ | a coefficient to establish the desired weight given to cost improvement contributions of variation terms on the $i^{\text{th}}$ trajectory leg   |
| $C_L$     | the vehicle lift coefficient   |
| $C_{L_a}$ | the lift increment coefficient for the basic vehicle derived from the Langley data base (a function of $\alpha$ and $M_f$ )  |
| $C_{L_e}$ | the lift increment coefficient of the combined left and right elevons derived from the Langley data base (a function of $\alpha$ , $\delta_e$ , and $M_f$ ) - it has a value of zero after the rocket engine turn-on switch time   |
| $C_m$     | the vehicle pitch moment coefficient relative to the moment reference center   |
| $C_{m_a}$ | the pitch moment increment coefficient for the basic vehicle, relative to the moment reference center, derived from the Langley data base (a function of $\alpha$ and $M_f$ )  |
| $C_{m_e}$ | the pitch moment increment coefficient of the combined left and right elevons, relative to the moment reference center, derived from the Langley data base (a function of $\alpha$ , $\delta_e$ , and $M_f$ ) - it has a value of zero after the rocket engine turn-on switch time |
| $C_{m_q}$ | the vehicle pitching moment increment coefficient with pitch rate derivative, relative to the moment reference center, derived from the Langley data base (a function of $\alpha$ and $M_f$ )  |
| $C_Q$     | the dynamic pressure constraint cost weighting term  |
| $C_T$     | the vehicle air-breathing engine thrust coefficient derived from the Langley data base with dimension $\text{ft}^2$ (a function of $\Phi_\alpha$ , $M_f$ , and weakly of $Q$ ) - it has a value of zero after the air-breathing engine turn-off switch time                        |
| $C_\Psi$  | a diagonal matrix of constant coefficients to establish the desired weights given to equality constraint violation improvements in variation terms   |

|                     |  |
|---------------------|--|
| $C_{\psi_i}$        | a diagonal matrix of constant coefficients to establish the desired weights given to equality constraint violation improvements in variation terms on the $i^{\text{th}}$ trajectory segment |
| $D$                 | the drag force acting on the vehicle   |
| DFY                 | Draper fiscal year   |
| $f$                 | the derivative of the state vector $x$ with respect to time  |
| $f_i$               | the derivative of $x_i$ with respect to time   |
| $f_R$               | The contribution to the equation for $f$ due to the rocket thrust  |
| $f_{s_i}$           | the derivative of the state vector $x$ with respect to time evaluated at the $i^{\text{th}}$ switch point  |
| $f_u$               | the partial derivative of the vector $f$ with respect to the control vector $u$  |
| $f_x$               | the partial derivative of the vector $f$ with respect to the state vector $x$  |
| $F$                 | the LVLH vector of forces acting on the vehicle  |
| $F_g$               | the gravity force acting on the vehicle  |
| $F_T$               | the force component parallel to the vehicle free stream velocity vector  |
| $F_N$               | the force component normal to the vehicle free stream velocity vector, pointing down in the vehicle plane of symmetry  |
| $F_1$               | the force component normal to $F_2$ and $F_3$ , pointing toward increasing $\mu$   |
| $F_2$               | the force component parallel to the equatorial plane, pointing eastward, normal to $F_3$   |
| $F_3$               | the force component parallel to $r$ - points toward Earth  |
| $g$                 | a vector term in the variation equations   |
| $g_0$               | a constant representing the number of pounds mass per slug (approx. 32.2)  |
| G&C                 | guidance and control   |
| $h$                 | vehicle altitude   |
| $H$                 | the Hamiltonian  |
| $H_u$               | the partial derivative of the Hamiltonian $H$ with respect to the control vector $u$   |
| HSV                 | hypersonic vehicle   |
| $I_{JJ}$            | a scalar influence function of cost  |
| $I_{J_i J_i}$       | a scalar influence function of cost for the $i^{\text{th}}$ trajectory leg   |
| $I_{s p_a}$         | the air-breathing engine specific impulse derived from the Langley data base with dimension sec (a function of $\Phi_a$ , $M_f$ , and weakly of $Q$ )  |
| $I_{s p_R}$         | the rocket engine specific impulse (a constant)  |
| $I_{yy}$            | the vehicle pitch moment of inertia derived from the Langley data base with dimension slug-ft <sup>2</sup>   |
| $I_{\psi J}$        | a vector influence function of constraints and cost  |
| $I_{\psi_i J_i}$    | a vector influence function of constraints and cost for the $i^{\text{th}}$ trajectory segment   |
| $I_{\psi \psi}$     | a matrix influence function of constraints   |
| $I_{\psi_i \psi_i}$ | a matrix influence function of constraints for the $i^{\text{th}}$ trajectory segment  |

|           |  |
|-----------|--|
| IR&D      | internal research and development  |
| J         | a mathematical cost imposed on the system  |
| $J_i$     | a mathematical cost imposed on the system for the $i^{\text{th}}$ ascent trajectory leg                                  |
| $J_s$     | a heuristically determined specified cost improvement  |
| L         | the distributed mathematical cost term   |
| $L_u$     | the partial derivative of the distributed mathematical cost term L with respect to the control vector $u$                |
| $L_x$     | the partial derivative of the distributed mathematical cost term L with respect to the state vector $x$                  |
| $K_{Q_i}$ | the distributed cost weighting term on the $i^{\text{th}}$ ascent trajectory leg   |
| $K_1$     | a coefficient in the equation used to find $\delta_e$ for vehicle moment trim - a function of $\alpha$ and $m$           |
| $K_2$     | a coefficient in the equation used to find $\delta_e$ for vehicle moment trim - a function of $\alpha$ and $m$           |
| $K_3$     | a coefficient in the equation used to find $\delta_e$ for vehicle moment trim - a function of $\alpha$ , $m$ , and $M_f$ |
| L         | the distributed mathematical cost term   |
| $L$       | the lift force acting on the vehicle   |
| $L_i$     | the distributed mathematical cost term for the $i^{\text{th}}$ ascent trajectory leg                                     |
| $L_{i,x}$ | the partial derivative of the distributed mathematical cost term $L_i$ with respect to the control vector $x$            |
| $L_u$     | the partial derivative of the distributed mathematical cost term L with respect to the control vector $u$                |
| LaRC      | Langley Research Center  |
| LVLH      | the local vertical/local horizontal reference frame  |
| $m$       | the vehicle mass   |
| $m_a$     | the air-breathing engine fuel mass   |
| $m_R$     | the rocket engine propellant mass  |
| $m_0$     | the vehicle mass at takeoff  |
| M         | a matrix term used in the trajectory optimization variation equations  |
| $M_f$     | the free stream Mach number  |
| $M_q$     | the pitch moment acting on the vehicle   |
| NM        | nautical miles   |
| psf       | pounds per square foot   |
| $q$       | the vehicle pitch rate   |
| $q_0$     | the vehicle takeoff pitch rate   |
| Q         | the dynamic pressure   |
| $Q_D$     | the desired dynamic pressure constraint bound  |
| $r$       | the vehicle distance from the center of the Earth  |
| $r_e$     | the radius of the Earth  |

|              |  |
|--------------|--|
| $r_{targ}$   | the target circular orbit altitude   |
| $r_0$        | the vehicle distance from the center of the Earth at takeoff   |
| $S_{ref}$    | the vehicle reference wing area  |
| <b>SSTO</b>  | single-stage-to-orbit  |
| $t$          | time   |
| $t_s$        | the switch time vector   |
| $t_{s_i}$    | the $i^{th}$ switch time   |
| $T$          | the thrust force acting on the vehicle   |
| $T_R$        | the rocket thrust at full throttle - it has a value of zero before the rocket engine turn-on switch time   |
| $u$          | the control vector   |
| $u_\alpha$   | the control for the air-breathing engine   |
| $u_i$        | the $i^{th}$ element of the control vector   |
| $u_R$        | the control for the rocket   |
| $u_0$        | a step function which changes from 0 to 1 at a functional value designated in brackets   |
| $U$          | a diagonal matrix of functions of time to weight different elements of the control variation vector  |
| $v_f$        | the vehicle velocity magnitude relative to the free stream   |
| $v_{targ}$   | the target velocity magnitude at the desired circular orbit condition  |
| $v_{targ_i}$ | the target velocity magnitude for the end of $i^{th}$ ascent trajectory leg  |
| $v_1$        | the free stream velocity component normal to $v_2$ and $v_3$ , pointing toward increasing $\mu$  |
| $v_{1_0}$    | the northerly component of the takeoff velocity  |
| $v_2$        | the free stream velocity component parallel to the equatorial plane, pointing eastward, normal to $v_3$  |
| $v_{2_0}$    | the easterly component of the takeoff velocity   |
| $v_3$        | the vehicle free stream velocity component parallel to $r$ (points toward Earth)   |
| $v_{3_0}$    | the vehicle free stream velocity component at takeoff parallel to $r$ (points toward Earth)  |
| $V$          | a diagonal matrix of constant coefficients to weight different elements of the switch time variation vector  |
| $x$          | the state vector   |
| $x_{CG}$     | the longitudinal distance from the current vehicle center of gravity to the moment reference center derived from the Langley data base with dimension ft |
| $x_i$        | the $i^{th}$ component of the state vector $x$   |
| $x_R$        | the longitudinal distance from the vehicle moment reference center to the point of rocket thrust application   |
| $x_0$        | the vehicle state vector at takeoff  |
| $\alpha$     | the vehicle angle of attack  |

A wide variety of HSV design concepts and applicable subsystem technologies are under consideration. Unique trajectory management strategies are likely to be necessary for each proposed vehicle configuration to assure efficient payload performance while satisfying critical physical constraints. The generic analysis technique implemented under this subtask permits a common tool to be applied to all proposed HSV SSTO configurations. Use of the tool supplies information needed for a valid comparison of expected performance and key sensitivities for alternative vehicle concepts.

The methodology applies a generalized gradient two-point boundary value problem solution algorithm to the HSV problem. Equality constraints are adjoined to the problem. Inequality constraints are treated by either mathematical remapping of the function space or penalty functions. Dynamic discontinuities, such as phasing of propulsive modes, are treated by an extension of the control vector to include the times at which the discontinuities occur. The integrated analysis data are generated by optimizing a mathematical performance index which emphasizes payload performance.

## **IV.B. Longer Term Research Objectives**

The task statement of work identifies several investigation paths which are intended as directions for research under possible continuations of the effort. These are summarized below:

### **IV.B.1. Treatment of Vehicle Thrust Direction and Pitch Moment Changes with Angle of Attack**

The initial example HSV model included a propulsion system that represented thrust magnitude as independent of angle of attack and forced thrust direction to always be in the longitudinal body axis. More realistic vehicle models specify the thrust magnitude and direction as functions of angle of attack, which also implies associated longitudinal moment variations. This subtask would characterize the changes in HSV trajectory management and control strategies that result from explicit consideration of angle of attack effects on propulsion performance.

### **IV.B.2. Incorporation of Thermal Constraints Into Trajectory Results**

The integrated trajectory/control analysis methodology supports treatment of inequality constraints which are functionally dependent on both states and controls. However, the initial demonstration was restricted to studying the effects of dynamic pressure inequality constraints which are only state dependent. Treatment of thermal constraints would address an important physical performance limitation that has both state and control dependencies. This subtask would incorporate a vehicle stagnation point thermal flux constraint and assess its qualitative effects on mission performance and G&C strategies.

### **IV.B.3. HSV G&C Performance Robustness Studies**

Uncertainty in the environment model and expected vehicle dynamics are important design considerations for HSV G&C systems. The atmosphere can experience significant density variations at the higher HSV air-breathing altitudes. The aerodynamic and propulsion performance of HSVs may not be accurately modelled before there is significant flight experience and may vary between vehicles or for a given vehicle on different flights. The likelihood of successfully accomplishing specific mission objectives depends on understanding the effects of these uncertainties and designing a G&C system that is robust enough to handle them. This subtask would evaluate the performance of the near-fuel-optimal HSV trajectories and candidate closed-loop G&C systems in the presence of aerodynamic variations, propulsion modelling uncertainties, and atmospheric disturbances. These uncertainty effects would be evaluated for a range of applicable inequality constraint bounds.

## V. Progress for June 1990 to March 1991

### V.A. Formulation of an Integrated Trajectory/Control Analysis Methodology

#### V.A.1. Overview

A major objective of this task has been to demonstrate the ability of the Draper integrated trajectory/control analysis methodologies to derive useful G&C design information when applied to realistic HSV ascent models. To accomplish this, the resulting tools were adapted to develop near-minimum-fuel, horizontal take-off-to-orbit trajectories for an example configuration, a winged-cone vehicle which is defined in a tabulated parametric database [11]. The model features lift, drag, side forces, and moments as functions of  $\alpha$ , Mach number, and  $\delta_e$ . Also, the air-breathing propulsion system thrust and specific impulse are represented as a function of  $\Phi_\alpha$ , Mach number, and  $Q$ .

The target orbit of interest in the study is polar, circular, and low altitude (e.g. 110 NM). The target requires some rocket thrust outside the sensible atmosphere to achieve the circularization. Therefore, full trajectory development requires evaluation of both air-breathing engine and rocket throttle setting histories. This requires treatment of the flight condition at which the air-breathing engine is fully shut down, the flight condition at which the rocket engine is first turned on, and aerosurface and rocket engine deflection histories. A suitable trajectory must minimize fuel consumption, satisfy physical design limits such as an upper bound on dynamic pressure, and must match both desired takeoff conditions and the desired target orbit state.

An open loop trajectory optimization algorithm general enough to handle all the considerations of concern for HSVs has already been developed and demonstrated for other HSV designs [2,4,12]. While the mathematics of the algorithm remain similar in each application, it is necessary to develop a performance index and apply constraints unique to each application. In addition, each vehicle model and associated partial derivatives must be defined. These features as well as a standard atmosphere model must be implemented in a form compatible with the optimization algorithm.

Air-breathing HSVs have highly nonlinear dynamics during powered flight that vary greatly with Mach number. In addition to extensive coupling between propulsion and control, there is little relevant flight experience. Construction of nearly fuel-optimal take-off-to-orbit trajectories cannot be accomplished from existing analytic formulas or by reliance on previous results. However, use of an applicable optimization algorithm can generate a desired trajectory. The algorithm must explicitly consider an appropriate performance index, boundary conditions, physically derived inequality constraints, and the phasing of discrete propulsion system operations.

The following specific methodology capabilities have been demonstrated in the trajectory development for the example HSV:

- Use of the example vehicle model's multidimensional tabulated database.
- Horizontal launch to near orbital velocities on a polar orbit track.
- Application of an upper bound on dynamic pressure.
- Achievement of near minimum propellant consumption.
- Consideration of elevon aerodynamics and longitudinal rotation dynamics.
- Development of an algorithm feature that can determine nearly optimal phasing of the air-breathing engine shutdown and rocket ignition.

## V.A.2. Data Smoothing Techniques

For the purpose of interpolating the aerodynamic and propulsion data, a new multidimensional cubic spline algorithm was developed to replace the B-spline method that has been used previously at Draper for similar applications.

B-splines are a basis set of overlapping polynomial splines from which interpolated values are obtained through linear combination over each interval. The main advantage of this approach is its generality. B-splines can be applied to multidimensional interpolation problems and can be used to obtain any desired degree of smoothness (continuous  $N^{\text{th}}$  order derivatives) at any point (including extreme points) in the data set. Continuity of the derivatives is achieved through the use of knot sequences along the independent axes. For more details about B-spline algorithms and their properties refer to ref. [13]. The disadvantage of using B-splines is that for problems not requiring such flexibility there is a significant degree of overhead in terms of transforming the data into B-spline tables, performing tensor algebra for multidimensional problems, and generating the required software.

The new interpolation algorithm is a multidimensional extension of the basic cubic spline procedure found in many calculus textbooks. It is also a variation of the so called "Cubic Hermite Interpolation" and provides a very efficient local scheme that is continuous up to the second-order derivatives. For problems requiring only smooth first-order derivatives it is a much faster algorithm than the B-spline approach.

The data set is assumed to be in the form of an N-dimensional table with uniformly spaced grid points along each of the axes of the independent variables. Prior to performing any interpolations, the entire data set is preprocessed to generate derivative information at the grid points. Since no a priori information is available to bias the choice of these derivatives, they are computed based on the straight line slope between the bounding grid points on each axis. For example, in one dimension, along the x-axis, x being an independent variable, at grid point  $x(2)$  :

$$\frac{df}{dx} = \frac{f(x(3)) - f(x(1))}{x(3) - x(1)} \quad (\text{Eq. V.1})$$

At the data set boundaries the last interval slope is used. For example, at  $x(0)$  :

$$\frac{df}{dx} = \frac{f(x(1)) - f(x(0))}{x(1) - x(0)} \quad (\text{Eq. V.2})$$

Precomputing the derivatives is not necessary, however it greatly improves the efficiency of the on-line interpolation.

The interpolation algorithm is best visualized using a two-dimensional example as illustrated in figure V-1. Consider the case of a dependent variable, such as drag coefficient, tabulated as a function of two independent variables, such as Mach Number and angle-of-attack. During an interpolation, one first finds the two-dimension grid cell containing the current flight condition. In the figure (xcoord, ycoord) represents the flight condition (Mach number and angle of attack), and the coordinates (a,c), (b,c), (b,d), and (a,d) represent the bounding cell. The function values, and the associated derivatives (along each axis), are then looked up for each of these coordinates. Using these values, several one-dimensional cubic splines are constructed in the same direction along the vertices of the bounding region. Note from the figure that two splines were required in the x-axis direction for a two-dimensional problem (labeled as fit1 and fit2). In three dimensions, this first step would have required four splines, and in more dimensions  $2^{N-1}$  splines. These one-dimensional splines are then used to obtain function values at the coordinates (xcoord,c) and (xcoord,d), while the derivatives at these points are obtained by linearly interpolating the slopes at the end-points of each spline. This completes the first interpolation step which effectively reduces the problem by one dimension. Now a simple cubic spline (fit3) can be generated along the y-axis using the new function values and slopes. The final interpolated value at (xcoord,ycoord)

is then obtained from this last spline at  $y=y_{\text{coord}}$ . This method works equally well for higher order interpolations, using one-dimensional splines to reduce the number of dimensions step-by-step until one final spline gives the desired interpolated value. It can be shown that the interpolated values using this algorithm are continuous with respect to the independent variables, and that their first-order derivatives are smooth.

The interpolation of aerodynamic and propulsion data was performed using the cubic spline algorithm described above. Although a general N-dimensional routine could have been implemented, separate two-dimensional and three-dimensional versions were written for speed and simplicity of the code. The interpolation software is divided into three sets of routines representing a preprocessor to generate derivatives, a table look up function to locate the cell boundaries, and then the actual code to perform the interpolation. The resulting interpolation code is efficient in terms of code size as well as execution speed. The only penalty is related to the additional storage space required to store the derivatives.

### V.A.3. Mathematical Basis of Analysis Algorithm

#### V.A.3.a. The Optimization Problem Formulation and Features

The trajectory optimization algorithm uses a generalized steepest descent gradient two-point boundary value problem solution technique. The most general form of the Draper developed methodology is capable of solving simultaneously for vehicle configuration, trajectory, dynamic discontinuity times, and controls [2,4]. It can accommodate equality and inequality constraints while optimizing with respect to a performance index of states, vehicle design parameters, controls, and time. In the current application, vehicle geometry is assumed fixed, eliminating consideration of design parameters. The optimization performance index  $J$  as applied to this problem has the form:

$$J(\tau) = \phi(x(\tau)) + \int_0^{\tau} L(x(t), u(t)) dt \quad (\text{Eq. V.3})$$

where  $\tau$  is the time at which the target orbit state is reached,  $x$  is the vehicle state vector:

$$x = \begin{pmatrix} r \\ v \\ \mu \\ v_1 \\ v_2 \\ v_3 \\ \theta \\ q \\ m \end{pmatrix} \quad (\text{Eq. V.4})$$

and  $u$  is the control vector:

$$u = \begin{pmatrix} u_1 \\ u_2 \\ u_3 \\ u_4 \end{pmatrix} = \begin{pmatrix} u_a \\ u_R \\ \delta_e \\ \delta_R \end{pmatrix} \quad (\text{Eq. V.5})$$

The relationship between the control vector elements and the actual propulsion system throttle variables are:

$$\Phi_a = (u_a)^2 \quad (\text{Eq. V.6})$$

$$\Phi_R = \frac{1}{1 + (u_R)^2} \quad (\text{Eq. V.7})$$

The terminal cost term  $\phi$  is used to minimize the consumed fuel mass.

$$\phi = m_0 - m(\tau) \quad (\text{Eq. V.8})$$

The integral function  $I$  treats inequality constraints. In this application where dynamic pressure is constrained,  $I$  is a function only of states since dynamic pressure is a function of velocity states and density, and density is a function of  $r$  when using a standard atmosphere model.

$$I = C_Q(Q - Q_D)^2 u_0 [Q - Q_D] \quad (\text{Eq. V.9})$$

where:

$$Q = \frac{\rho(v_f)^2}{2} \quad (\text{Eq. V.10})$$

and where  $u_0 [Q - Q_D]$  is a unit step function that changes from zero to one at  $Q = Q_D$ .

A costate like function  $\Lambda$  is adjoined to the problem to explicitly treat a vector of applicable equality constraints functions called  $\Psi$ . The specific equations for  $\Lambda$  are developed in section V.B.2.c in Eqs. V.45 and V.46. With the initial take-off conditions given, the equality constraints are needed to enforce the target orbit conditions at time  $\tau$ . One smoothly varying target orbit state equality constraint is needed to determine  $\tau$ . The target orbital velocity is used in this application and is therefore excluded from the adjoined function list. This trajectory integration cutoff function called  $\Omega$  helps determine boundary conditions on the costate function  $\lambda$ , while the remaining equality constraints determine boundary conditions used in the adjoined function  $\Lambda$ . The specific formulation for  $\lambda$  is also detailed in section V.B.2.c in Eqs. V.42,43.

An algorithm feature that locates the most efficient times for dynamic discontinuity events,  $t_s$ , is used to optimize propulsive phasing of the air-breathing engine and rocket. The discontinuities are factored into the vehicle state dynamics model (see Eq. V.38) and are treated in the costate and adjoined function dynamics (see Eqs. V.47,48). A discrete air-breathing engine

shutdown time and a separate discrete rocket ignition time can be evaluated by this means. The implementation permits staggered or overlapping engine operation as dictated by minimum fuel considerations.

Given an initial control history and propulsive phasing time guess, the algorithm iteratively computes perturbations to the controls and discontinuity times to improve the performance index while maintaining boundary conditions. Additive perturbation contributions are derived to improve the cost as well as to drive down violations of the equality constraints. Weighting functions balance the relative contributions of each additive perturbation term.

Numerical stability of the algorithm requires that the initial trajectory guess nearly satisfies the equality constraints even if far from optimal in performance. Since the vehicle dynamics are very dissimilar from a simple rocket, a strategy to develop a suitable initial guess is required.

#### V.A.3.b. A Technique to Construct an Initial Trajectory Guess

An air-breathing SSTO HSV is likely to have three distinct flight phases when subjected to a dynamic pressure upper bound. The first phase seeks efficient performance in the subsonic to low supersonic flight regime while remaining below the dynamic pressure bound. When the bound is reached, the vehicle is likely to fly along it while accelerating to high hypersonic velocities. Finally, there is a climb to orbit, utilizing the rocket as necessary, while experiencing declining dynamic pressure. An appropriate procedure to construct an initial trajectory guess is to develop feasible trajectory segments in each of the three identified flight phases. An engineer's experience-based intuition can be better applied to determination of likely vehicle flight characteristics in the simplified envelope of each of the separate flight segments. Solution of the segments in sequence from the ground up assures matching conditions between each segment and provides a suitable initial guess for the overall trajectory analysis problem.

A separate, simplified, optimization problem has been posed for each flight segment. In each case, the propellant mass consumption has still been minimized. However, it remained necessary to construct an initial control history guess on each segment which flies a trajectory that nearly satisfies the locally applicable boundary conditions (though without regard to performance). To simplify this development, the following assumptions have been made:

- The active control used for pitch attitude is  $\alpha$  rather than  $\delta_e$  and  $\delta_R$ . Elevon aerodynamic effects are retained by requiring maintenance of moment trim. Use of  $\alpha$  (combined with  $\phi_\alpha$  and  $\phi_R$ ) is more intuitive for raw trajectory construction than  $\delta_e$  and  $\delta_R$  histories. The resulting control vector is:

$$u = \begin{pmatrix} u_1 \\ u_2 \\ u_3 \end{pmatrix} = \begin{pmatrix} u_\alpha \\ u_R \\ \alpha \end{pmatrix} \quad (\text{Eq. V.11})$$

- Rotation dynamics are not tracked (reducing the state dimensionality). The resulting state vector is:

$$X = \begin{pmatrix} r \\ v \\ \mu \\ u_1 \\ u_2 \\ u_3 \\ m \end{pmatrix} \quad (\text{Eq. V.12})$$

- Only air-breathing propulsion is assumed available on the first two segments, eliminating

## V.B. Demonstration Case Preliminaries

### V.B.1. Vehicle/Environment Models

A 4200+ line file of data was used [11] to define the aerodynamic and propulsive characteristics, as well as mass properties of the example winged-cone hypersonic vehicle (HSV). Aerodynamic effects of rotational control aerosurfaces are included. The data is in table look-up form, involving up to trivariant dependencies for specified parameters, including some which evidence highly nonlinear behavior with respect to one or more variables.

#### V.B.1.a. Available Database

*Variable Definitions and Dependencies:* The variables in tables V.1,2,3 are included in the example vehicle model:

**Table V.1**  
**Example Model Aerodynamic Force Coefficients**

| Variable       | Functional Dependencies | Description                                      |
|----------------|-------------------------|--|
| $C_{D,u}$      | $M, \alpha$             | Drag increment coefficient for the basic vehicle |
| $C_{D,da}$     | $M, \alpha, \delta$     | Drag increment coefficient for the right elevon  |
| $C_{D,de}$     | $M, \alpha, \delta$     | Drag increment coefficient for the left elevon   |
| $C_{D,dr}$     | $M, \alpha, \delta$     | Drag increment coefficient for the rudder        |
| $C_{D,dc}$     | $M, \alpha, \delta$     | Drag increment coefficient for the canard        |
| $C_{L,\alpha}$ | $M, \alpha$             | Lift increment coefficient for the basic vehicle |
| $C_{L,da}$     | $M, \alpha, \delta$     | Lift increment coefficient for the right elevon  |
| $C_{L,de}$     | $M, \alpha, \delta$     | Lift increment coefficient for the left elevon   |
| $C_{L,dc}$     | $M, \alpha, \delta$     | Lift increment coefficient for the canard        |
| $C_{Y,da}$     | $M, \alpha, \delta$     | Side force increment for the right elevon        |

**Table V.2**  
**Example Model Aerodynamic Moment Coefficients**

| <b>Variable</b> | <b>Functional Dependencies</b> | <b>Description</b>                                       |
|-----------------|--------------------------------|--|
| $C_{l, da}$     | $M, \alpha, \delta$            | Rolling moment coefficient for the right elevon          |
| $C_{l, de}$     | $M, \alpha, \delta$            | Rolling moment coefficient for the left elevon           |
| $C_{l, dr}$     | $M, \alpha, \delta$            | Rolling moment coefficient for the rudder                |
| $C_{ma}$        | $M, \alpha$                    | Pitch moment increment for the basic vehicle             |
| $C_{m, da}$     | $M, \alpha, \delta$            | Pitch moment increment for the right elevon              |
| $C_{m, de}$     | $M, \alpha, \delta$            | Pitch moment increment for the left elevon               |
| $C_{m, dr}$     | $M, \alpha, \delta$            | Pitch moment increment for the rudder                    |
| $C_{m, dc}$     | $M, \alpha, \delta$            | Pitch moment increment for the canard                    |
| $C_{m_q}$       | $M, \alpha$                    | Pitching moment with pitch rate derivative               |
| $C_{n, da}$     | $M, \alpha, \delta$            | Yawing moment increment coefficient for the right elevon |
| $C_{n, de}$     | $M, \alpha, \delta$            | Yawing moment increment coefficient for the left elevon  |
| $C_{n, dr}$     | $M, \alpha, \delta$            | Yawing moment increment coefficient for the rudder       |
| $C_{n_p}$       | $M, \alpha$                    | Yawing moment with roll rate dynamic derivative          |

**Table V.3**  
**Example Model Propulsion and Mass Property Coefficients**

| <b>Variable</b> | <b>Functional Dependencies</b> | <b>Description</b>  |
|-----------------|--------------------------------|---|
| $C_T$           | $M, \phi, Q$                   | Thrust coefficient  |
| $I_{sp}$        | $M, \phi, Q$                   | Specific impulse  |
| $x_{cg}$        | $m$                            | Longitudinal distance from moment reference center to vehicle center of gravity |
| $I_{yy}$        | $m$                            | Pitch moment of inertia   |

**Observations About Supplied Data:** A number of parameter identities apply to the example vehicle model as a result of some of the symmetry used in its formulation:

$$\begin{aligned}
 C_{D, d\alpha} &= C_{D, d\epsilon} & C_{L, d\alpha} &= -C_{L, d\epsilon} & C_{L, d\alpha} &= C_{L, d\epsilon} \\
 C_{m, d\alpha} &= C_{m, d\epsilon} & C_{Y, d\alpha} &= -C_{Y, d\epsilon} & C_{n, d\alpha} &= -C_{n, d\epsilon} \\
 C_{D, dr}(\alpha) &= C_{D, dr}(-\alpha)
 \end{aligned}$$

Some of the variables are nearly perfectly linear with respect to variations in angle of attack ( $\alpha$ ), eliminating the need to fit the data with respect to this parameter. These variables include:  $C_{Y, dr}, C_{L, dr}, C_{m, dr}, C_{n, dr}, C_{n_p}$

The canard is assumed to be retracted above Mach 1, so data are only provided for its aerodynamic contributions under subsonic flight conditions.

**Environment Model - Atmosphere:** A standard 1976 atmosphere model that only treats altitude dependencies for physical properties has been used. Data are tabulated at one kilometer altitude increments. An exponential fit between altitude break points has been used. The atmosphere is assumed to rotate uniformly with the Earth's surface directly below a specified location.

**Environment Model - Gravity:** The gravity is modelled as an inverse square field based on the assumption of a homogeneous spherical Earth. Oblateness effects were ignored.

#### V.B.1.b. Simplifications

**Reduced Rotational Dynamics:** The trajectory analysis under this task was restricted to include the pitch plane rotational dynamics in order to reduce the computational burden required to accomplish the G&C analysis of the NASA/LaRC HSV design concept. This amounts to consideration of constant heading angle cases only, ignoring side forces. With this assumption, only the following variables are retained, where left and right elevon contributions are merged into combined coefficients (by adding them together) since they act in unison for pitch control:

$$C_{D\alpha}, (C_{D, d\alpha} + C_{D, d\epsilon}), C_{D, dc}, C_{L\alpha}, (C_{L, d\alpha} + C_{L, d\epsilon}), C_{L, dc}, \\
 C_{m\alpha}, (C_{m, d\alpha} + C_{m, d\epsilon}), C_{m, dc}, C_{m_q}, C_T, I_{sp}, I_{yy}, x_{cg}$$

Consistent with the exclusion of vehicle roll and yaw dynamics, the pitch dynamics are treated in a strictly planer sense. The vehicle wing axis is assumed to always be level with the local horizontal, and no sideslip is treated. Inertial coupling and frame rotation effects can eventually be added when 3-dimensional rotation dynamics are included (along with the aerosurfaces to provide the other rotational degrees of freedom).

**Exclude Canard Use:** The canard in the example vehicle model is assumed to be usable only at low velocities (data ends at Mach = 0.9). It is excluded in the analysis methodology demonstration cases. All pitch control is accomplished with elevon usage.

**Curve Fits for the Vehicle Mass Properties Model:** Since the data for the moments of inertia values and center of mass location included in the example winged-cone vehicle model was quite smooth, it was decided to develop a polynomial fit of their functional dependence.

For the relationship of  $x_{CG}$  to mass, a quadratic fit gave good accuracy. The resulting function is:

$$x_{CG} = -24.227373830 + .00008264665m - .00000000011m^2 \quad (\text{Eq. V.14})$$

where mass is expressed in pounds and  $x_{CG}$  in feet. In the analysis code, the masses are in slugs. Figure V-2 shows the fit curve and the data points (noted by circles).

A cubic fit was chosen for the  $I_{yy}$  data, with the following result:

$$I_{yy} = 2.8896578089m + .00028207479m^2 - .00000000061m^3 \quad (\text{Eq. V.15})$$

The fit function for  $I_{yy}$  is shown in figure V-3.

**Propulsion Phasing:** The example vehicle data provides an air-breathing propulsion model to orbital velocities. However, to achieve the desired 110 NM circular orbit, some propulsive capability is required above the sensible atmosphere. A constant specific impulse rocket with throttle and a maximum thrust magnitude is assumed. Separate, discrete air-breathing engine off-time and rocket on-time values are defined as optimization switch points. The rocket is assumed to stay on from computed on-time to final orbit insertion. If a split rocket thrust history is necessary (similar to a Hohmann transfer), then intermediate zero throttle settings will result from the optimization solution.

**Rotation Effector Phasing:** Use of aerosurface effectors for pitch control will be terminated at rocket ignition with control moments subsequently provided by rocket gimbal rotation of the thrust vector. Changes in rocket thrust along the vehicle longitudinal body axis will be ignored and normal force components due to gimbal rotation will not be included.

**Unconstrained Orbit Phasing:** The target circular, polar orbit will be assumed to have an unconstrained phase angle. Any circular orbit of proper altitude will be deemed an acceptable result.

## V.B.2. Strategy for Final Near-Fuel-Optimal Trajectory Development

### V.B.2.a. Trajectory Definition (Boundary Conditions)

Initial and final state conditions need to be set to complete the specification of the desired optimization problem. The initial condition is defined just after vehicle takeoff:

$$x(0) = \begin{pmatrix} r_e \\ v_0 \\ \mu_0 \\ v_{1_0} \\ v_{2_0} \\ v_{3_0} \\ \theta_0 \\ q_0 \\ m_0 \end{pmatrix} \quad (\text{Eq. V.16})$$

Only three of the terminal states are constrained as the problem is posed (including simplifications). The target orbit velocity is used to determine the forward integration cutoff condition  $\Omega$ . The target orbit altitude and a zero target vertical velocity (for a circular orbit) fill out the equality constraint set, defining the two element constraint vector  $\Psi$ .

$$\Omega = (v_1)^2 + (v_2 + r\omega_e \cos\mu)^2 - (v_{targ})^2 \quad (\text{Eq. V.17})$$

$$\Psi = \begin{pmatrix} r(\tau) - r_{targ} \\ v_3(\tau) \end{pmatrix} \quad (\text{Eq. V.18})$$

### V.B.2.b. Nine State Vehicle Dynamics Model

A nine state vehicle dynamics model permits treatment of longitudinal rotational dynamics using the aerosurfaces (elevons in the example vehicle) for rotational control. The state equations consistent with the LVLH coordinate system shown in figure V.4 and the modelling simplifications noted in section V.B.1.b can be written as follows:

$$\dot{f} = \begin{pmatrix} -x_6 \\ \frac{x_5}{x_1 \cos x_3} \\ \frac{x_4}{x_1} \\ \frac{x_4 x_6 - (x_5)^2 \tan x_3}{x_1} - 2\omega_e x_5 \sin x_3 - x_1 (\omega_e)^2 \sin x_3 \cos x_3 + \frac{F_1}{x_9} \\ x_5 \frac{(x_6 + x_4 \tan x_3)}{x_1} + 2\omega_e (x_4 \sin x_3 + x_6 \cos x_3) + \frac{F_2}{x_9} \\ \frac{-((x_4)^2 + (x_5)^2)}{x_1} - 2\omega_e x_5 \cos x_3 - x_1 (\omega_e \cos x_3)^2 + \frac{F_3}{x_9} \\ x_8 \\ \frac{M_q}{I_{yy}} \\ \frac{1}{g_0} \left( \frac{Qc_T}{I_{sp_a}} + \frac{T_R \Phi_R}{I_{sp_R}} \right) \end{pmatrix} \quad (\text{Eq. V.19})$$

where:

$$x = \begin{pmatrix} r \\ v \\ \mu \\ u_1 \\ u_2 \\ u_3 \\ \theta \\ q \\ m \end{pmatrix} \quad (\text{Eq. V.20})$$

Using the zero bank angle assumption, the following force equations in the vehicle LVLH frame result assuming an arc tangent function definition over the range from -90 deg to +90 deg:

$$F = \begin{pmatrix} F_1 \\ F_2 \\ F_3 \end{pmatrix} = \begin{pmatrix} \text{sign}(v_1) \cos \psi (F_T \cos \gamma + F_N \sin \gamma) \\ \text{sign}(v_1) \sin \psi (F_T \cos \gamma + F_N \sin \gamma) \\ -F_T \sin \gamma + F_N \cos \gamma + F_g \end{pmatrix} \quad (\text{Eq. V.21})$$

where  $\text{sign}(v_1)$  has a value of 1 for  $v_1 \geq 0$ , and a value of -1 for  $v_1 < 0$ . Also, note that only two force components remain in the body frame (no side force):

$$F_T = T \cos \alpha - D \quad (\text{Eq. V.22})$$

$$F_N = -(T \sin \alpha + L) \quad (\text{Eq. V.23})$$

The following equations are used to relate flight angles to states:

$$\alpha = \theta - \gamma \quad (\text{Eq. V.24})$$

$$\gamma = \tan^{-1} \left( \frac{-x_6}{\sqrt{(x_4)^2 + (x_5)^2}} \right) \quad (\text{Eq. V.25})$$

$$\psi = \tan^{-1} \left( \frac{x_5}{x_4} \right) \quad (\text{Eq. V.26})$$

The lift, drag, pitch moments, and engine thrust can be written in the following form involving coefficient functions specified in the example model data tables:

$$L = C_L Q S_{ref} \quad (\text{Eq. V.27})$$

$$D = C_D Q S_{ref} \quad (\text{Eq. V.28})$$

$$M_q = C_m Q c S_{ref} - x_{CG} (D \sin \alpha + L \cos \alpha) + (x_R - x_{CG}) \Phi_R T_R \sin \delta_R \quad (\text{Eq. V.29})$$

$$T = Q C_T + \Phi_R T_R \quad (\text{Eq. V.30})$$

where:

$$C_L = C_{L_\alpha} + C_{L_e} \quad (\text{Eq. V.31})$$

$$C_D = C_{D_\alpha} + C_{D_e} \quad (\text{Eq. V.32})$$

$$C_m = C_{m_\alpha} + C_{m_e} + C_{m_q} \left( \frac{qc}{2v_f} \right) \quad (\text{Eq. V.33})$$

$$v_f = \sqrt{(v_1)^2 + (v_2)^2 + (v_3)^2} \quad (\text{Eq. V.34})$$

When using the example model database,  $v_f$  and  $\alpha$  are required, where  $v_f$  is used along with  $r$  in an atmosphere model to compute  $M_f$ .

It is intended that eventually a model of moments from air-breathing engine thrust as a function of Mach number and angle of attack will be developed, the use of which will require additional terms in the vehicle pitch moment equation above.

The gravity force acting on the vehicle can be written in the following form:

$$F_g = \frac{M_e X_g}{(X_1)^2} \quad (\text{Eq. V.35})$$

The following equations are used to transform the throttle controls on the propulsion to unbounded control vector components. They are based on the assumption that  $\Phi_\alpha \geq 0$  and  $0 < \Phi_R \leq 1$ .

$$\Phi_\alpha = (u_\alpha)^2 \quad (\text{Eq. V.36})$$

$$\Phi_R = \frac{1}{1 + (u_R)^2} \quad (\text{Eq. V.37})$$

#### V.B.2.c. Optimization Algorithm Formulation for the Example Application

To perform closed-loop G&C studies on an air-breathing HSV during powered ascent to orbit, it is necessary first to construct a representative, realizable trajectory under nominal flight conditions. The most appropriate way to construct the desired trajectory is to perform an open-loop analysis with the help of a trajectory optimization algorithm. Since the flight path must accommodate physical constraints such as limits on dynamic pressure, the methodology must directly treat the constraints to obtain a realistic trajectory. Also, since discrete phasing of propulsive components is likely, the trajectory generation methodology must treat discontinuities in the system dynamics. A steepest descent, gradient-based optimization algorithm that treats all these concerns, as well as other features that would allow vehicle configuration characterization within the optimization, has already been developed and demonstrated [2]. To use this technique in the example application, it is necessary to formulate the optimization algorithm in an applicable form, and to define the vehicle dynamics in a compatible state space representation.

**The Algorithms Used:** The trajectory optimization algorithm is based on a gradient/steepest descent technique for solving two-point boundary value problems. Predicated on the techniques reviewed in greater detail in refs. [2,4,12], the algorithm can accommodate equality and inequality constraints while optimizing performance with respect to state. The method can also be generalized to treat variations in vehicle design, also as discussed in refs. [2,4,12]. To address the optimization problem, the vehicle state equation is first defined for use in the algorithm forward integration:

$$\frac{dx}{dt} = f(x, u, t_s) \quad (\text{Eq. V.38})$$

Then the algorithm development starts by definition of an applicable performance index:

$$J(\tau) = \phi(x(\tau)) + \int_0^{\tau} L(x(t), u(t)) dt \quad (\text{Eq. V.39})$$

A forward integration cutoff condition is defined (e.g. target orbital velocity):

$$\Omega(x(\tau)) = 0 \quad (\text{Eq. V.40})$$

A Hamiltonian is constructed after defining a costate vector  $\lambda$  which is determined by backwards integration:

$$H = L + \lambda^T f \quad (\text{Eq. V.41})$$

where:

$$\frac{d\lambda}{dt} = -f_x^T \lambda - L_x^T \quad (\text{Eq. V.42})$$

and where the backwards integration boundary condition is evaluated at the forward integration cutoff time  $\tau$ :

$$\lambda^T(\tau) = \left( \phi_x - \left( \frac{\phi_x f + L}{\Omega_x f} \right) \Omega_x \right) \Big|_{x(\tau), u(\tau)} \quad (\text{Eq. V.43})$$

An equality constraint vector is constructed to accommodate the terminal state boundary conditions defined at the forward integration cutoff time  $\tau$ :

$$\Psi(x(\tau)) = 0 \quad (\text{Eq. V.44})$$

An additional adjoint variable, also determined by backwards integration, is defined to factor in the equality constraint functions (boundary conditions) at the terminal time:

$$\frac{d\Lambda}{dt} = -f_x^T \Lambda \quad (\text{Eq. V.45})$$

where the backwards integration boundary condition is evaluated at the forward integration cutoff time  $\tau$ :

$$\Lambda^T(\tau) = \left( \Psi_x - \frac{\Psi_x f \Omega_x}{\Omega_x f} \right) \Big|_{x(\tau), u(\tau)} \quad (\text{Eq. V.46})$$

It is helpful to introduce the following variables for subsequent notational simplicity where  $U$  and  $V$  are diagonal matrices of coefficients used to weight the relative size of perturbations to the controls and propulsive phasing switch times, respectively:

$$g = \begin{pmatrix} -\Lambda^T(t_{s_1})(f_{s_1}^+ - f_{s_1}^-) \\ -\Lambda^T(t_{s_2})(f_{s_2}^+ - f_{s_2}^-) \\ \vdots \\ \vdots \\ \vdots \end{pmatrix} \quad (\text{Eq. V.47})$$

$$M = \left[ -\Lambda^T(t_{s_1})(f_{s_1}^+ - f_{s_1}^-) \mid -\Lambda^T(t_{s_2})(f_{s_2}^+ - f_{s_2}^-) \mid \cdots \right] \quad (\text{Eq. V.48})$$

$$I_{\Psi\Psi} = \int_0^\tau \Lambda^T f_u U f_u^T \Lambda dt \quad (\text{Eq. V.49})$$

$$I_{\Psi J} = \int_0^\tau \Lambda^T f_u U H_u^T dt \quad (\text{Eq. V.50})$$

$$I_{JJ} = \int_0^\tau H_u U H_u^T dt \quad (\text{Eq. V.51})$$

$$B = (I_{\Psi\Psi} + M V M^T)^{-1} \quad (\text{Eq. V.52})$$

$$C = (I_{\Psi J} + M V g) \quad (\text{Eq. V.53})$$

The resulting algorithm variational equations for the control vector  $u$  and the propulsive phasing switch times  $t_s$  (where dynamic discontinuities occur) are:

$$\delta u = -U(f_u^T \Lambda B C_\Psi \Psi + C_J(H_u^T - f_u^T \Lambda B C)) \quad (\text{Eq. V.54})$$

$$\delta t_s = -V(M^T B C_\Psi \Psi + C_J(g - M^T B C)) \quad (\text{Eq. V.55})$$

where:

$$C_J = -\frac{dJ_s + (I_{\Psi J}^T B + g^T V M^T B) C_\Psi \Psi}{I_{JJ} - I_{\Psi J}^T B C + g^T V g - g^T V M^T B C} \quad (\text{Eq. V.56})$$

With specification of  $dJ_s$  and  $C_\Psi$ , the variational equations can be used to perturb the desired control history on successive iterations through use of Eqs. V.54,55 to eventually achieve vehicle performance optimality while satisfying all applicable constraints. The scalar  $dJ_s$  reflects the specified cost improvement sought on each optimization algorithm iteration. The diagonal matrix  $C_\Psi$  weights the relative size of equality constraint improvements on each optimization algorithm iteration. Proper selection of these weightings as well as  $U$  and  $V$  is critical to the numerical stability and convergence rate of the optimization process. A block diagram showing the signal flow and processing order of the optimization algorithm is shown in figure V-5.

**Treating Constraints:** There are several types of constraints applicable to HSV trajectory optimization. As is true for any two-point boundary value problem, it is necessary to apply equality constraints at the trajectory final target condition. These are treated by adjoining the variable  $\Lambda$ , thereby incorporating the influence of the boundary conditions.

There are constraints on some of the controls. An example would be a lower bound (fuel flow off) on throttle setting. Often such constraints can be treated by nonlinear mapping into a control space without bounds. Care must be taken when using nonlinear mapping to avoid initial solution guesses that specify mapped control values in insensitive regions of the actual control space.

Inequality constraints need to be applied as a result of physical design constraints such as dynamic pressure and thermal limits. For this methodology, penalty functions are introduced through the integral performance index  $I$ . This approach requires periodic adjustment of penalty function gains as the optimal solution is approached.

**Required Special Features:** As is generally true when two-point boundary problem optimization algorithms are used, some application specific considerations are required to assure good algorithm performance for the HSV problem. These include the careful choice of the integration cutoff condition as well as special approaches to balancing the perturbations to boundary value constraint violations against perturbations to controls needed to improve performance. Failure to carefully treat these issues can prevent acceptable algorithm numerical behavior.

Unlike a rocket ascent to orbit, HSVs are more likely to follow a trajectory at low Mach numbers akin to supersonic fighter aircraft minimum time to climb profiles. Often this results in a "zoom maneuver" in the transonic range, where the vehicle uses already acquired potential energy (altitude), combined with thrust, to quickly transit the maximum drag environment near Mach 1 [14]. The resulting ascent can involve a negative vertical velocity component for a short interval. The nonmonotonic behavior of this velocity component makes it an unacceptable parameter for algorithm integration cutoff. Either horizontal velocity or orbital energy state provides much greater likelihood of achieving acceptable state conditions at integration cutoff.

Successful convergence of the optimization algorithm to the desired minimum cost solution requires that the effort to drive the violation of the boundary conditions to zero be balanced against the effort to find an optimal control history. Each parameter requiring perturbation must be separately weighted, with the emphasis that each receives chosen to stress those variables that currently promise the most improvement without numerically destabilizing the algorithm. (Bad choices could induce highly nonlinear steps.) As the interim trajectory solution approaches optimality, the relative sensitivity of the perturbed parameters change. Techniques must be applied to determine current sensitivity and modify the weightings as the algorithm progresses. In some instances, this may require acceptance of perturbations that do not uniformly improve all boundary value violations. A composite measure of proposed algorithm step acceptability can be constructed that takes precedence over individual variation effects, as discussed in ref. [4].

**Cost Function Specification:** Of primary importance in applying an optimization algorithm to a trajectory analysis problem is specification of the terms of a cost index. For this task the terminal cost term was used to minimize vehicle propellant mass usage to go from the ground to orbit, and the integral cost term was used to constrain the dynamic pressure. The resulting functional forms are:

$$\phi = m_0 - m(\tau) \quad (\text{Eq. V.57})$$

$$L = C_Q(Q - Q_D)^2 u_0[Q - Q_D] \quad (\text{Eq. V.58})$$

where  $u_0[Q - Q_D]$  is a unit step function that has zero value for  $Q < Q_D$  and has a value of 1 otherwise.

### V.B.2.d. Relevant Partial Derivatives

**Boundary Condition Derivatives:** The following two equations are the example specific derivatives of the boundary condition equality constraint functions needed in Eqs V.43,46:

$$\Omega_x^T = \begin{pmatrix} 2\omega_e \cos \mu (v_2 + r\omega_e \cos \mu) \\ 0 \\ -2r\omega_e \sin \mu (v_2 + r\omega_e \cos \mu) \\ 2v_1 \\ 2(v_2 + r\omega_e \cos \mu) \\ 0 \\ 0 \\ 0 \\ 0 \end{pmatrix} \quad (\text{Eq. V.59})$$

$$\Psi_x = \begin{pmatrix} 1 & 0 & 0 & 0 & 0 & 0 & 0 & 0 & 0 \\ 0 & 0 & 0 & 0 & 0 & 1 & 0 & 0 & 0 \end{pmatrix} \quad (\text{Eq. V.60})$$

**Cost Function Derivatives:** The following two equations are the example specific derivatives of the performance index function J needed in Eqs. V.42,43:

$$\phi_x = (0 \quad 0 \quad -1) \quad (\text{Eq. V.61})$$

$$L_x = 2C_Q(Q - Q_D)u_0[Q - Q_D] \frac{\partial Q}{\partial x} \quad (\text{Eq. V.62})$$

where:

$$\frac{\partial Q}{\partial x} = \begin{pmatrix} \frac{\partial \rho (v_f)^2}{\partial r} \frac{1}{2} & 0 & 0 & \rho v_1 & \rho v_2 & \rho v_3 & 0 & 0 & 0 \end{pmatrix} \quad (\text{Eq. V.63})$$

and where  $Q_D$  is assumed to be a constant. The values for  $\rho$  and  $\frac{\partial \rho}{\partial r}$  must be derived from a standard atmosphere model.

The Hamiltonian derivative with respect to controls needed in Eqs V.50,51,54 can be expressed by the relationship  $H_u = L_u + \lambda^T f_u$  which requires a partial of the integral cost function with respect to the control vector. For the function of L in the example here,  $L_u$  has zero value.

**State Equation Derivatives:** The partials of the state equation  $f$  in Eq. V.19 with respect to states  $x$  is required for use in Eqs. V.42,45. Because of the number of equations required to complete the definition of  $f_x$  for the example model, details are provided in appendix A.1.

The partials of  $f$  with respect to controls  $u$  is required in Eqs. V.49,50,54. Because of the number of equations required to complete the definition of  $f_u$  for the example model, details are provided in appendix A.2.

### V.B.3. Preliminary Near-Fuel-Optimal Trajectory Development

A general methodology to perform integrated trajectory and control analysis on SSTO HSVs has been devised, and the mathematical basis for demonstrating the complete minimum-fuel-to-orbit trajectory analysis of the example vehicle has been presented above. However, to use the methodology, it is first necessary to construct a complete, mathematically realizable trajectory, from horizontal takeoff to orbit, which initializes the optimization algorithm. While manual iteration of the vehicle dynamics model could be performed to provide an overall trajectory guess, the job can be made much less labor intensive by breaking the problem into a series of simpler initial trajectory development problems (each still requiring a manually developed starting trajectory profile). Sequential development of the trajectory segment guesses from the ground up supports local optimization of each segment, resulting in a composite trajectory that is likely to be better behaved when used to initiate the entire ground to orbit trajectory optimization analysis.

The formulation of three representative trajectory segments are presented here to support the initial complete trajectory definition demonstration. To further reduce the computational complexity of the initial example trajectory segment development, rotational states of the vehicle are not tracked, and the moments are only included to treat vehicle lift and drag effects which result from maintaining pitch trim throughout flight. Engine throttle and vehicle angle of attack are treated as the controls (not aerosurface and rocket gimbal deflection angles). A simpler seven state vehicle dynamics model results.

#### V.B.3.a. A Representative Trajectory Partition

Three ascent trajectory legs were defined, each with special characteristics, which simplify development of an initial trajectory guess. The first leg flies from a horizontal takeoff up until the dynamic pressure constraint is reached at a target velocity in the Mach 2 range. The second leg flies as close to constant dynamic pressure as possible. The third leg ascends to the orbital condition from the end of the constant dynamic pressure segment. The following subsections further discuss each leg.

*Leg 1 - Takeoff to the dynamic pressure limit:* This segment is solved first using the desired vehicle horizontal takeoff conditions as initial conditions. A target terminal time velocity is defined, selected on the basis of the desired dynamic pressure limit (near Mach 2 for a dynamic pressure bound of 1000 psf). Terminal time constraints on the trajectory segment conditions are selected so the dynamic pressure bound is approached with near zero slope to provide proper initial conditions for the next leg which seeks constant dynamic pressure. Inequality constraints are applied only if required to keep the peak dynamic pressure close to the terminal constraint value. Propulsion is limited to the air-breathing system. This results in the elimination of the switch points in the trajectory leg analysis. When applying the optimization algorithm  $g$  and  $M$  have zero value, and the variations  $\delta t_s$  disappear. Also the following simplified equations result:

$$B = (I_{\psi_1 \psi_1})^{-1} \quad (\text{Eq. V.64})$$

$$\delta u = -U \left( f_u^T \wedge B C_{\psi_1} \Psi_1 + C_{J_1} \left( H_u^T - f_u^T \wedge B I_{\psi_1 J_1} \right) \right) \quad (\text{Eq. V.65})$$

$$C_{J_1} = - \frac{dJ_s + I_{\psi_1 J_1}^T B C_{\psi_1} \Psi_1}{I_{J_1 J_1} - I_{\psi_1 J_1}^T B I_{\psi_1 J_1}} \quad (\text{Eq. V.66})$$

*Leg 2 - Constant dynamic pressure:* This segment is solved second, using the terminal conditions from leg 1 as initial conditions. A target terminal time velocity is defined, selected on the basis of where constant dynamic pressure air-breathing flight, with net acceleration, is still barely sustainable (assumed to be 20,000 ft/s air speed). The same terminal time constraints are applied as those used on the first trajectory leg. A distributed cost term is applied to the trajectory segment to nearly maintain the desired constant dynamic pressure for the entire leg. Propulsion is limited

to the air-breathing system. As for leg 1, this results in the elimination of the switch points in the trajectory leg analysis. When applying the optimization algorithm  $\Lambda, g, M$  and the variations  $\delta t_s$  disappear. Also the following simplified equations result:

$$B = (I_{\Psi_2 \Psi_2})^{-1} \quad (\text{Eq. V.67})$$

$$\delta u = -U \left( f_u^T \Lambda B C_{\Psi_2} \Psi_2 + C_{J_2} \left( H_u^T - f_u^T \Lambda B I_{\Psi_2 J_2} \right) \right) \quad (\text{Eq. V.68})$$

$$C_{J_2} = - \frac{dJ_s + I_{\Psi_2 J_2}^T B C_{\Psi_2} \Psi_2}{I_{J_2 J_2} - I_{\Psi_2 J_2}^T B I_{\Psi_2 J_2}} \quad (\text{Eq. V.69})$$

**Leg 3 - Final Ascent to orbit:** This segment is solved third, using the terminal conditions from leg 2 as initial conditions. The target circular orbit velocity is used as the terminal time cutoff condition with the orbit altitude and radial velocity also constrained at terminal time. The inequality constraint on dynamic pressure is still enforced as required. Propulsion can include the air-breathing system and the rocket. The mathematical form of the problem is the same as discussed above for the entire trajectory solution, but using  $\Psi_3$  as the terminal constraint function and  $J_3$  as the cost.

#### V.B.3.b. Simpler Seven State Vehicle Dynamics Model

The simpler seven state vehicle dynamics can be written as follows in state equation form consistent with the frame of reference given in figure V.4:

$$f = \begin{pmatrix} -x_6 \\ \frac{x_5}{x_1 \cos x_3} \\ \frac{x_4}{x_1} \\ \frac{x_4 x_6 - (x_5)^2 \tan x_3}{x_1} - 2\omega_e x_5 \sin x_3 - x_1 (\omega_e)^2 \sin x_3 \cos x_3 + \frac{F_1}{x_7} \\ x_5 \frac{(x_6 + x_4 \tan x_3)}{x_1} + 2\omega_e (x_4 \sin x_3 + x_6 \cos x_3) + \frac{F_2}{x_7} \\ \frac{-((x_4)^2 + (x_5)^2)}{x_1} - 2\omega_e x_5 \cos x_3 - x_1 (\omega_e \cos x_3)^2 + \frac{F_3}{x_7} \\ \frac{1}{g_0} \left( \frac{QC_T}{I_{sp_a}} + f_R \right) \end{pmatrix} \quad (\text{Eq. V.70})$$

where:

$$x = \begin{pmatrix} r \\ v \\ \mu \\ v_1 \\ v_2 \\ v_3 \\ m \end{pmatrix} \quad (\text{Eq. V.71})$$

and where  $f_R$  has zero value for ascent legs 1 and 2. For the orbit insertion leg 3:

$$f_R = \frac{T_R \Phi_R}{I_{SPR}} \quad (\text{Eq. V.72})$$

Using the zero bank angle assumption, the following force equations in the vehicle LVLH frame result assuming an arc tangent definition over the range from -90 deg to +90 deg:

$$F = \begin{pmatrix} F_1 \\ F_2 \\ F_3 \end{pmatrix} = \begin{pmatrix} \text{sign}(v_1) \cos \psi (F_T \cos \gamma + F_N \sin \gamma) \\ \text{sign}(v_1) \sin \psi (F_T \cos \gamma + F_N \sin \gamma) \\ -F_T \sin \gamma + F_N \cos \gamma + F_g \end{pmatrix} \quad (\text{Eq. V.73})$$

where  $\text{sign}(v_1)$  has a value of 1 for  $v_1 \geq 0$ , and a value of -1 for  $v_1 < 0$ . Also note that only two force components remain in the body frame (no side force):

$$F_T = T \cos \alpha - D \quad (\text{Eq. V.74})$$

$$F_N = -(T \sin \alpha + L) \quad (\text{Eq. V.75})$$

Also, the following equations are used to relate flight angles to states:

$$\gamma = \tan^{-1} \left( \frac{-x_6}{\sqrt{(x_4)^2 + (x_5)^2}} \right) \quad (\text{Eq. V.76})$$

$$\psi = \tan^{-1} \left( \frac{x_5}{x_4} \right) \quad (\text{Eq. V.77})$$

The lift, drag, pitch moments, and engine thrust can be written in the following form involving coefficient functions specified in the example vehicle model data tables, utilizing the assumption that the elevons are used only to maintain a vehicle pitch trim condition. With moment balance, pitch rates must be assumed zero, eliminating the need for a moment coefficient due to pitch rates  $C_{m_q}$ . This further simplifies the dynamics model considerably, but introduces some mathematical inconsistency since a time variant angle of attack actually implies vehicle rotation rates:

$$L = C_L Q S_{ref} \quad (\text{Eq. V.78})$$

$$D = C_D Q S_{ref} \quad (\text{Eq. V.79})$$

$$M_q = 0 = C_m Q c S_{ref} - x_{CG} (D \sin \alpha + L \cos \alpha) \quad (\text{Eq. V.80})$$

$$T = Q C_T + \Phi_R T_R \quad (\text{Eq. V.81})$$

where:

$$C_L = C_{L_a} + C_{L_e} \quad (\text{Eq. V.82})$$

$$C_D = C_{D_a} + C_{D_e} \quad (\text{Eq. V.83})$$

$$C_m = C_{m_a} + C_{m_e} \quad (\text{Eq. V.84})$$

$$v_f = \sqrt{(u_1)^2 + (u_2)^2 + (u_3)^2} \quad (\text{Eq. V.85})$$

When using the example vehicle model database,  $M_f$ ,  $\alpha$ , and  $\delta_e$  are required, where  $v_f$  is used along with  $r$  in an atmosphere model to compute  $M_f$ . An implicit equation to determine  $\delta_e$  is derived from the moment balance relationship. Only the elevon drag, lift, and moment terms are dependent on  $\delta_e$ . Other terms, and the other degrees of freedom for the elevon dependent terms, are determined by the currently stored history of  $\alpha$ ,  $m$ , and  $M_f$ . Using the following equation (and the associated relations defining the equation coefficients), a value of  $\delta_e$  can be found iteratively.

$$C_{m_e} - K_1 C_{D_e} - K_2 C_{L_e} = K_3 \quad (\text{Eq. V.86})$$

where:

$$K_1 = \frac{x_{CG}}{c} \sin \alpha \quad (\text{Eq. V.87})$$

$$K_2 = \frac{x_{CG}}{c} \cos \alpha \quad (\text{Eq. V.88})$$

$$K_3 = \frac{x_{CG}}{c} (C_{D_a} \sin \alpha + C_{L_a} \cos \alpha) - C_{m_a} \quad (\text{Eq. V.89})$$

The gravity force acting on the vehicle can be written in the following form:

$$F_g = \frac{\mu_e x_7}{(x_1)^2} \quad (\text{Eq. V.90})$$

Finally, the following equations are used to transform the throttle controls on the propulsion to unbounded control vector components. They are based on the assumption that  $\Phi_\alpha \geq 0$  and  $0 < \Phi_R \leq 1$ . Also,  $\Phi_R$  only applies to leg 3 of the ascent trajectory.

$$\Phi_u = (u_a)^2 \quad (\text{Eq. V.91})$$

$$\Phi_R = \frac{1}{1 + (u_R)^2} \quad (\text{Eq. V.92})$$

### V.B.3.c. The Boundary Conditions

Boundary conditions are set for each of the trajectory legs based on the criteria discussed above. Velocities are used to identify the end of each trajectory leg  $\Omega_i$ . Relative air speeds are used for legs 1 and 2, and Earth centered inertial velocity is used for leg 3 (assuming no radial velocity term). Other terminal time conditions ( $\Psi_i$ ) apply to trajectories 1 and 3. For leg 1, the dynamic pressure limit to be applied on leg 2 must be matched, and have zero slope. For leg 3, the additional constraint conditions assure a circular orbit at the desired altitude. If a Hohmann type transfer is required on leg 3 (two separate burns with the later being a circularization impulse), then the optimization solution will accomplish that result by forcing the rocket throttle setting to zero for a coast interval.

$$\Omega_1 = (v_1)^2 + (v_2)^2 + (v_3)^2 - (v_{targ_1})^2 \quad (\text{Eq. V.93})$$

$$\Omega_2 = (v_1)^2 + (v_2)^2 + (v_3)^2 - (v_{targ_2})^2 \quad (\text{Eq. V.94})$$

$$\Omega_3 = (v_1)^2 + (v_2 + r\omega_e \cos\mu)^2 - (v_{targ_3})^2 \quad (\text{Eq. V.95})$$

$$\Psi_1 = \begin{pmatrix} Q - Q_D \\ \frac{dQ}{dt} \end{pmatrix} \quad (\text{Eq. V.96})$$

$$\Psi_2 = \begin{pmatrix} Q - Q_D \\ \frac{dQ}{dt} \end{pmatrix} \quad (\text{Eq. V.97})$$

$$\Psi_3 = \begin{pmatrix} r(\tau_3) - r_{targ_3} \\ v_3(\tau_3) \end{pmatrix} \quad (\text{Eq. V.98})$$

### V.B.3.d. Cost Function Specification

Of primary importance in applying an optimization algorithm to a trajectory analysis problem is specification of the terms of cost indices. The basic function forms are:

$$J_1(\tau_1) = \phi_1(x(\tau_1)) + \int_0^{\tau_1} L_1(x(t), u(t)) dt \quad (\text{Eq. V.99})$$

$$J_2(\tau_2) = \phi_2(x(\tau_2)) + \int_{\tau_1}^{\tau_2} L_2(x(t), u(t)) dt \quad (\text{Eq. V.100})$$

$$J_3(\tau_3) = \phi_3(x(\tau_3)) + \int_{\tau_2}^{\tau_3} L_3(x(t), u(t)) dt \quad (\text{Eq. V.101})$$

where:

$$u = \begin{pmatrix} u_1 \\ u_2 \\ u_3 \end{pmatrix} = \begin{pmatrix} u_a \\ u_R \\ \alpha \end{pmatrix} \quad (\text{Eq. V.102})$$

Note that  $u_2$  is only used in leg 3 of the ascent trajectory.

For the current example, the cost terms used are as follows:

$$\phi_1 = m_0 - m(\tau_1) \quad (\text{Eq. V.103})$$

$$\phi_2 = m(\tau_1) - m(\tau_2) \quad (\text{Eq. V.104})$$

$$\phi_3 = m(\tau_2) - m(\tau_3) \quad (\text{Eq. V.105})$$

Set:

$$I_{.1} = K_{Q_1} (Q - Q_D)^2 u_0 [Q - Q_D] \quad (\text{Eq. V.106})$$

For subsequent flight segments:

$$I_{.2} = K_{Q_2} (Q - Q_D)^2 \quad (\text{Eq. V.107})$$

$$I_{.3} = K_{Q_3} (Q - Q_D)^2 u_0 [Q - Q_D] \quad (\text{Eq. V.108})$$

### V.B.3.e. Relevant Partial Derivatives

**Boundary Condition Derivatives:** The following equations are the required derivatives of the boundary condition functions in Eqs. V.93-98 used in Eqs. V.43,46:

$$\Omega_{1_x} = (0 \quad 0 \quad 0 \quad 2v_1 \quad 2v_2 \quad 2v_3 \quad 0) \quad (\text{Eq. V.109})$$

$$\Omega_{2_x} = (0 \quad 0 \quad 0 \quad 2v_1 \quad 2v_2 \quad 2v_3 \quad 0) \quad (\text{Eq. V.110})$$

$$\Omega_{3_x}^T = \begin{pmatrix} 2\omega_e \cos \mu (v_2 + r\omega_e \cos \mu) \\ 0 \\ -2r\omega_e \sin \mu (v_2 + r\omega_e \cos \mu) \\ 2v_1 \\ 2(v_2 + r\omega_e \cos \mu) \\ 0 \\ 0 \end{pmatrix} \quad (\text{Eq. V.111})$$

$$\Psi_{1_x} = \begin{pmatrix} \frac{\partial Q(\tau_1)}{\partial x} \\ \frac{\partial \dot{Q}(\tau_1)}{\partial x} \end{pmatrix} \quad (\text{Eq. V.112})$$

$$\Psi_{2_x} = \begin{pmatrix} \frac{\partial Q(\tau_1)}{\partial x} \\ \frac{\partial \dot{Q}(\tau_1)}{\partial x} \end{pmatrix} \quad (\text{Eq. V.113})$$

$$\Psi_{3_x} = \begin{pmatrix} 1 & 0 & 0 & 0 & 0 & 0 & 0 \\ 0 & 0 & 0 & 0 & 0 & 1 & 0 \end{pmatrix} \quad (\text{Eq. V.114})$$

where:

$$\frac{\partial Q}{\partial x} = \begin{pmatrix} \frac{d\rho(v_f)^2}{dr} & 0 & 0 & \rho v_1 & \rho v_2 & \rho v_3 & 0 \end{pmatrix} \quad (\text{Eq. V.115})$$

$$\frac{dQ}{dt} = \frac{f_1(v_f)^2}{2} \frac{d\rho}{dr} + \rho(x_4 f_4 + x_5 f_5 + x_6 f_6) \quad (\text{Eq. V.116})$$

$$\left( \frac{\partial \left( \frac{dQ}{dt} \right)}{\partial x} \right)^T = \begin{pmatrix} -x_6 \frac{v_f^2}{2} \frac{d^2 \rho}{dr^2} + (x_4 f_4 + x_5 f_5 + x_6 f_6) \frac{d\rho}{dr} \\ 0 \\ 0 \\ -x_4 x_6 \frac{d\rho}{dr} + \rho f_4 \\ -x_5 x_6 \frac{d\rho}{dr} + \rho f_5 \\ -\frac{3}{2} x_6^2 \frac{d\rho}{dr} + \rho f_6 \\ 0 \end{pmatrix} \quad (\text{Eq. V.117})$$

$$+ \rho \left( x_4 \frac{\partial f_4}{\partial x} + x_5 \frac{\partial f_5}{\partial x} + x_6 \frac{\partial f_6}{\partial x} \right)^T$$

where the last term of the previous equation was written in vector form for notational simplicity. Also, note that since  $\rho$  is assumed to be only a function of  $r$ ,  $\frac{\partial \rho}{\partial r} = \frac{d\rho}{dr}$ .

**Cost Function Derivatives:** The following equations are the derivatives of the cost functions  $J_i$  defined in Eqs. V.103-108 that are required in Eqs. V.42,43:

$$\phi_{1,x} = (0 \quad 0 \quad 0 \quad 0 \quad 0 \quad 0 \quad -1) \quad (\text{Eq. V.118})$$

$$\phi_{2,x} = (0 \quad 0 \quad 0 \quad 0 \quad 0 \quad 0 \quad -1) \quad (\text{Eq. V.119})$$

$$\phi_{3,x} = (0 \quad 0 \quad 0 \quad 0 \quad 0 \quad 0 \quad -1) \quad (\text{Eq. V.120})$$

For the first segment,  $L_{1,x} = 0$  if  $Q < Q_D$ , and when  $Q \geq Q_D$ :

$$L_{1,x} = 2K_{Q1}(Q - Q_D) \frac{\partial Q}{\partial x} \quad (\text{Eq. V.121})$$

For the second segment:

$$L_{2,x} = 2K_{Q2}(Q - Q_D) \frac{\partial Q}{\partial x} \quad (\text{Eq. V.122})$$

For the third segment, as for the first,  $L_{3,x} = 0$  if  $Q < Q_D$ , and when  $Q \geq Q_D$ :

$$L_{3,x} = 2K_{Q3}(Q - Q_D) \frac{\partial Q}{\partial x} \quad (\text{Eq. V.123})$$

The Hamiltonian derivative with respect to controls can be expressed by the relationship  $\Pi_u = L_u + \lambda^T f_u$  which requires a partial of the integral cost function with respect to the control vector. For the functions of  $I$  selected in the example here,  $L_u$  has zero value.

**State Equation Derivatives:** The partials of the seven state vehicle dynamics equation  $f$  given in Eq. V.70 with respect to states is required for use in Eqs. V.42,45. Because of the complexity of its specification, details are given in Appendix B.1.

The partials of the seven state vehicle dynamics equation  $f$  given in Eq. V.70 with respect to controls is required for use in Eqs. V.49,50,54. Because of the complexity of its specification, details are given in Appendix B.2.

#### V.B.3.f. Calculation of Elevon Trim Deflection

**Calculation Method for Elevon Trim Deflection:** A general numerical method has been devised to calculate an aerosurface deflection that trims a vehicle's moments resulting from aerodynamic loading. In the example application, the method has been adapted to calculate elevon trim deflections. The vehicle longitudinal moment balance equation is given by:

$$QS_{ref}c(C_{m_\alpha} + C_{m_\epsilon}) = QS_{ref}x_{cg}((C_{D_\alpha} + C_{D_\epsilon})\sin(\alpha) + (C_{L_\alpha} + C_{L_\epsilon})\cos(\alpha)) \quad (\text{Eq. V.124})$$

where the left side is the intrinsic aerodynamic moment, and the right side is the added moment caused by center of gravity offset. If  $x_{CG}$  is zero, the trim deflection is found by obtaining the value of  $\delta_\epsilon$  such that:

$$C_{m_\epsilon}(\delta_\epsilon) = -C_{m_\alpha} \quad (\text{Eq. V.125})$$

When  $N_{CC}$  is nonzero, as is generally the case, the flap deflection enters the balance equation through  $C_{L_e}$  and  $C_{D_e}$  in addition to  $C_{m_e}$ . To find the value of  $\delta_e$  that satisfies the above equation we rewrite the equation in the form:

$$f(\delta_e) = C_{m_e} - K_1 C_{D_e} - K_2 C_{L_e} - K_3 = 0 \quad (\text{Eq. V.126})$$

where the  $K_i$  coefficients are independent of  $\delta_e$ . We then apply a Newtonian iteration that finds a zero of the above expression for the solution value of  $\delta_e$ . The iteration is of the form:

$$\delta_e(i) = \delta_e(i-1) - f(\delta_e(i-1)) / df(\delta_e(i-1)) \quad (\text{Eq. V.127})$$

with:

$$f(\delta_e(i)) = C_{m_e}(i) - C_{D_e}(i)K_1 - C_{L_e}(i)K_2 - K_3 \quad (\text{Eq. V.128})$$

$$df(\delta_e(i)) = (f(\delta_e(i)) - f(\delta_e(i-1))) / (\delta_e(i) - \delta_e(i-1)) \quad (\text{Eq. V.129})$$

To speed convergence, the previous solution for  $\delta_e$  is used as the starting point for successive time steps, and the resulting convergence typically requires just a few iterations. To stay within the 20 degree limit on angle of attack, the starting perturbation values of  $\delta_e$  that are used to establish the derivative  $df(\delta_e)$  are set one degree towards zero from the previous trim position. For example, if the previous trim was -16 degrees, the perturbation point is chosen as -15 degrees.

**Calculation Method for Elevon Deflection Partial Derivatives:** Close examination of the elevon deflection partial equation  $\frac{\partial \delta_e}{\partial x}$  reveals that on the right hand side, the partials  $\frac{\partial D}{\partial x}$  and  $\frac{\partial L}{\partial x}$  are themselves functions of  $\frac{\partial \delta_e}{\partial x}$ . To solve for  $\frac{\partial \delta_e}{\partial x}$  we write:

$$\frac{\partial \delta_e}{\partial x_i} = C0_i + C1 \frac{\partial D}{\partial x_i} + C2 \frac{\partial L}{\partial x_i} \quad (\text{Eq. V.130})$$

where  $i$  is an index over the states, and the coefficients  $C$  are given by:

$$C0_i = \left[ - \left( \frac{\partial C_{m_e}}{\partial M_f} + \frac{\partial C_{m_a}}{\partial M_f} \right) \frac{\partial M_f}{\partial x_i} + \frac{\partial}{\partial x_i} \left( \frac{x_{cg}}{QCS_{ref}} \right) (D \sin \alpha + L \cos \alpha) \right] \left( \frac{\partial C_{m_e}}{\partial \delta_e} \right)^{-1} \quad (\text{Eq. V.131})$$

$$C1 = \left( \frac{\partial C_{m_e}}{\partial \delta_e} \right)^{-1} \left( \frac{x_{cg}}{QCS_{ref}} \right) \sin \alpha \quad (\text{Eq. V.132})$$

$$C2 = \left( \frac{\partial C_{m_e}}{\partial \delta_e} \right)^{-1} \left( \frac{x_{cg}}{QCS_{ref}} \right) \cos \alpha \quad (\text{Eq. V.133})$$

Next we expand  $\frac{\partial L}{\partial x_i}$  and  $\frac{\partial D}{\partial x_i}$  in a similar manner, namely:

$$\frac{\partial D}{\partial x_i} = A1_i + B1 \frac{\partial \delta_e}{\partial x_i} \quad (\text{Eq. V.134})$$

$$\frac{\partial L}{\partial x_i} = A2_i + B2 \frac{\partial \delta_e}{\partial x_i} \quad (\text{Eq. V.135})$$

where:

$$A1_i = QS_{ref} \left( \frac{\partial C_{D\alpha}}{\partial M_f} \frac{\partial M_f}{\partial x_i} + \frac{\partial C_{D_e}}{\partial M_f} \frac{\partial M_f}{\partial x_i} \right) + C_{D_e} S_{ref} \frac{\partial Q}{\partial x_i} \quad (\text{Eq. V.136})$$

$$A2_i = QS_{ref} \left( \frac{\partial C_{L\alpha}}{\partial M_f} \frac{\partial M_f}{\partial x_i} + \frac{\partial C_{L_e}}{\partial M_f} \frac{\partial M_f}{\partial x_i} \right) + C_{L_e} S_{ref} \frac{\partial Q}{\partial x_i} \quad (\text{Eq. V.137})$$

$$B1 = QS_{ref} \frac{\partial C_{D_e}}{\partial \delta_e} \quad (\text{Eq. V.138})$$

$$B2 = QS_{ref} \frac{\partial C_{L_e}}{\partial \delta_e} \quad (\text{Eq. V.139})$$

Substituting the expansions for  $\frac{\partial D}{\partial x_i}$  and  $\frac{\partial L}{\partial x_i}$  into the expansion for  $\frac{\partial \delta_e}{\partial x}$  gives the equation:

$$\frac{\partial \delta_e}{\partial x_i} = C0_i + C1 A1_i + C1 B1 \frac{\partial \delta_e}{\partial x_i} + C2 A2_i + C2 B2 \frac{\partial \delta_e}{\partial x_i} \quad (\text{Eq. V.140})$$

which has the desired solution:

$$\frac{\partial \delta_e}{\partial x_i} = \frac{C0_i + C1 A1_i + C2 A2_i}{1 - (C1 B1 + C2 B2)} \quad (\text{Eq. V.141})$$

### V.B.3.g. Initial Conditions

The initial conditions assumed for the example vehicle in the analysis demonstration are set immediately after horizontal takeoff:

$$x_0 = \begin{pmatrix} r_0 \\ v_0 \\ \mu_0 \\ v_{1_0} \\ v_{2_0} \\ v_{3_0} \\ m_0 \end{pmatrix} = \begin{pmatrix} 20,909,723 \text{ ft} \\ 280 \text{ deg} \\ 28.5225 \text{ deg} \\ 444.889 \text{ ft/s} \\ -37.5695 \text{ ft/s} \\ -6.46676 \text{ ft/s} \\ 299,000 \text{ lb} \end{pmatrix} \quad (\text{Eq. V.142})$$

## **V.C. Analysis Demonstration Results**

### **V.C.1. Cases Run**

An analysis methodology demonstration case was run using the example vehicle model. The case was run from the moment of horizontal takeoff to 20,000 ft/s relative air speed. The trajectory optimization objective was to achieve a near minimum propellant consumption condition while applying a dynamic pressure constraint of 1000 psf. The presented results are an aggregate of computation on two flight legs: Takeoff to Mach 2 (leg 1); Mach 2 to 20,000 ft/sec (leg 2). The second leg was constructed from two shorter segments which were merged at 10,000 ft/s.

Originally, the leg 1 results were run first, using a preliminary version of the example vehicle model database, and the terminal conditions for that trajectory segment were used as initial conditions for leg 2 analysis. After starting the leg 2 computations, the final version of the example vehicle model was prepared which amended the sign of the center of mass to moment reference center distance. Based on the model update, the leg 2 analysis was restarted, and run to completion. Subsequently an effort was also made, using the amended data set, to regenerate leg 1 results. To get a reasonable new interface boundary condition between the two trajectory legs, matches were mathematically forced on the dynamic pressure, its time derivative, and the vehicle mass at the interface point. (The dynamic pressure and derivative matching conditions had the effect of forcing an altitude match given the combination of the atmospheric model used and the fixed trajectory segment cutoff velocity.) The effects of these matching conditions on trajectory results are discussed in section V.C.2.d.

### **V.C.2. Observations from Demonstration Case Results**

Many significant vehicle dynamics and control characteristics are apparent from inspection of the plotted data. These results are indicative of the benefits of the generic integrated trajectory/control analysis methodology. There are features that provide evidence of flight characteristics that should be treated explicitly rather than by being buried in data tables (particularly discovered propulsive discontinuities). Some results provide information essential to closed-loop G&C system design requirements development. Also, vehicle performance sensitivities to modelling uncertainty have become apparent.

#### **V.C.2.a. Observations from Specific Variable Plots**

##### ***Angle of Attack***

Figures V-6,7 plot the computed angle of attack vs Mach number and time, respectively. The history shows the high angle of attack at takeoff necessary to get sufficient lift. It reaches a local minimum in the transonic region allowing the vehicle to use more of available engine thrust to accelerate through the high drag phase, rather than fighting lift related drag and gravity. Generally thereafter a gradual increase occurs to Mach 6. Above Mach 8 the angle of attack declines smoothly with Mach number as a result of orbital mechanics (the lift requirement declines as velocity approaches orbital speed). Some of the additional detail in the plot structure is discussed below.

##### ***Equivalence Ratio***

Figures V-8,9 plot the engine throttle equivalence ratio vs Mach number and time, respectively. The history shows a local peak in the transonic region to get more thrust in the high drag flight phase. Another local peak occurs near Mach 6 where initial scramjet use is likely, and neither a ramjet nor a scramjet is capable of particularly good performance. Above Mach 8 the equivalence ratio undergoes very little variation.

### *Elevon Deflection*

Figures V-10,11 plot elevon deflection vs Mach number and time, respectively. The history shows a maximum value near Mach 2 and reflects a change in vehicle trim as a result of combined changes in aerodynamic loading and center of mass shift due to fuel consumption. Above Mach 8 elevon deflections eventually diminish as the angle of attack declines (figures V-6,7), offsetting the effects of center of mass shifts due to fuel consumption.

### *Dynamic Pressure*

Figures V-12,13 plot the vehicle dynamic pressure and the dynamic pressure time derivative respectively vs Mach number. The profile shows a capture of the 1000 psf constraint at about Mach 2. Most of the leg 1 flight phase is unaffected by the dynamic pressure constraint until very near Mach 2. By contrast, the leg 2 results reflect a near constant dynamic pressure flight condition objective. Note that the leg 2 results were still very slightly sub-optimal when computation was stopped, accounting for the  $\pm 2-4$  psf oscillations in the dynamic pressure around the 1000 psf constraint.

### *Flight Path Angle*

Figures V-14,15 plot the vehicle flight path angle and flight path angle time derivative respectively, vs Mach number. The flight path is very steep in the initial flight phases to gain altitude quickly, thereby assuring that the vehicle remains within the dynamic pressure constraint as it accelerates at higher Mach. As the vehicle accelerates toward orbital velocity, the angle tapers off to near zero.

### *Vehicle Acceleration*

Figures V-16,17 plot the vehicle ground (also air) relative acceleration and inertial relative acceleration respectively vs Mach number. Both plots indicate that maximum acceleration occurs between Mach 2 and 6. Above Mach 8 the vehicle acceleration initially drops due to declining engine performance, but eventually starts rising again due to declining vehicle mass. While the inertial acceleration is much lower than the ground relative acceleration at low Mach (due to ground motion), both become almost identical at high Mach.

### *Vehicle Mass Behavior*

Figures V-18,19 plot the vehicle mass and mass flow respectively vs Mach number. The overall mass trend is a nearly linear decline with Mach number (as opposed to an exponential decay typical of a rocket). However, above Mach 8 the fuel mass flow magnitude goes through an oscillation that reflects the nonlinear propulsion system (specific impulse) model and associated curve fit.

### *Altitude History*

Figure V-20 plots the vehicle altitude vs Mach number which shows the square root function-like shape characteristic of HSVs going to orbit. As the Mach number increases, less altitude rise is required to maintain the dynamic pressure constraint for a given velocity change.

### *Mach History*

Figure V-21 plots the vehicle Mach number vs time. The acceleration drops near 400 seconds at Mach 8 leading to a lower Mach increase slope for the remainder of the flight.

## V.C.2.b. Observed Acceleration and/or Mass Flow Discontinuities

A number of discontinuities are observed in vehicle acceleration characteristics that probably reflect discrete transitions in air-breathing propulsive modes. The acceleration plots (figures V-16,17) are consistent with the use of a multi-mode propulsion system, possibly a turbojet to near Mach 3.5, followed by a ramjet to near Mach 6, with a scramjet for the remainder of air-breathing flight. These characteristics were not explicitly identified before performing the numerical analysis. The strong nonlinearities that they induce caused a large increase in computational effort to achieve near-minimum-fuel trajectory convergence. If the propulsive phases

were treated explicitly in the analysis, there would have been less computational burden along with the added benefit of being able to assess the optimal timing of the propulsive phasing. Also, the separation of the specific impulse and thrust coefficient data in the example vehicle model makes possible inadvertent introduction of model inconsistencies by incorrect specification of individual data points. Some model inconsistencies do seem to have been identified by the numerical analysis of the trajectory. These unspecified discontinuities and modelling inconsistencies are evidence of a situation where there should be close coordination between developers of propulsion system models and G&C system analysts. Specific examples follow:

- At Mach 3.5, there is a steep change in vehicle acceleration (see figures V-16,17) that correlates with a sudden change in fuel mass flow rate. Inspection of the example vehicle model propulsion data shows the cause of the odd behavior seen in the plots is a sudden change in modelled specific impulse behavior at Mach 3.5 (data is supplied at Mach 3, 3.5, and 4). This may reflect a change from turbojet to ramjet operations.
- A steady rise in the equivalence ratio begins at about Mach 5.45 (see figures V-8,9). The start of the equivalence ratio rise correlates with propulsion data that suddenly results in higher specific impulse values at equivalence ratios between 1 and 2.5 in the flight range between Mach 4 and 6. This may correlate with a transition from ramjet mode to a scramjet mode as Mach 6 is approached.
- There are some significant data variations between Mach 7 and 8. Below Mach 7.5, a sharp local maximum occurs in the angle of attack (figures V-6,7), a rapid drop occurs in the equivalence ratio (figures V-8,9), and a local minimum occurs in the mass flow rate (figure V-19). At Mach 8.0, there is a nearly discrete change in vehicle acceleration (figures V-16,17) that correlates with a sudden change in fuel mass flow rate (figure V-19) and a nearly discrete change in the desired equivalence ratio (figures V-8,9). Inspection of the example vehicle propulsion model shows major changes between Mach 6 and 8 in the character of both the thrust coefficient and specific impulse tabulated data, somewhat akin to the behavior observed at Mach 3.5. This probably reflects some propulsion model fidelity problems and possible inconsistencies in the specific impulse and thrust coefficient data trends. While spline routines have been used to smooth out corners in the tabulated vehicle model data, the routines were not intended to effectively handle nearly discrete, multidimensional changes in functional characteristics.
- The most significant remaining variations from the 1000 psf dynamic pressure constraint (figures V-12,13) are at Mach 3.5 and near Mach 6. These points correspond exactly with propulsion model data points and behavioral changes intrinsic in the tabulated example vehicle model data. Transients in the elevon trim angle (figures V-10,11), equivalence ratio (figures V-8,9), angle of attack (figures V-6,7), acceleration (figures V-16,17), and engine mass flow (figure V-19) occur at the same Mach numbers. This is more evidence of unspecified discrete changes in the propulsion model. The ground relative acceleration plot shows classic turbojet performance below Mach 3.5, with a sudden jump in acceleration (figures V-16,17) to a ramjet like profile. Above Mach 5.5, the acceleration profile looks more like a scramjet, peaking just beyond Mach 6.

#### V.C.2.c. Analysis Observations Affecting G&C Design

The power of the integrated trajectory/control analysis methodology to identify vehicle flight characteristics with critical impact on the desired closed-loop G&C system design is evident in some of the demonstration case data. Examples include large elevon trim deflections which indicate important limits in available effector control moments for broad flight regimes, and episodic tendencies to seek rapid angle of attack variations which are evidence of a requirement for a highly responsive controller. These two effects actually provide conflicting G&C development guidelines, creating narrow constraints on an acceptable design. Some specific observations based on the plotted data follow.

- The elevon deflection angle history (figures V-10,11) reflects changing vehicle trim characteristics due to Mach number dependent aerodynamic effects and vehicle center of mass changes that result from fuel consumption. The direction of vehicle trim moments reverses at about Mach 4. As the Mach number increases beyond Mach 4, the increasingly negative trim angles induce added drag that must be overcome by propulsion settings. Much of the net vehicle drag losses at high Mach is due to the elevon trim deflection. Between Mach 10 and 15, the elevon trim angle exceeds 16 deg (peaking at 17 deg) leaving less than 4 deg authority for active control.
- A steep perturbation in the angle of attack (figures V-6,7) occurs at about Mach 5.24, and reverses at about Mach 5.45. It seems to correlate with some large, highly nonlinear changes in the engine model specific impulse data that occur between Mach 4 and 6 for the equivalence ratio range (figures V-8,9) applicable to the profile.
- The gamma dot plot (figure V-15) has steep variations between Mach 5 and 6 in direct correlation with the angle of attack variations (figures V-6,7) noted above. These variations have similar but smaller effect on vehicle acceleration (figures V-16,17) and mass flow (figure V-19).
- A sharp local minimum occurs in the angle of attack (figures 6,7) at Mach 6.35. It is also seen in the flight path angle time derivative data (figure V-15). The physical (model based) origins of this effect are not yet fully understood.

#### V.C.2.d. The Mach 2 Transients

As was noted above, an amendment to the vehicle model as its final version was prepared resulted in the assessment of the takeoff to Mach 2 leg and the Mach 2 to 20,000 ft/sec leg to be evaluated in reverse of the usual order for trajectory segment generation. As a result, and in spite of enforcement of several interface matching conditions, not all the state function and control histories were continuous across the interface. This behavior is evident in transients in some plots at Mach 2 that are identified below. The transients are confined to state and/or control functions not forced to satisfy matching conditions at the trajectory leg interface. If the very brief Mach 2 transients are ignored, the plots still give a good indication of the constrained near-fuel-optimal trajectory and control flight characteristics for the example vehicle. The specific Mach 2 data problems seen in the figures are as follows:

- There is a sharp angle of attack drop and recovery (figures V-6,7).
- There is a sharp equivalence ratio drop and recovery (figures V-8,9).
- There is a very brief drop and recovery in the elevon deflection angle (figures V-10,11).
- The flight path angle shows a negative spike (figure V-14). With a full state match at the trajectory segment interface, this state function transient would not be physically possible.
- The flight path angle time derivative (figure V-15) shows a spike corresponding the path angle transient.
- There are sharp drops and recoveries of the vehicle acceleration (figures V-16,17).
- There is a negative then positive change in the propellant mass flow rate (figure V-19). Results processed before the model amendment suggest that the positive direction transient is real. (It may be the result of a propulsive mode change.) However, the spike in the negative direction is probably due to the trajectory segment interface matching problems.

#### V.C.2.e. Performance Sensitivity to Modelling Uncertainty

Significant differences in the effective dynamics of specific HSV models can result from alternative methods of computing data table based performance. Analysis of the example vehicle model propulsion system data indicated that steep changes in response occur near specific Mach numbers. These changes can induce significant differences in engine performance

estimates in the vicinity of those data points when different interpolation schemes are used. Trajectories computed with spline fitted vehicle model representations were compared with trajectories computed with linearly interpolated models. One comparison showed nearly a 5,000 lb variation in propellant used between Mach 2 and Mach 3.5 as a result of the dissimilar interpolation strategies.

The differences in vehicle performance estimates due to interpolation methodology have been shown to have the potential of drastically affecting the predicted vehicle payload to orbit. This indicates that the integrated trajectory/control analysis methodology can identify vehicle model fidelity inadequacies in sensitive flight regimes. It also is evidence that the methodology can determine when the specific vehicle designs and/or engine moding strategies result in unacceptable consequences as a result of modelling uncertainty.

## **V.D. Progress Toward AIPS Requirements Specification**

The HSV integrated trajectory and control analysis methodology developed under this task provides information that is essential to development of closed-loop G&C system design requirements. The demonstration winged-cone vehicle results have provided enough trajectory management strategy and performance sensitivity information (reviewed in the previous subsection) to immediately support development of a strawman G&C requirements specification. A complete G&C specification would permit characterization of a closed-loop G&C algorithm, including input/output processing rates and redundancy requirements. Completion of all these steps, to accommodate assessment of expected overall G&C related throughput and computational processing rates, is a mandatory part of the AIPS requirements specification [15].

## VI. Conclusions

A generic methodology to permit integrated trajectory/control analysis, including the effects of physically derived constraints, has been successfully adapted for assessment of single-stage-to-orbit hypersonic vehicles with multi-mode propulsion systems. Both an overall trajectory evaluation algorithm and a preliminary near-fuel-optimal trajectory development tool have been mathematically formulated and implemented for use in a work station computational environment. The methodology is capable of assessing the relative performance of alternative vehicles and/or subsystem technologies with respect to a single mathematically valid measure. To assure good numerical behavior of the analysis algorithms, a cubic spline based data smoothing routine was developed and included in the resulting tool to permit use of multidimensional tabulated vehicle models.

Hypersonic vehicle designs demand complex integration of the airframes and propulsion systems. As a result, there is an expectation that there will be a strong dependence between configuration details, the mission performance, and trajectory management and control strategies. To assure that an overall vehicle design would have a high probability of achieving mission objectives, it was thought to be essential to have a means to perform an early assessment of how specific vehicle designs and their guidance and control system characteristics would interact. Justification of this argument for the research demanded a specific demonstration of the generic analysis tool.

In support of the demonstration objective, two applicable vehicle dynamics models were derived including all relevant analytic partial derivatives. A nine state model incorporates all translational and longitudinal (pitch) dynamics and uses throttle and elevon controls. A somewhat simpler seven state model should help bootstrap to the use of the nine state model. The simpler model restricts treatment of longitudinal effects to the calculation of elevon deflections and the resulting incremental forces which maintain vehicle pitch trim. Angle of attack in the seven state model replaces elevon deflection in the nine state model as a control, which should permit more intuitive analysis to be applied.

A specific test case of the hypersonic vehicle integrated trajectory/control analysis methodology was defined, performed, and evaluated to demonstrate the power of the algorithm to derive information of critical importance to developers of guidance and control systems. The example vehicle model was based on an air-breathing accelerator, winged-cone vehicle database. Performance from horizontal takeoff to 20,000 ft/s relative airspeed on a polar orbit track was determined. A dynamic pressure constraint of 1000 psf was enforced. The following list summarizes some of the most significant conclusions:

- Three near-fuel-optimal flight segments were derived that satisfy the applied constraints. They successively cover flight from horizontal takeoff to Mach 2, Mach 2 to 10,000 ft/s, and 10,000 ft/s to 20,000 ft/s (where velocity is specified in terms of relative air speed). Segment boundary condition matching criteria were enforced to permit the merger of the individual segment results into a single full trajectory usable for overall optimization.
- The analysis methodology was able to identify previously unspecified discontinuities and propulsive phasing characteristics in the vehicle model. This information can be used to directly treat these strong model nonlinearities so as to reduce the computational burden in subsequent work.
- Flight regimes with strong performance sensitivities and inadequate model fidelity were highlighted. Failure to consider these effects can leave the vehicle design at great risk of unacceptable performance losses.
- Data to determine lower bound control effector response times and the remaining effector control authority after accounting for trim was generated.

- Drag losses due to required control effector activity was shown to be very high, demonstrating the importance of also including vehicle design characteristics in the integrated analysis.

When analysis results are considered collectively, they provide much of the information needed to define guidance and control system design requirements. The methodology supports treatment of important effects not considered in the demonstration case, such as accommodating thermal constraints and determining efficient propulsive mode phasing, which would provide even more realistic inputs to the design process.

## VII. References

- [1] Hattis, Philip D., "An Optimal Design Methodology for a Class of Air-Breathing Launch Vehicles", Doctor of Philosophy Thesis, Massachusetts Institute of Technology, June 1980.
- [2] Hattis, Philip D., "Optimal Air-Breathing Launch Vehicle Design", **Journal of Guidance and Control**, Vol. 4, No. 5, Sept. - Oct. 1981, pp. 543-550.
- [3] National Aerospace Plane Configuration and Trajectory Assessment, C. S. Draper Laboratory Fiscal Year 89 IR&D Technical Plan, Report CSDL-R-2087, Project Number 236.
- [4] Adams, Neil J. and Philip D. Hattis, "An Integrated Configuration and Control Analysis Technique for Hypersonic Vehicles", presented at the 1989 American Control Conference, Pittsburgh, Pennsylvania, June 21-23, 1989, pp. 1105-1110 of the proceedings.
- [5] Mattson, Erik A., "An Implicit Algorithm for Analysis of an Airframe-Integrated Scramjet Propulsion Cycle", Master of Science Thesis, Massachusetts Institute of Technology, May 1988.
- [6] Lewis, Mark J., "The Prediction of Inlet Flow Stratification and Its Influence on the Performance of Air-Breathing Hypersonic Propulsion Systems", Doctor of Science Thesis, Massachusetts Institute of Technology, June 1988.
- [7] Biasca, Rodger J., "Chemical Kinetics of Scramjet Propulsion", Master of Science Thesis, Massachusetts Institute of Technology, September 1988.
- [8] Ren, Chiang-Hwa, "A Computer Based Model for the Performance Analysis of a Scramjet Propulsion System", Master of Science Thesis, Massachusetts Institute of Technology, January 1989.
- [9] Paradiso, Joseph A., "A Highly Adaptable Method of Managing Jets and Aerosurfaces for Control of Aerospace Vehicles", presented at the 1989 AIAA Guidance and Control Conference, Boston, Massachusetts, August 14-16, 1989.
- [10] Hattis, Philip D., "Hypersonic Vehicle Air Data Collection: Assessing the Relationship Between the Sensor and Guidance and Control System Requirements", Proceedings of the 1990 American Control Conference, San Diego, California, May 23-25, 1990, pp. 1811-1818.
- [11] John D. Shaughnessy, S. Zane Pinckney, John D. McMinn, Christopher I. Cruz, and Marie-Louise Kelley, "Hypersonic Vehicle Simulation Model: Winged-Cone Configuration", NASA TM 102610, November 1990.
- [12] P.D. Hattis and R.K. Smolskis, "Optimal Trajectory Generation and Design Trades for Hypersonic Vehicles", proceedings of the 1989 American Control Conf., Pittsburgh, Penn., June 21-23, 1989, pp. 1125-1130.
- [13] Carl de Boor, **A Practical Guide to Splines**, Springer-Verlag, New York, 1978.
- [14] A.E. Bryson and W.F. Denham, "A Steepest-Ascent Method for Solving Optimum Programming Problems", **Journal of Applied Mechanics**, June 1962, pp. 247-257.
- [15] J.H. Lala, R.E. Harper, K.R. Jaskowiak, G. Rosch, L.S. Alger, A.L. Schor, "Advanced Information Processing System for Advanced Launch System: Avionics Architecture Synthesis", C.S. Draper Laboratory Report on Contract NAS1-18565, NASA CR-187554, 1991.

## Appendix A

### Nine State Function Partial Derivatives for the Example Model

#### A.1. Derivatives with Respect to States

The matrix  $f_{,}$  for the example application with nine states (derived from differentiating Eq. V.19) is too large to print as a single equation, so it is specified here on a column by column basis. The equations for  $f_{,}$  are simplified by the knowledge that the following derivatives have zero value:  $\frac{\partial Q}{\partial v}; \frac{\partial M_f}{\partial v}; \frac{\partial Q}{\partial \mu}; \frac{\partial M_f}{\partial \mu}; \frac{\partial Q}{\partial \theta}; \frac{\partial M_f}{\partial \theta}; \frac{\partial Q}{\partial q}; \frac{\partial M_f}{\partial q}; \frac{\partial Q}{\partial m}; \frac{\partial M_f}{\partial m}$ . Simplifications are also made by utilizing the knowledge that  $I_{yy}$  is a function only of  $m$ , and  $M_f$  is a function only of  $r$  and  $v_f$ .

$$\frac{\partial f}{\partial x_1} = \frac{\partial f}{\partial r} = \begin{pmatrix} 0 \\ -x_5 \\ \frac{-x_4}{(x_1)^2 \cos x_3} \\ \frac{-x_4}{(x_1)^2} \\ \frac{(x_5)^2 \tan x_3 - x_4 x_6}{(x_1)^2} - \frac{(\omega_s)^2 \sin 2x_3}{2} + \frac{1}{x_9} \frac{\partial F_1}{\partial x_1} \\ \frac{-x_5(x_6 + x_4 \tan x_3)}{(x_1)^2} + \frac{1}{x_9} \frac{\partial F_2}{\partial x_1} \\ \frac{(x_4)^2 + (x_5)^2}{(x_1)^2} - (\omega_s \cos x_3)^2 + \frac{1}{x_9} \frac{\partial F_3}{\partial x_1} \\ 0 \\ \frac{1}{I_{yy}} \frac{\partial M_q}{\partial x_1} \\ \frac{1}{g_0} \left( \left( \frac{C_T}{I_{sp_0}} + \frac{Q}{I_{sp_0}} \frac{\partial C_T}{\partial Q} - \frac{QC_T}{(I_{sp_0})^2} \frac{\partial I_{sp_0}}{\partial Q} \right) \frac{\partial Q}{\partial x_1} + \left( \frac{Q}{I_{sp_0}} \frac{\partial C_T}{\partial M_f} - \frac{QC_T}{(I_{sp_0})^2} \frac{\partial I_{sp_0}}{\partial M_f} \right) \frac{\partial M_f}{\partial x_1} \right) \end{pmatrix} \quad (\text{Eq. A.1})$$

$$\frac{\partial f}{\partial x_2} = \frac{\partial f}{\partial v} = \begin{pmatrix} 0 \\ 0 \\ 0 \\ \frac{1}{x_9} \frac{\partial F_1}{\partial x_2} \\ \frac{1}{x_9} \frac{\partial F_2}{\partial x_2} \\ \frac{1}{x_9} \frac{\partial F_3}{\partial x_2} \\ 0 \\ \frac{1}{I_{yy}} \frac{\partial M_q}{\partial x_2} \\ 0 \end{pmatrix} \quad (\text{Eq. A.2})$$

$$\frac{\partial f}{\partial x_3} = \frac{\partial f}{\partial \mu} = \begin{pmatrix} 0 \\ \frac{x_5 \sin x_3}{x_1 (\cos x_3)^2} \\ 0 \\ \frac{-(x_5)^2}{x_1 (\cos x_3)^2} - 2\omega_e x_5 \cos x_3 - x_1 (\omega_e)^2 \cos 2x_3 + \frac{1}{x_9} \frac{\partial F_1}{\partial x_3} \\ \frac{x_5 x_4}{x_1 (\cos x_3)^2} + 2\omega_e (x_4 \cos x_3 - x_6 \sin x_3) + \frac{1}{x_9} \frac{\partial F_2}{\partial x_3} \\ 2\omega_e x_5 \sin x_3 + x_1 (\omega_e)^2 \sin 2x_3 + \frac{1}{x_9} \frac{\partial F_3}{\partial x_3} \\ 0 \\ \frac{1}{I_{yy}} \frac{\partial M_q}{\partial x_3} \\ 0 \end{pmatrix} \quad (\text{Eq. A.3})$$

$$\frac{\partial f}{\partial x_4} = \frac{\partial f}{\partial v_1} = \begin{pmatrix} 0 \\ 0 \\ \frac{1}{x_1} \\ \frac{x_6}{x_1} + \frac{1}{x_9} \frac{\partial F_1}{\partial x_4} \\ \frac{x_5 \tan x_3}{x_1} + 2\omega_e \sin x_3 + \frac{1}{x_9} \frac{\partial F_2}{\partial x_4} \\ -\frac{2x_4}{x_1} + \frac{1}{x_9} \frac{\partial F_3}{\partial x_4} \\ 0 \\ \frac{1}{I_{yy}} \frac{\partial M_q}{\partial x_4} \\ \frac{1}{g_0} \left( \left( \frac{C_T}{I_{sp_0}} + \frac{Q}{I_{sp_0}} \frac{\partial C_T}{\partial Q} - \frac{QC_T}{(I_{sp_0})^2} \frac{\partial I_{sp_0}}{\partial Q} \right) \frac{\partial Q}{\partial x_4} + \left( \frac{Q}{I_{sp_0}} \frac{\partial C_T}{\partial M_f} - \frac{QC_T}{(I_{sp_0})^2} \frac{\partial M_f}{\partial M_f} \right) \frac{\partial M_f}{\partial x_4} \right) \end{pmatrix} \quad (\text{Eq. A.4})$$

$$\frac{\partial f}{\partial x_5} = \frac{\partial f}{\partial v_2} = \begin{pmatrix} 0 \\ \frac{1}{x_1 \cos x_3} \\ 0 \\ -\frac{2x_5 \tan x_3}{x_1} - 2\omega_e \sin x_3 + \frac{1}{x_9} \frac{\partial F_1}{\partial x_5} \\ \frac{x_6 + x_4 \tan x_3}{x_1} + \frac{1}{x_9} \frac{\partial F_2}{\partial x_5} \\ -\frac{2x_5}{x_1} - 2\omega_e \cos x_3 + \frac{1}{x_9} \frac{\partial F_3}{\partial x_5} \\ 0 \\ \frac{1}{I_{yy}} \frac{\partial M_q}{\partial x_5} \\ \frac{1}{g_0} \left( \left( \frac{C_T}{I_{sp_0}} + \frac{Q}{I_{sp_0}} \frac{\partial C_T}{\partial Q} - \frac{QC_T}{(I_{sp_0})^2} \frac{\partial I_{sp_0}}{\partial Q} \right) \frac{\partial Q}{\partial x_5} + \left( \frac{Q}{I_{sp_0}} \frac{\partial C_T}{\partial M_f} - \frac{QC_T}{(I_{sp_0})^2} \frac{\partial M_f}{\partial M_f} \right) \frac{\partial M_f}{\partial x_5} \right) \end{pmatrix} \quad (\text{Eq. A.5})$$

$$\frac{\partial f}{\partial x_6} = \frac{\partial f}{\partial u_3} = \begin{pmatrix} -1 \\ 0 \\ 0 \\ \frac{x_4}{x_1} + \frac{1}{x_9} \frac{\partial F_1}{\partial x_6} \\ \frac{x_5}{x_1} + 2\omega_0 \cos x_3 + \frac{1}{x_9} \frac{\partial F_2}{\partial x_6} \\ \frac{1}{x_9} \frac{\partial F_3}{\partial x_6} \\ 0 \\ \frac{1}{I_{yy}} \frac{\partial M_q}{\partial x_6} \\ \frac{1}{g_0} \left( \left( \frac{C_T}{I_{sp_0}} + \frac{Q}{I_{sp_0}} \frac{\partial C_T}{\partial Q} - \frac{QC_T}{(I_{sp_0})^2} \frac{\partial I_{sp_0}}{\partial Q} \right) \frac{\partial Q}{\partial x_6} + \left( \frac{Q}{I_{sp_0}} \frac{\partial C_T}{\partial M_I} - \frac{QC_T}{(I_{sp_0})^2} \frac{\partial I_{sp_0}}{\partial M_I} \right) \frac{\partial M_I}{\partial x_6} \right) \end{pmatrix} \quad (\text{Eq. A.6})$$

$$\frac{\partial f}{\partial x_7} = \frac{\partial f}{\partial \theta} = \begin{pmatrix} 0 \\ 0 \\ 0 \\ \frac{1}{x_9} \frac{\partial F_1}{\partial x_7} \\ \frac{1}{x_9} \frac{\partial F_2}{\partial x_7} \\ \frac{1}{x_9} \frac{\partial F_3}{\partial x_7} \\ 0 \\ \frac{1}{I_{yy}} \frac{\partial M_q}{\partial x_7} \\ 0 \end{pmatrix} \quad (\text{Eq. A.7})$$

$$\frac{\partial f}{\partial x_8} = \frac{\partial f}{\partial q} = \begin{pmatrix} 0 \\ 0 \\ 0 \\ \frac{1}{x_9} \frac{\partial F_1}{\partial x_8} \\ \frac{1}{x_9} \frac{\partial F_2}{\partial x_8} \\ \frac{1}{x_9} \frac{\partial F_3}{\partial x_8} \\ 1 \\ \frac{1}{I_{yy}} \frac{\partial M_q}{\partial x_8} \\ 0 \end{pmatrix} \quad (\text{Eq. A.8})$$

$$\frac{\partial f}{\partial x_9} = \frac{\partial f}{\partial m} = \begin{pmatrix} 0 \\ 0 \\ 0 \\ \frac{1}{x_9} \frac{\partial F_1}{\partial x_9} - \frac{F_1}{(x_9)^2} \\ \frac{1}{x_9} \frac{\partial F_2}{\partial x_9} - \frac{F_2}{(x_9)^2} \\ \frac{1}{x_9} \frac{\partial F_3}{\partial x_9} - \frac{F_3}{(x_9)^2} \\ 0 \\ \frac{1}{I_{yy}} \left( \frac{\partial M_a}{\partial x_9} - \frac{1}{I_{yy}} \frac{\partial I_{yy}}{\partial x_9} \right) \\ 0 \end{pmatrix} \quad (\text{Eq. A.9})$$

where:

$$\begin{aligned} \frac{\partial F_1}{\partial x} = \text{sign} \psi [ & -\sin \psi (F_T \cos \gamma + F_N \sin \gamma) \frac{\partial \psi}{\partial x} + \cos \psi \left( \frac{\partial F_T}{\partial x} \cos \gamma + \frac{\partial F_N}{\partial x} \sin \gamma \right) \\ & + \cos \psi \frac{\partial \gamma}{\partial x} (-F_T \sin \gamma + F_N \cos \gamma) ] \end{aligned} \quad (\text{Eq. A.10})$$

$$\begin{aligned} \frac{\partial F_2}{\partial x} = \text{sign} \psi [ & \cos \psi (F_T \cos \gamma + F_N \sin \gamma) \frac{\partial \psi}{\partial x} + \sin \psi \left( \frac{\partial F_T}{\partial x} \cos \gamma + \frac{\partial F_N}{\partial x} \sin \gamma \right) \\ & + \sin \psi \frac{\partial \gamma}{\partial x} (-F_T \sin \gamma + F_N \cos \gamma) ] \end{aligned} \quad (\text{Eq. A.11})$$

$$\frac{\partial F_3}{\partial x} = -\frac{\partial F_T}{\partial x} \sin \gamma + \frac{\partial F_N}{\partial x} \cos \gamma + \frac{\partial F_C}{\partial x} - \frac{\partial \gamma}{\partial x} (F_T \cos \gamma + F_N \sin \gamma) \quad (\text{Eq. A.12})$$

$$\begin{aligned} \frac{\partial M_a}{\partial x} = c S_{ref} \left( C_m \frac{\partial Q}{\partial x} + Q \frac{\partial C_m}{\partial x} \right) - (D \sin \alpha + L \cos \alpha + \Phi_R T_R \sin \delta_R) \frac{\partial x_{CG}}{\partial x} \\ - x_{CG} \left( \frac{\partial D}{\partial x} \sin \alpha + \frac{\partial L}{\partial x} \cos \alpha + (D \cos \alpha - L \sin \alpha) \frac{\partial \alpha}{\partial x} \right) \end{aligned} \quad (\text{Eq. A.13})$$

$$\frac{\partial \psi}{\partial x} = \begin{pmatrix} 0 & 0 & 0 & \frac{-x_5}{(x_4)^2 + (x_5)^2} & \frac{x_4}{(x_4)^2 + (x_5)^2} & 0 & 0 & 0 & 0 \end{pmatrix} \quad (\text{Eq. A.14})$$

$$\frac{\partial F_T}{\partial x} = \frac{\partial T}{\partial x} \cos \alpha - \frac{\partial D}{\partial x} - \frac{\partial \alpha}{\partial x} T \sin \alpha \quad (\text{Eq. A.15})$$

$$\frac{\partial F_N}{\partial x} = -\frac{\partial T}{\partial x} \sin \alpha - \frac{\partial L}{\partial x} - \frac{\partial \alpha}{\partial x} T \cos \alpha \quad (\text{Eq. A.16})$$

$$\left(\frac{\partial \Upsilon}{\partial x}\right)^T = \begin{pmatrix} 0 \\ 0 \\ 0 \\ \frac{x_4 x_6}{(v_f)^2 \sqrt{(x_4)^2 + (x_5)^2}} \\ \frac{x_5 x_6}{(v_f)^2 \sqrt{(x_4)^2 + (x_5)^2}} \\ \frac{-\sqrt{(x_4)^2 + (x_5)^2}}{(v_f)^2} \\ 0 \\ 0 \\ 0 \end{pmatrix} \quad (\text{Eq. A.17})$$

$$\frac{\partial F_g}{\partial x} = \begin{pmatrix} \frac{-2\mu_e x_9}{(x_1)^3} & 0 & 0 & 0 & 0 & 0 & 0 & 0 & \frac{\mu_e}{(x_1)^2} \end{pmatrix} \quad (\text{Eq. A.18})$$

$$\frac{\partial C_m}{\partial x} = \frac{\partial C_{m_a}}{\partial x} + \frac{\partial C_{m_o}}{\partial x} + \frac{q_c}{2v_f} \frac{\partial C_{m_q}}{\partial x} + \frac{c C_{m_q}}{2} \frac{\partial}{\partial x} \left( \frac{q}{v_f} \right) \quad (\text{Eq. A.19})$$

$$\frac{\partial C_{m_a}}{\partial x} = \frac{\partial C_{m_a}}{\partial \alpha} \frac{\partial \alpha}{\partial x} + \frac{\partial C_{m_a}}{\partial M_f} \frac{\partial M_f}{\partial x} \quad (\text{Eq. A.20})$$

$$\frac{\partial C_{m_o}}{\partial x} = \frac{\partial C_{m_o}}{\partial \alpha} \frac{\partial \alpha}{\partial x} + \frac{\partial C_{m_o}}{\partial M_f} \frac{\partial M_f}{\partial x} \quad (\text{Eq. A.21})$$

$$\frac{\partial C_{m_q}}{\partial x} = \frac{\partial C_{m_q}}{\partial \alpha} \frac{\partial \alpha}{\partial x} + \frac{\partial C_{m_q}}{\partial M_f} \frac{\partial M_f}{\partial x} \quad (\text{Eq. A.22})$$

$$\frac{\partial}{\partial x} \left( \frac{q}{v_f} \right) = \begin{pmatrix} 0 & 0 & 0 & \frac{-x_4 x_8}{(v_f)^3} & \frac{-x_5 x_8}{(v_f)^3} & \frac{-x_6 x_8}{(v_f)^3} & 0 & \frac{1}{v_f} & 0 \end{pmatrix} \quad (\text{Eq. A.23})$$

$$\frac{\partial x_{CG}}{\partial x} = \begin{pmatrix} 0 & 0 & 0 & 0 & 0 & 0 & 0 & 0 & \frac{\partial x_{CG}}{\partial x_9} \end{pmatrix} \quad (\text{Eq. A.24})$$

$$\frac{\partial D}{\partial x} = Q S_{ref} \frac{\partial C_D}{\partial x} + C_D S_{ref} \frac{\partial Q}{\partial x} \quad (\text{Eq. A.25})$$

$$\frac{\partial I}{\partial x} = Q S_{ref} \frac{\partial C_L}{\partial x} + C_L S_{ref} \frac{\partial Q}{\partial x} \quad (\text{Eq. A.26})$$

$$\left( \frac{\partial \alpha}{\partial x} \right)^T = \begin{pmatrix} 0 \\ 0 \\ 0 \\ \frac{-x_4 x_6}{(v_f)^2 \sqrt{(x_4)^2 + (x_5)^2}} \\ \frac{-x_5 x_6}{(v_f)^2 \sqrt{(x_4)^2 + (x_5)^2}} \\ \frac{\sqrt{(x_4)^2 + (x_5)^2}}{(v_f)^2} \\ 1 \\ 0 \\ 0 \end{pmatrix} \quad (\text{Eq. A.27})$$

$$\frac{\partial T}{\partial x} = Q \frac{\partial C_T}{\partial x} + C_T \frac{\partial Q}{\partial x} \quad (\text{Eq. A.28})$$

$$M_f = \frac{v_f}{\alpha} \quad (\text{Eq. A.29})$$

$$\frac{\partial M_f}{\partial x} = \left( \frac{-v_f \partial \alpha}{\alpha^2 \partial r} \quad 0 \quad 0 \quad \frac{v_1}{\alpha v_f} \quad \frac{v_2}{\alpha v_f} \quad \frac{v_3}{\alpha v_f} \quad 0 \quad 0 \quad 0 \right) \quad (\text{Eq. A.30})$$

$$\frac{\partial C_D}{\partial x} = \frac{\partial C_{D_a}}{\partial x} + \frac{\partial C_{D_e}}{\partial x} \quad (\text{Eq. A.31})$$

$$\frac{\partial C_{D_a}}{\partial x} = \frac{\partial C_{D_a}}{\partial \alpha} \frac{\partial \alpha}{\partial x} + \frac{\partial C_{D_a}}{\partial M_f} \frac{\partial M_f}{\partial x} \quad (\text{Eq. A.32})$$

$$\frac{\partial C_{D_e}}{\partial x} = \frac{\partial C_{D_e}}{\partial \alpha} \frac{\partial \alpha}{\partial x} + \frac{\partial C_{D_e}}{\partial M_f} \frac{\partial M_f}{\partial x} \quad (\text{Eq. A.33})$$

$$\frac{\partial C_L}{\partial x} = \frac{\partial C_{L_a}}{\partial x} + \frac{\partial C_{L_e}}{\partial x} \quad (\text{Eq. A.34})$$

$$\frac{\partial C_{L_u}}{\partial x} = \frac{\partial C_{L_u}}{\partial \alpha} \frac{\partial \alpha}{\partial x} + \frac{\partial C_{L_u}}{\partial M_f} \frac{\partial M_f}{\partial x} \quad (\text{Eq. A.35})$$

$$\frac{\partial C_{L_e}}{\partial x} = \frac{\partial C_{L_e}}{\partial \alpha} \frac{\partial \alpha}{\partial x} + \frac{\partial C_{L_e}}{\partial M_f} \frac{\partial M_f}{\partial x} \quad (\text{Eq. A.36})$$

$$\frac{\partial C_T}{\partial x} = \frac{\partial C_T}{\partial M_f} \frac{\partial M_f}{\partial x} + \frac{\partial C_T}{\partial Q} \frac{\partial Q}{\partial x} \quad (\text{Eq. A.37})$$

To complete the evaluation of  $f_x$ , the following partial derivatives are derived from the example vehicle model tables:  $\frac{\partial I_{yy}}{\partial m}$ ;  $\frac{\partial x_{CG}}{\partial m}$ ;  $\frac{\partial C_{m_a}}{\partial \alpha}$ ;  $\frac{\partial C_{m_a}}{\partial M_f}$ ;  $\frac{\partial C_{m_e}}{\partial \alpha}$ ;  $\frac{\partial C_{m_e}}{\partial M_f}$ ;  $\frac{\partial C_{m_q}}{\partial \alpha}$ ;  $\frac{\partial C_{m_q}}{\partial M_f}$ ;  $\frac{\partial C_{D_a}}{\partial \alpha}$ ;  $\frac{\partial C_{D_a}}{\partial M_f}$ ;  $\frac{\partial C_{D_e}}{\partial \alpha}$ ;  $\frac{\partial C_{D_e}}{\partial M_f}$ ;  $\frac{\partial C_{L_u}}{\partial \alpha}$ ;  $\frac{\partial C_{L_u}}{\partial M_f}$ ;  $\frac{\partial C_{L_e}}{\partial \alpha}$ ;  $\frac{\partial C_{L_e}}{\partial M_f}$ ;  $\frac{\partial C_T}{\partial Q}$ ;  $\frac{\partial C_T}{\partial M_f}$ . Also  $\alpha$  and  $\frac{\partial \alpha}{\partial r}$  are derived from a standard atmosphere model.

## A.2. Derivatives with Respect to Controls

All the equations required to compute the matrix  $f_u$  for the example application with nine states, required for use in Eqs. V.49,50,54, are derived from differentiating Eq. V.19. The equations for  $f_u$  are simplified by the knowledge that the following partial derivatives have zero value:

$$\frac{\partial C_{D_a}}{\partial u} ; \frac{\partial C_{L_a}}{\partial u} .$$

$$f_u = \begin{pmatrix} 0 & 0 & 0 & 0 \\ 0 & 0 & 0 & 0 \\ 0 & 0 & 0 & 0 \\ \frac{1}{x_9} \left( \frac{\partial F_1}{\partial u_1} \right) & \frac{1}{x_9} \left( \frac{\partial F_1}{\partial u_2} \right) & \frac{1}{x_9} \left( \frac{\partial F_1}{\partial u_3} \right) & \frac{1}{x_9} \left( \frac{\partial F_1}{\partial u_4} \right) \\ \frac{1}{x_9} \left( \frac{\partial F_2}{\partial u_1} \right) & \frac{1}{x_9} \left( \frac{\partial F_2}{\partial u_2} \right) & \frac{1}{x_9} \left( \frac{\partial F_2}{\partial u_3} \right) & \frac{1}{x_9} \left( \frac{\partial F_2}{\partial u_4} \right) \\ \frac{1}{x_9} \left( \frac{\partial F_3}{\partial u_1} \right) & \frac{1}{x_9} \left( \frac{\partial F_3}{\partial u_2} \right) & \frac{1}{x_9} \left( \frac{\partial F_3}{\partial u_3} \right) & \frac{1}{x_9} \left( \frac{\partial F_3}{\partial u_4} \right) \\ 0 & 0 & 0 & 0 \\ \frac{\partial \frac{dx_8}{dt}}{\partial u_1} & \frac{\partial \frac{dx_8}{dt}}{\partial u_2} & \frac{\partial \frac{dx_8}{dt}}{\partial u_3} & \frac{\partial \frac{dx_8}{dt}}{\partial u_4} \\ \frac{Q}{g_0} \frac{\partial}{\partial u_1} \left( \frac{C_T}{I_{sp_a}} \right) & \frac{T_R}{g_0 I_{sp_R}} \frac{\partial \Phi_R}{\partial u_2} & 0 & 0 \end{pmatrix} \quad (\text{Eq. A.38})$$

where:

$$\frac{\partial F_1}{\partial u_i} = \text{sign} \psi \cos \psi \left( \frac{\partial F_T}{\partial u_i} \cos \gamma + \frac{\partial F_N}{\partial u_i} \sin \gamma \right) \quad (\text{Eq. A.39})$$

$$\frac{\partial F_2}{\partial u_i} = \text{sign} \psi \sin \psi \left( \frac{\partial F_T}{\partial u_i} \cos \gamma + \frac{\partial F_N}{\partial u_i} \sin \gamma \right) \quad (\text{Eq. A.40})$$

$$\frac{\partial F_3}{\partial u_i} = -\frac{\partial F_T}{\partial u_i} \sin \gamma + \frac{\partial F_N}{\partial u_i} \cos \gamma \quad (\text{Eq. A.41})$$

$$\frac{\partial \dot{x}_8}{\partial u} = \frac{1}{I_{yy}} \left( Q_C S_{ref} \frac{\partial C_{m_e}}{\partial u} - N_{CG} \left( \sin \alpha \frac{\partial D}{\partial u} + \cos \alpha \frac{\partial L}{\partial u} \right) \right) \quad (\text{Eq. A.42})$$

$$+ (N_R - N_{CG}) T_R \frac{\partial}{\partial u} (\Phi_R \sin \delta_R)$$

$$\frac{\partial}{\partial u_i} \left( \frac{C_T}{I_{sp_a}} \right) = \frac{2u_a}{I_{sp_a}} \left( \frac{\partial C_T}{\partial \Phi_a} - \frac{C_T}{I_{sp_a}} \frac{\partial I_{sp_a}}{\partial \Phi_a} \right) \quad (\text{Eq. A.43})$$

To complete the evaluation of  $f_u$ , the following partial derivatives are derived from the example vehicle model tables:  $\frac{\partial C_T}{\partial \Phi_a}$ ;  $\frac{\partial I_{sp_a}}{\partial \Phi_a}$ ;  $\frac{\partial C_{m_e}}{\partial u_3}$ ;  $\frac{\partial C_{D_e}}{\partial u_3}$ ;  $\frac{\partial C_{L_e}}{\partial u_3}$ .

## Appendix B

### Seven State Function Partial Derivatives for the Example Model

#### B.1. Derivatives with Respect to States

The matrix  $f_v$  for the example application with seven states (derived from differentiating Eq. V.70) is too large to print as a single equation, so it is specified here on a column by column basis. The equations for  $f_v$  are simplified by the knowledge that the following derivatives have zero value:  $\frac{\partial Q}{\partial v}$ ;  $\frac{\partial M_f}{\partial v}$ ;  $\frac{\partial Q}{\partial \mu}$ ;  $\frac{\partial M_f}{\partial \mu}$ ;  $\frac{\partial Q}{\partial m}$ ;  $\frac{\partial M_f}{\partial m}$ . Simplifications are also made by utilizing the knowledge that  $M_f$  is a function only of  $r$  and  $v_f$ .

$$\frac{\partial f}{\partial x_1} = \frac{\partial f}{\partial r} = \begin{pmatrix} 0 \\ -x_5 \\ \frac{-x_4}{(x_1)^2 \cos x_3} \\ \frac{-x_4}{(x_1)^2} \\ \frac{(x_5)^2 \tan x_3 - x_4 x_6}{(x_1)^2} - \frac{(\omega_*)^2 \sin 2x_3}{2} + \frac{1}{x_7} \frac{\partial F_1}{\partial x_1} \\ \frac{-x_5(x_6 + x_4 \tan x_3)}{(x_1)^2} + \frac{1}{x_7} \frac{\partial F_2}{\partial x_1} \\ \frac{(x_4)^2 + (x_5)^2}{(x_1)^2} - (\omega_* \cos x_3)^2 + \frac{1}{x_7} \frac{\partial F_3}{\partial x_1} \\ \frac{1}{g_0} \left( \left( \frac{C_T}{l_{sp_0}} + \frac{Q}{l_{sp_0}} \frac{\partial C_T}{\partial Q} - \frac{QC_T}{(l_{sp_0})^2} \frac{\partial l_{sp_0}}{\partial Q} \right) \frac{\partial Q}{\partial x_1} + \left( \frac{Q}{l_{sp_0}} \frac{\partial C_T}{\partial M_f} - \frac{QC_T}{(l_{sp_0})^2} \frac{\partial M_f}{\partial M_f} \right) \frac{\partial M_f}{\partial x_1} \right) \end{pmatrix} \quad (\text{Eq. B.1})$$

$$\frac{\partial f}{\partial x_2} = \frac{\partial f}{\partial v} = \begin{pmatrix} 0 \\ 0 \\ 0 \\ \frac{1}{x_7} \frac{\partial F_1}{\partial x_2} \\ \frac{1}{x_7} \frac{\partial F_2}{\partial x_2} \\ \frac{1}{x_7} \frac{\partial F_3}{\partial x_2} \\ 0 \end{pmatrix} \quad (\text{Eq. B.2})$$

$$\frac{\partial f}{\partial x_3} = \frac{\partial f}{\partial \mu} = \begin{pmatrix} 0 \\ \frac{x_5 \sin x_3}{x_1 (\cos x_3)^2} \\ 0 \\ \frac{-(x_5)^2}{x_1 (\cos x_3)^2} - 2\omega_e x_5 \cos x_3 - x_1 (\omega_e)^2 \cos 2x_3 + \frac{1}{x_7} \frac{\partial F_1}{\partial x_3} \\ \frac{x_5 x_4}{x_1 (\cos x_3)^2} + 2\omega_e (x_4 \cos x_3 - x_6 \sin x_3) + \frac{1}{x_7} \frac{\partial F_2}{\partial x_3} \\ 2\omega_e x_5 \sin x_3 + x_1 (\omega_e)^2 \sin 2x_3 + \frac{1}{x_7} \frac{\partial F_3}{\partial x_3} \\ 0 \end{pmatrix} \quad (\text{Eq. B.3})$$

$$\frac{\partial f}{\partial x_4} = \frac{\partial f}{\partial v_1} = \begin{pmatrix} 0 \\ 0 \\ \frac{1}{x_1} \\ \frac{x_6}{x_1} + \frac{1}{x_7} \frac{\partial F_1}{\partial x_4} \\ \frac{x_5 \tan x_3}{x_1} + 2\omega_e \sin x_3 + \frac{1}{x_7} \frac{\partial F_2}{\partial x_4} \\ -\frac{2x_4}{x_1} + \frac{1}{x_7} \frac{\partial F_3}{\partial x_4} \\ \frac{1}{g_0} \left( \left( \frac{C_T}{I_{sp_0}} + \frac{Q}{I_{sp_0}} \frac{\partial C_T}{\partial Q} - \frac{QC_T}{(I_{sp_0})^2} \frac{\partial I_{sp_0}}{\partial Q} \right) \frac{\partial Q}{\partial x_4} + \left( \frac{Q}{I_{sp_0}} \frac{\partial C_T}{\partial M_f} - \frac{QC_T}{(I_{sp_0})^2} \frac{\partial M_f}{\partial x_4} \right) \frac{\partial M_f}{\partial x_4} \right) \end{pmatrix} \quad (\text{Eq. B.4})$$

$$\frac{\partial f}{\partial x_5} = \frac{\partial f}{\partial v_2} = \begin{pmatrix} 0 \\ \frac{1}{x_1 \cos x_3} \\ 0 \\ -\frac{2x_5 \tan x_3}{x_1} - 2\omega_e \sin x_3 + \frac{1}{x_7} \frac{\partial F_1}{\partial x_5} \\ \frac{x_6 + x_4 \tan x_3}{x_1} + \frac{1}{x_7} \frac{\partial F_2}{\partial x_5} \\ -\frac{2x_5}{x_1} - 2\omega_e \cos x_3 + \frac{1}{x_7} \frac{\partial F_3}{\partial x_5} \\ \frac{1}{g_0} \left( \left( \frac{C_T}{I_{sp_0}} + \frac{Q}{I_{sp_0}} \frac{\partial C_T}{\partial Q} - \frac{QC_T}{(I_{sp_0})^2} \frac{\partial I_{sp_0}}{\partial Q} \right) \frac{\partial Q}{\partial x_5} + \left( \frac{Q}{I_{sp_0}} \frac{\partial C_T}{\partial M_f} - \frac{QC_T}{(I_{sp_0})^2} \frac{\partial M_f}{\partial x_5} \right) \frac{\partial M_f}{\partial x_5} \right) \end{pmatrix} \quad (\text{Eq. B.5})$$

$$\frac{\partial f}{\partial x_6} = \frac{\partial f}{\partial v_3} = \begin{pmatrix} -1 \\ 0 \\ 0 \\ \frac{x_4}{x_1} + \frac{1}{x_7} \frac{\partial F_1}{\partial x_6} \\ \frac{x_5}{x_1} + 2\omega_e \cos x_3 + \frac{1}{x_7} \frac{\partial F_2}{\partial x_6} \\ \frac{1}{x_7} \frac{\partial F_3}{\partial x_6} \\ \frac{1}{g_0} \left( \left( \frac{C_T}{I_{sp_0}} + \frac{Q}{I_{sp_0}} \frac{\partial C_T}{\partial Q} - \frac{QC_T}{(I_{sp_0})^2} \frac{\partial I_{sp_0}}{\partial Q} \right) \frac{\partial Q}{\partial x_6} + \left( \frac{Q}{I_{sp_0}} \frac{\partial C_T}{\partial M_f} - \frac{QC_T}{(I_{sp_0})^2} \frac{\partial M_f}{\partial x_6} \right) \frac{\partial M_f}{\partial x_6} \right) \end{pmatrix} \quad (\text{Eq. B.6})$$

$$\frac{\partial f}{\partial x_7} = \frac{\partial f}{\partial m} = \begin{pmatrix} 0 \\ 0 \\ 0 \\ \frac{1}{x_7} \frac{\partial F_1}{\partial x_7} - \frac{F_1}{(x_7)^2} \\ \frac{1}{x_7} \frac{\partial F_2}{\partial x_7} - \frac{F_2}{(x_7)^2} \\ \frac{1}{x_7} \frac{\partial F_3}{\partial x_7} - \frac{F_3}{(x_7)^2} \\ 0 \end{pmatrix} \quad (\text{Eq. B.7})$$

where:

$$\begin{aligned} \frac{\partial F_1}{\partial x} = \text{sign}\psi [ & -\sin\psi (F_T \cos\gamma + F_N \sin\gamma) \frac{\partial\psi}{\partial x} + \cos\psi \left( \frac{\partial F_T}{\partial x} \cos\gamma + \frac{\partial F_N}{\partial x} \sin\gamma \right) \\ & + \cos\psi \frac{\partial\gamma}{\partial x} (-F_T \sin\gamma + F_N \cos\gamma) ] \end{aligned} \quad (\text{Eq. B.8})$$

$$\begin{aligned} \frac{\partial F_2}{\partial x} = \text{sign}\psi [ & \cos\psi (F_T \cos\gamma + F_N \sin\gamma) \frac{\partial\psi}{\partial x} + \sin\psi \left( \frac{\partial F_T}{\partial x} \cos\gamma + \frac{\partial F_N}{\partial x} \sin\gamma \right) \\ & + \sin\psi \frac{\partial\gamma}{\partial x} (-F_T \sin\gamma + F_N \cos\gamma) ] \end{aligned} \quad (\text{Eq. B.9})$$

$$\frac{\partial F_3}{\partial x} = -\frac{\partial F_T}{\partial x} \sin\gamma + \frac{\partial F_N}{\partial x} \cos\gamma + \frac{\partial F_C}{\partial x} - \frac{\partial\gamma}{\partial x} (F_T \cos\gamma + F_N \sin\gamma) \quad (\text{Eq. B.10})$$

$$\frac{\partial\psi}{\partial x} = \begin{pmatrix} 0 & 0 & 0 & \frac{-x_5}{(x_4)^2 + (x_5)^2} & \frac{x_4}{(x_4)^2 + (x_5)^2} & 0 & 0 \end{pmatrix} \quad (\text{Eq. B.11})$$

$$\frac{\partial F_T}{\partial x} = \frac{\partial T}{\partial x} \cos\alpha - \frac{\partial D}{\partial x} \quad (\text{Eq. B.12})$$

$$\frac{\partial F_N}{\partial x} = -\frac{\partial T}{\partial x} \sin\alpha - \frac{\partial L}{\partial x} \quad (\text{Eq. B.13})$$

$$\left(\frac{\partial Y}{\partial x}\right)^T = \begin{pmatrix} 0 \\ 0 \\ 0 \\ \frac{x_4 x_6}{(v_f)^2 \sqrt{(x_4)^2 + (x_5)^2}} \\ \frac{x_5 x_6}{(v_f)^2 \sqrt{(x_4)^2 + (x_5)^2}} \\ \frac{-\sqrt{(x_4)^2 + (x_5)^2}}{(v_f)^2} \\ 0 \end{pmatrix} \quad (\text{Eq. B.14})$$

$$\frac{\partial F_g}{\partial x} = \begin{pmatrix} \frac{-2\mu_e x_7}{(x_1)^3} & 0 & 0 & 0 & 0 & 0 & \frac{\mu_e}{(x_1)^2} \end{pmatrix} \quad (\text{Eq. B.15})$$

$$\frac{\partial D}{\partial x} = Q S_{ref} \frac{\partial C_D}{\partial x} + C_D S_{ref} \frac{\partial Q}{\partial x} \quad (\text{Eq. B.16})$$

$$\frac{\partial L}{\partial x} = Q S_{ref} \frac{\partial C_L}{\partial x} + C_L S_{ref} \frac{\partial Q}{\partial x} \quad (\text{Eq. B.17})$$

$$\frac{\partial T}{\partial x} = Q \frac{\partial C_T}{\partial x} + C_T \frac{\partial Q}{\partial x} \quad (\text{Eq. B.18})$$

$$\frac{\partial C_D}{\partial x} = \frac{\partial C_{D_a}}{\partial x} + \frac{\partial C_{D_e}}{\partial x} \quad (\text{Eq. B.19})$$

$$\frac{\partial C_{D_a}}{\partial x} = \frac{\partial C_{D_a}}{\partial M_f} \frac{\partial M_f}{\partial x} \quad (\text{Eq. B.20})$$

$$\frac{\partial C_{D_e}}{\partial x} = \frac{\partial C_{D_e}}{\partial M_f} \frac{\partial M_f}{\partial x} + \frac{\partial C_{D_e}}{\partial \delta_e} \frac{\partial \delta_e}{\partial x} \quad (\text{Eq. B.21})$$

$$\frac{\partial C_L}{\partial x} = \frac{\partial C_{L_a}}{\partial x} + \frac{\partial C_{L_e}}{\partial x} \quad (\text{Eq. B.22})$$

$$\frac{\partial C_{L_a}}{\partial x} = \frac{\partial C_{L_a}}{\partial M_f} \frac{\partial M_f}{\partial x} \quad (\text{Eq. B.23})$$

$$\frac{\partial C_{L_e}}{\partial x} = \frac{\partial C_{L_e}}{\partial M_f} \frac{\partial M_f}{\partial x} + \frac{\partial C_{L_e}}{\partial \delta_e} \frac{\partial \delta_e}{\partial x} \quad (\text{Eq. B.24})$$

$$\frac{\partial C_T}{\partial x} = \frac{\partial C_T}{\partial M_f} \frac{\partial M_f}{\partial x} + \frac{\partial C_T}{\partial Q} \frac{\partial Q}{\partial x} \quad (\text{Eq. B.25})$$

$$M_f = \frac{v_f}{\alpha} \quad (\text{Eq. B.26})$$

$$\frac{\partial M_f}{\partial x} = \begin{pmatrix} -\frac{v_f}{\alpha^2} \frac{\partial \alpha}{\partial r} & 0 & 0 & \frac{v_1}{\alpha v_f} & \frac{v_2}{\alpha v_f} & \frac{v_3}{\alpha v_f} & 0 \end{pmatrix} \quad (\text{Eq. B.27})$$

$$\begin{aligned} \frac{\partial \delta_e}{\partial x} = & \left( \frac{\partial C_{m_e}}{\partial \delta_e} \right)^{-1} \left( - \left( \frac{\partial C_{m_e}}{\partial M_f} + \frac{\partial C_{m_a}}{\partial M_f} \right) \frac{\partial M_f}{\partial x} \right. \\ & + \frac{\partial}{\partial x} \left( \frac{x_{CG}}{QcS_{ref}} \right) (D \sin \alpha + L \cos \alpha) \\ & \left. + \frac{x_{cg}}{QcS_{ref}} \left( \frac{\partial D}{\partial x} \sin \alpha + \frac{\partial L}{\partial x} \cos \alpha \right) \right) \end{aligned} \quad (\text{Eq. B.28})$$

$$\frac{\partial}{\partial x} \left( \frac{x_{CG}}{QcS_{ref}} \right) = \frac{1}{QcS_{ref}} \left( \frac{\partial x_{CG}}{\partial x} - \frac{x_{CG}}{Q} \frac{\partial Q}{\partial x} \right) \quad (\text{Eq. B.29})$$

$$\frac{\partial x_{CG}}{\partial x} = \begin{pmatrix} 0 & 0 & 0 & 0 & 0 & 0 & \frac{\partial x_{CG}}{\partial m} \end{pmatrix} \quad (\text{Eq. B.30})$$

To complete the evaluation of  $f_x$ , the following partial derivatives are derived from the example vehicle model data tables:  $\frac{\partial C_{D_a}}{\partial M_f}$ ;  $\frac{\partial C_{D_e}}{\partial M_f}$ ;  $\frac{\partial C_{D_e}}{\partial \delta_e}$ ;  $\frac{\partial C_{L_a}}{\partial M_f}$ ;  $\frac{\partial C_{L_e}}{\partial M_f}$ ;  $\frac{\partial C_{L_e}}{\partial \delta_e}$ ;  $\frac{\partial C_{m_a}}{\partial M_f}$ ;  $\frac{\partial C_{m_e}}{\partial M_f}$ ;  $\frac{\partial C_{m_e}}{\partial \delta_e}$ ;  $\frac{\partial C_T}{\partial Q}$ ;  $\frac{\partial C_T}{\partial M_f}$ ;  $\frac{\partial x_{CG}}{\partial m}$ . Also  $\alpha$  and  $\frac{\partial \alpha}{\partial r}$  are derived from a standard atmosphere model.

## **B.2. Derivatives with Respect to Controls**

All the equations required to compute the matrix  $f_u$  for the example application with seven states, required for use in Eqs. V.49,50,54, are derived from differentiating Eq. V.70. The middle column of  $f_u$  only applies to leg 3 of the ascent trajectory:

$$f_u = \begin{pmatrix} 0 & 0 & 0 \\ 0 & 0 & 0 \\ 0 & 0 & 0 \\ \frac{1}{x_7} \left( \frac{\partial F_1}{\partial u_1} \right) & \frac{1}{x_7} \left( \frac{\partial F_1}{\partial u_2} \right) & \frac{1}{x_7} \left( \frac{\partial F_1}{\partial u_3} \right) \\ \frac{1}{x_7} \left( \frac{\partial F_2}{\partial u_1} \right) & \frac{1}{x_7} \left( \frac{\partial F_2}{\partial u_2} \right) & \frac{1}{x_7} \left( \frac{\partial F_2}{\partial u_3} \right) \\ \frac{1}{x_7} \left( \frac{\partial F_3}{\partial u_1} \right) & \frac{1}{x_7} \left( \frac{\partial F_3}{\partial u_2} \right) & \frac{1}{x_7} \left( \frac{\partial F_3}{\partial u_3} \right) \\ \frac{Q}{g_0} \frac{\partial}{\partial u_1} \left( \frac{C_T}{I_{sp_a}} \right) & \frac{T_R}{g_0 I_{sp_R}} \frac{\partial \Phi_R}{\partial u_2} & 0 \end{pmatrix} \quad (\text{Eq. B.31})$$

where  $\Phi_R$  is zero except for leg 3 of the ascent trajectory:

$$\frac{\partial F_1}{\partial u_i} = \text{sign} \psi \cos \psi \left( \frac{\partial F_T}{\partial u_i} \cos \gamma + \frac{\partial F_N}{\partial u_i} \sin \gamma \right) \quad (\text{Eq. B.32})$$

$$\frac{\partial F_2}{\partial u_i} = \text{sign} \psi \sin \psi \left( \frac{\partial F_T}{\partial u_i} \cos \gamma + \frac{\partial F_N}{\partial u_i} \sin \gamma \right) \quad (\text{Eq. B.33})$$

$$\frac{\partial F_3}{\partial u_i} = -\frac{\partial F_T}{\partial u_i} \sin \gamma + \frac{\partial F_N}{\partial u_i} \cos \gamma \quad (\text{Eq. B.34})$$

$$\frac{\partial}{\partial u_1} \left( \frac{C_T}{I_{sp_a}} \right) = \frac{2u_a}{I_{sp_a}} \left( \frac{\partial C_T}{\partial \Phi_a} - \frac{C_T}{I_{sp_a}} \frac{\partial I_{sp_a}}{\partial \Phi_a} \right) \quad (\text{Eq. B.35})$$

$$\frac{\partial \Phi_R}{\partial u_2} = \frac{-2u_R}{(1 + (u_R)^2)^2} \quad (\text{Eq. B.36})$$

$$\frac{\partial F_T}{\partial u_i} = \frac{\partial T}{\partial u_i} \cos \alpha - T \sin \alpha \frac{\partial \alpha}{\partial u_i} - \frac{\partial D}{\partial u_i} \quad (\text{Eq. B.37})$$

$$\frac{\partial F_N}{\partial u_i} = -\left( \frac{\partial T}{\partial u_i} \sin \alpha + T \cos \alpha \frac{\partial \alpha}{\partial u_i} + \frac{\partial L}{\partial u_i} \right) \quad (\text{Eq. B.38})$$

$$\frac{\partial \alpha}{\partial u_i} = (0 \quad 0 \quad 1) \quad (\text{Eq. B.39})$$

$$\frac{\partial D}{\partial u} = \begin{pmatrix} 0 & 0 & QS_{ref} \left( \frac{\partial C_{D_a}}{\partial u_3} + \frac{\partial C_{D_e}}{\partial u_3} \right) \end{pmatrix} \quad (\text{Eq. B.40})$$

$$\frac{\partial L}{\partial u} = \begin{pmatrix} 0 & 0 & QS_{ref} \left( \frac{\partial C_{L_a}}{\partial u_3} + \frac{\partial C_{L_e}}{\partial u_3} \right) \end{pmatrix} \quad (\text{Eq. B.41})$$

$$\frac{\partial T}{\partial u} = \begin{pmatrix} 2Qu_1 \frac{\partial C_T}{\partial \Phi_a} & \frac{-2T_R u_2}{(1 + (u_2)^2)^2} & 0 \end{pmatrix} \quad (\text{Eq. B.42})$$

Note that the middle terms in the above matrix equations for the partials with respect to controls disappear for legs 1 and 2 of the ascent trajectory.

To complete the evaluation of  $f_u$ , the following partial derivatives are derived from the example vehicle model data tables:  $\frac{\partial C_T}{\partial \Phi_a}$ ;  $\frac{\partial I_{sp_a}}{\partial \Phi_a}$ ;  $\frac{\partial C_{D_a}}{\partial u_3}$ ;  $\frac{\partial C_{D_e}}{\partial u_3}$ ;  $\frac{\partial C_{L_a}}{\partial u_3}$ ;  $\frac{\partial C_{L_e}}{\partial u_3}$ .



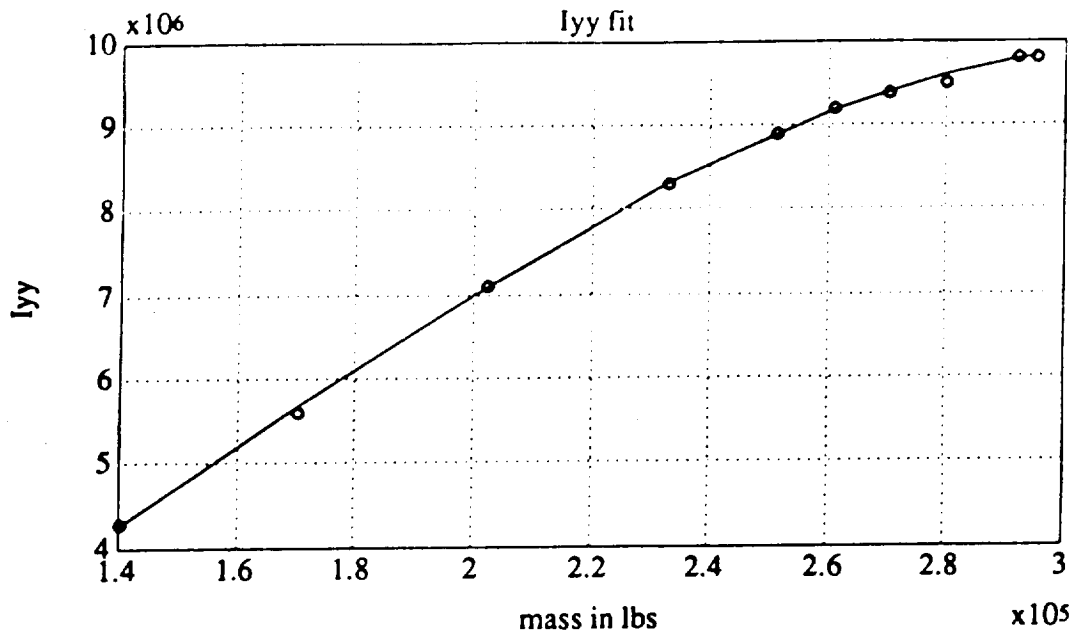


Figure V-2. Vehicle Mass Model Curve Fit

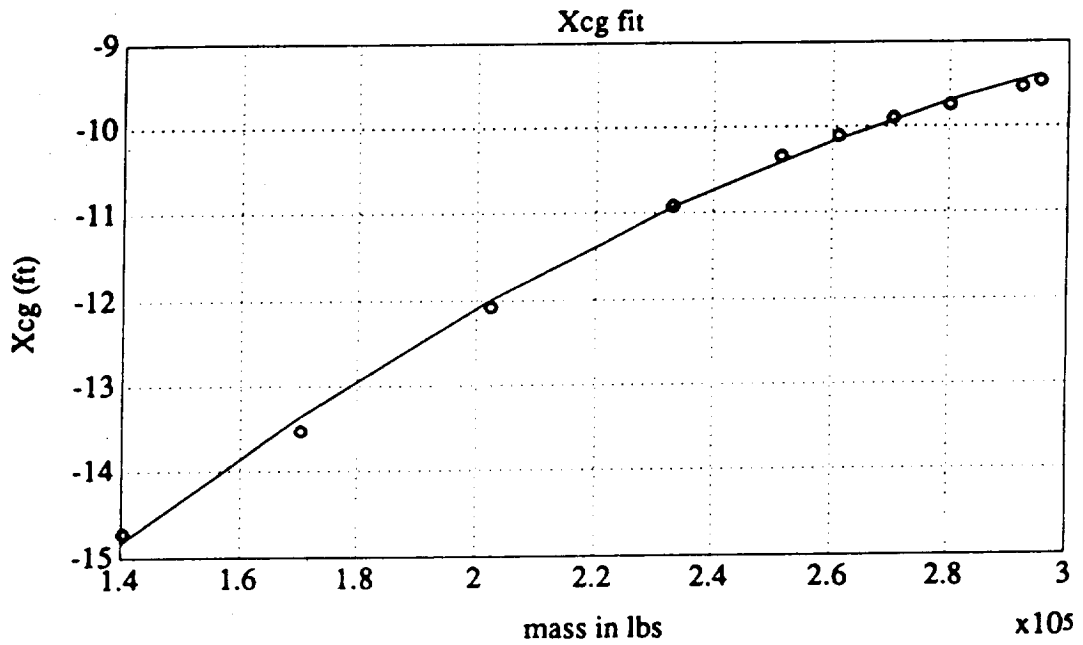
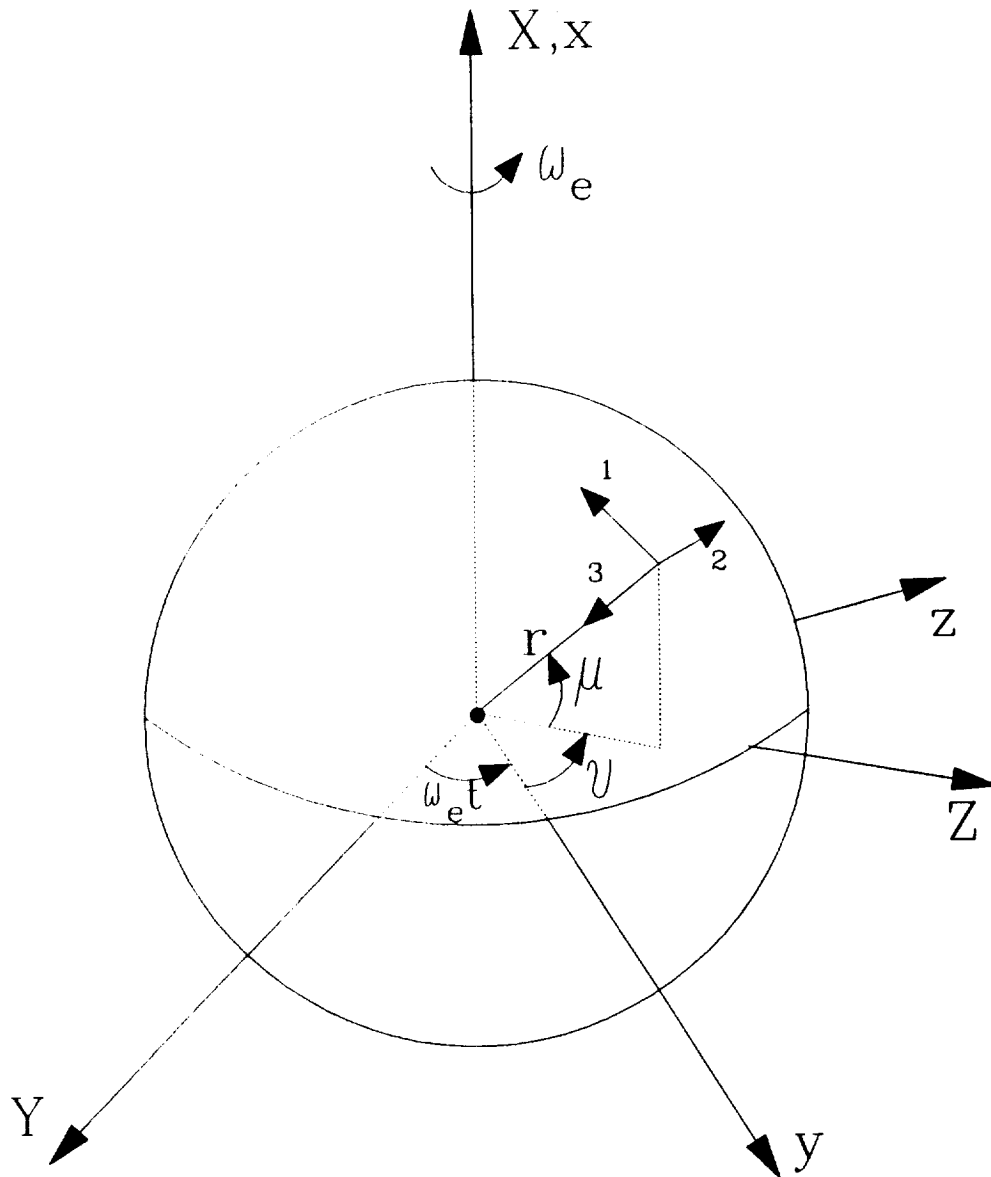


Figure V-3. Vehicle Pitch Inertia Moment Model Curve Fit



- $X-Y-Z$ : Earth centered inertial frame
- $x-y-z$ : Earth fixed frame (rotates with Earth)
- $1-2-3$ : Vehicle fixed LVLH frame

Figure V-4. Coordinate Systems for Dynamics Equations

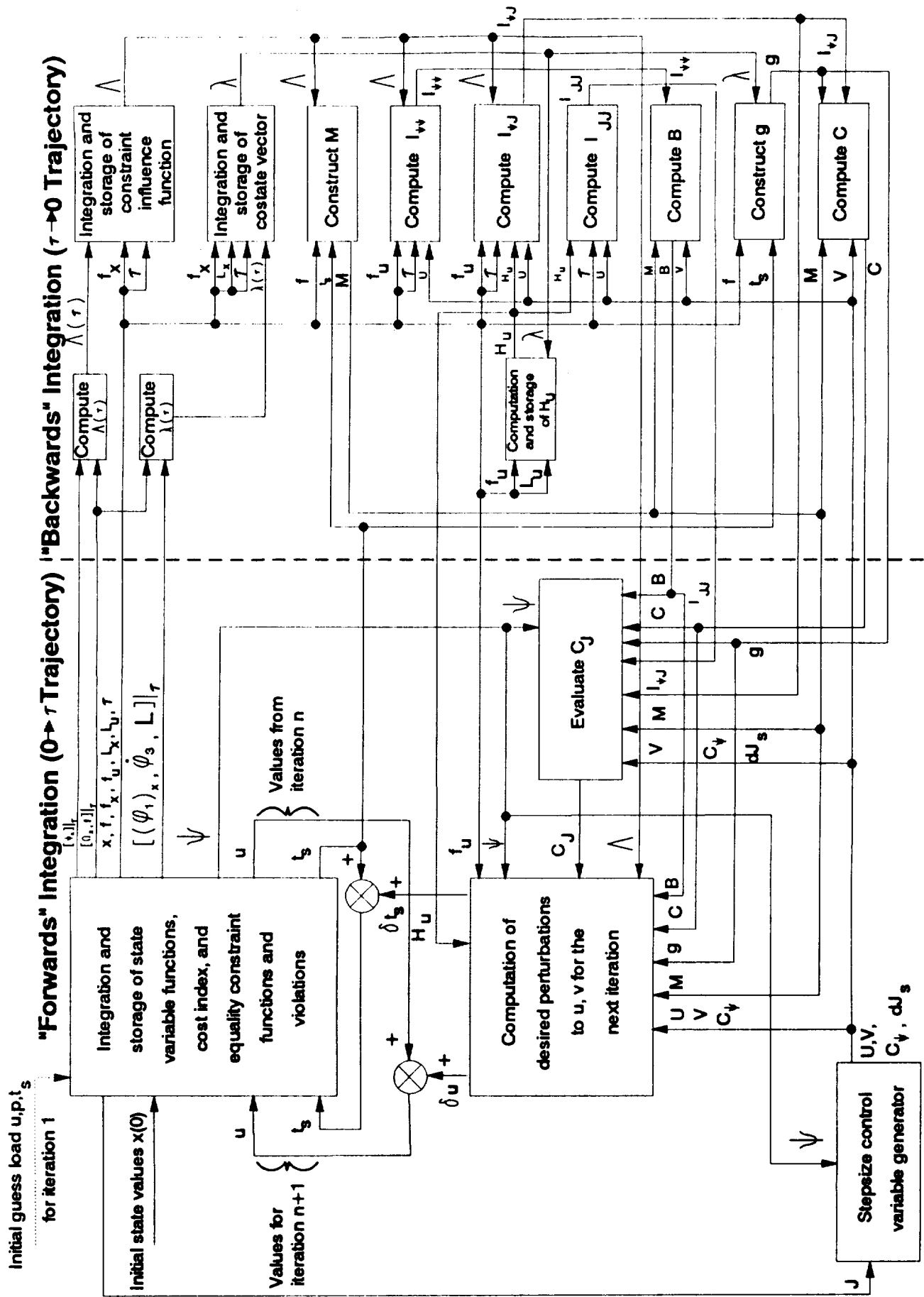


Figure V-5. Integrated Trajectory/Control Optimization Algorithm Structure

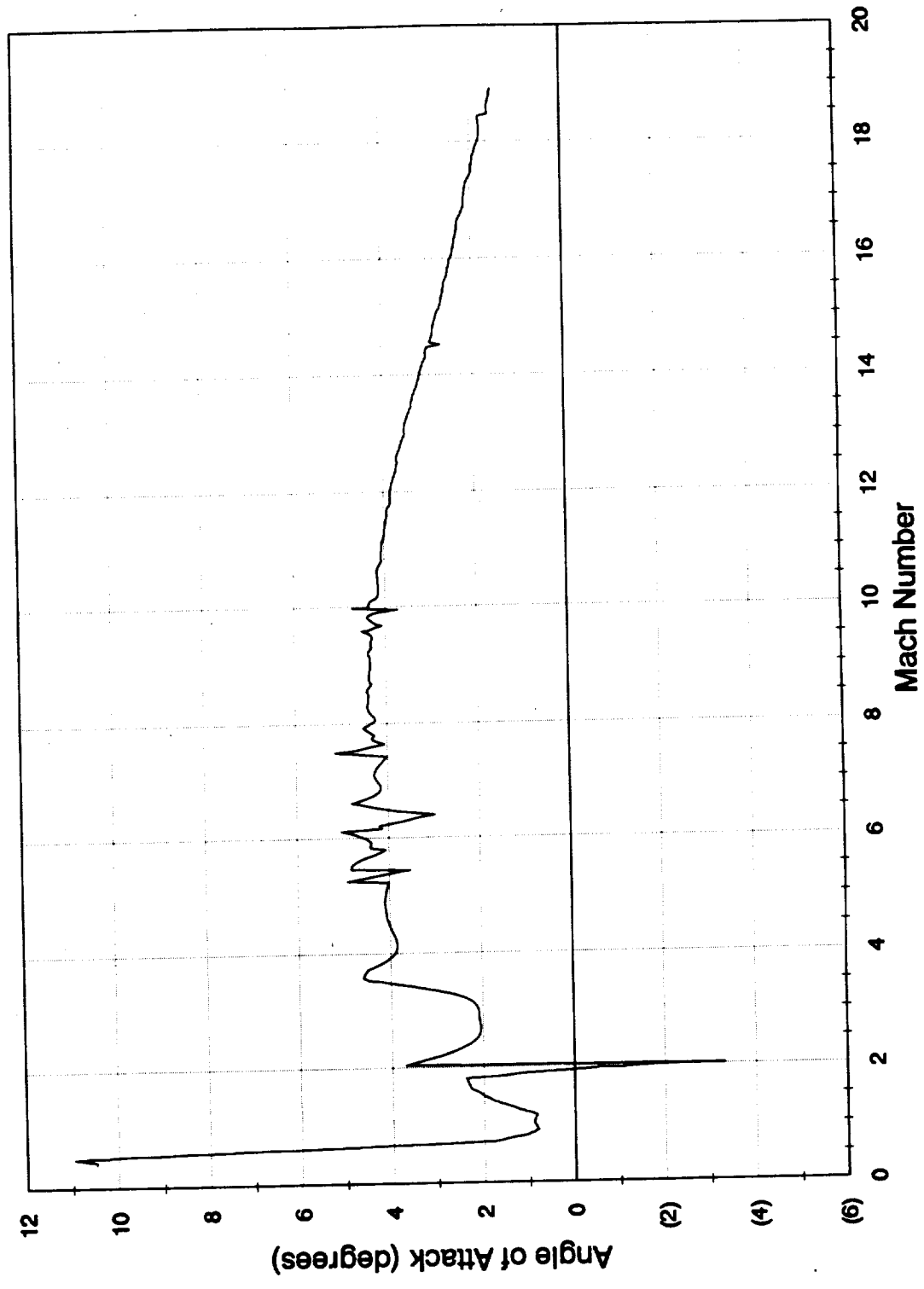


Figure V-6. Demonstration Case - Angle of Attack vs Mach Number

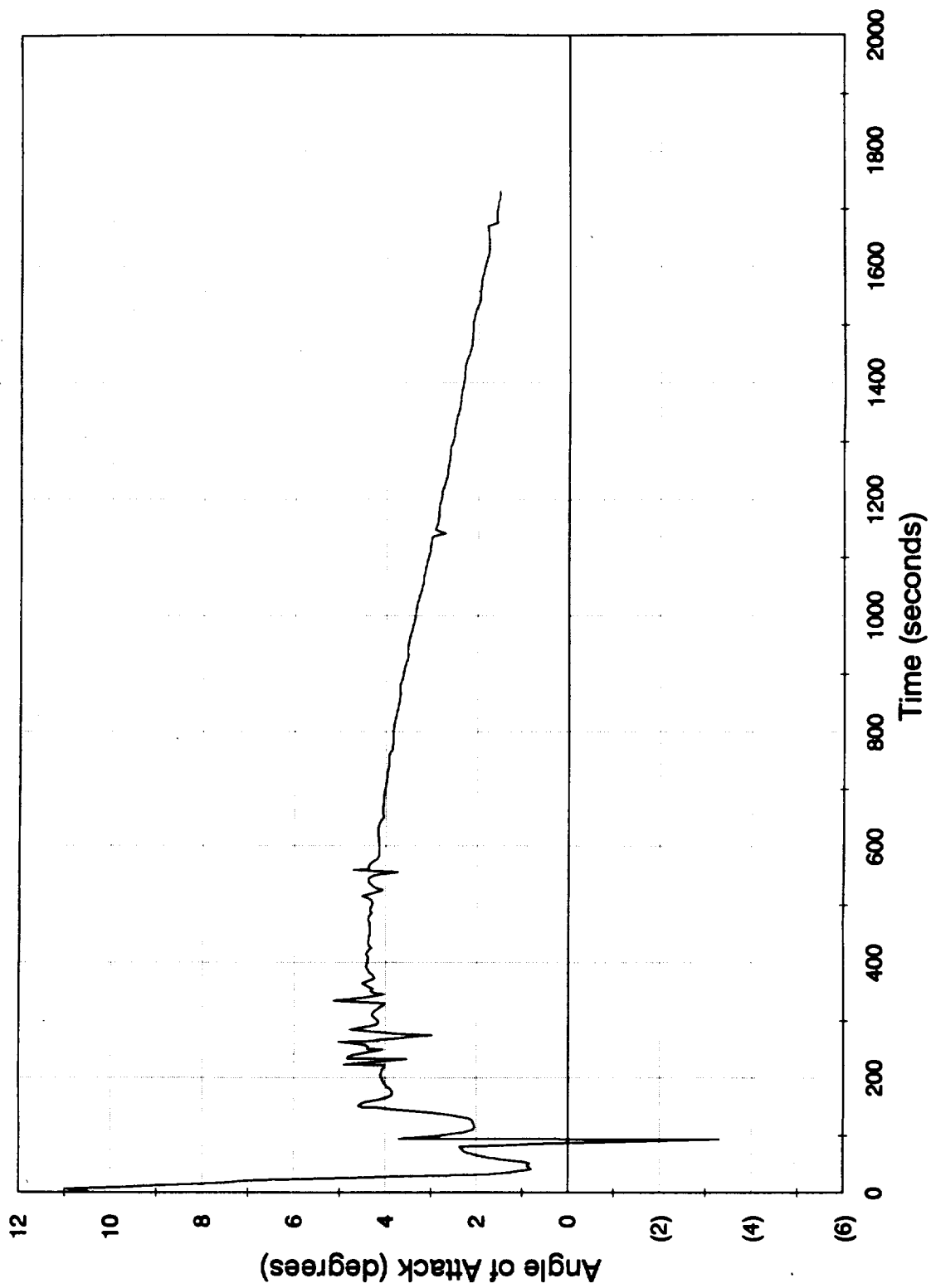


Figure V-7. Demonstration Case - Angle of Attack vs Time

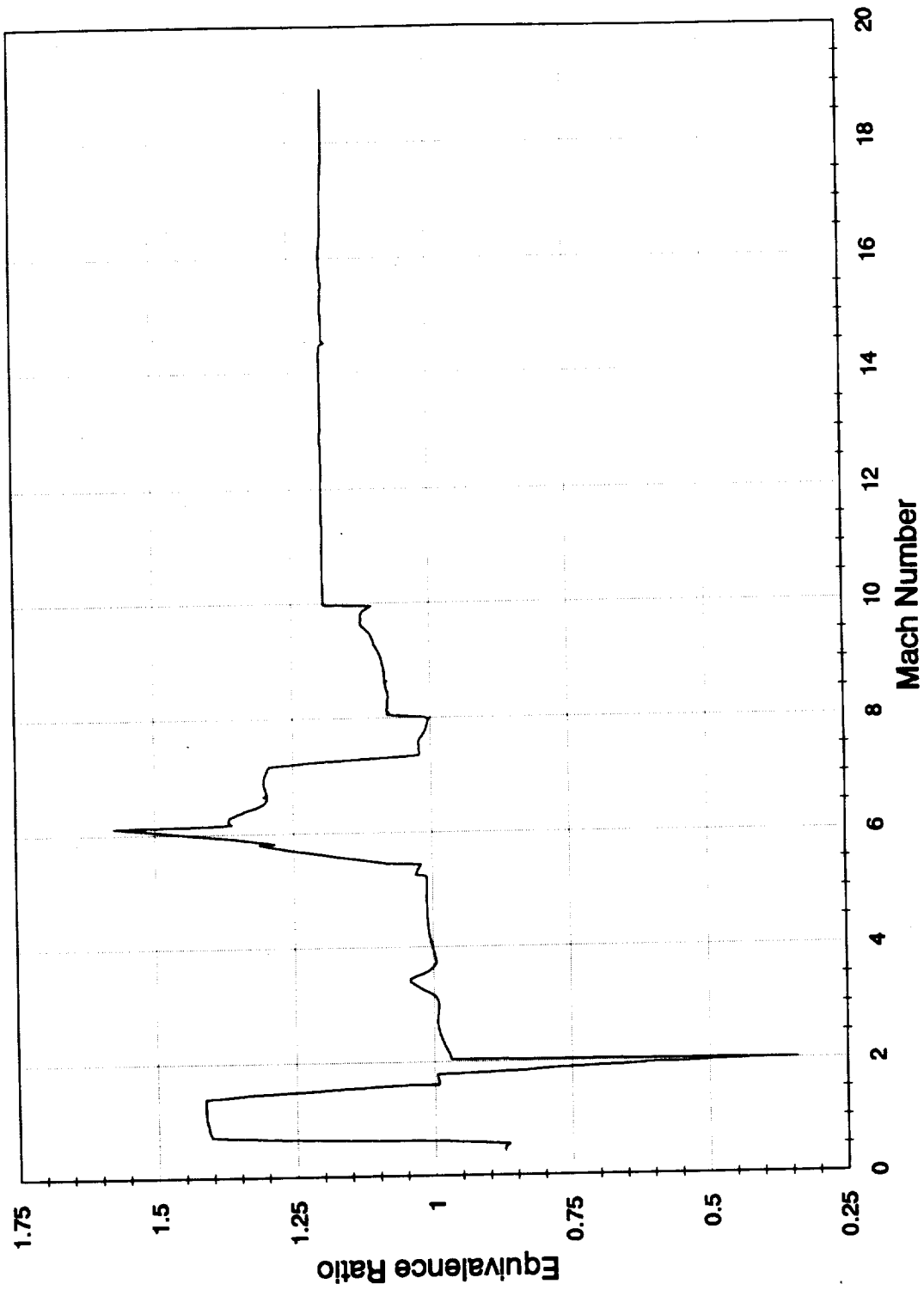


Figure V-8. Demonstration Case - Equivalence Ratio vs Mach Number

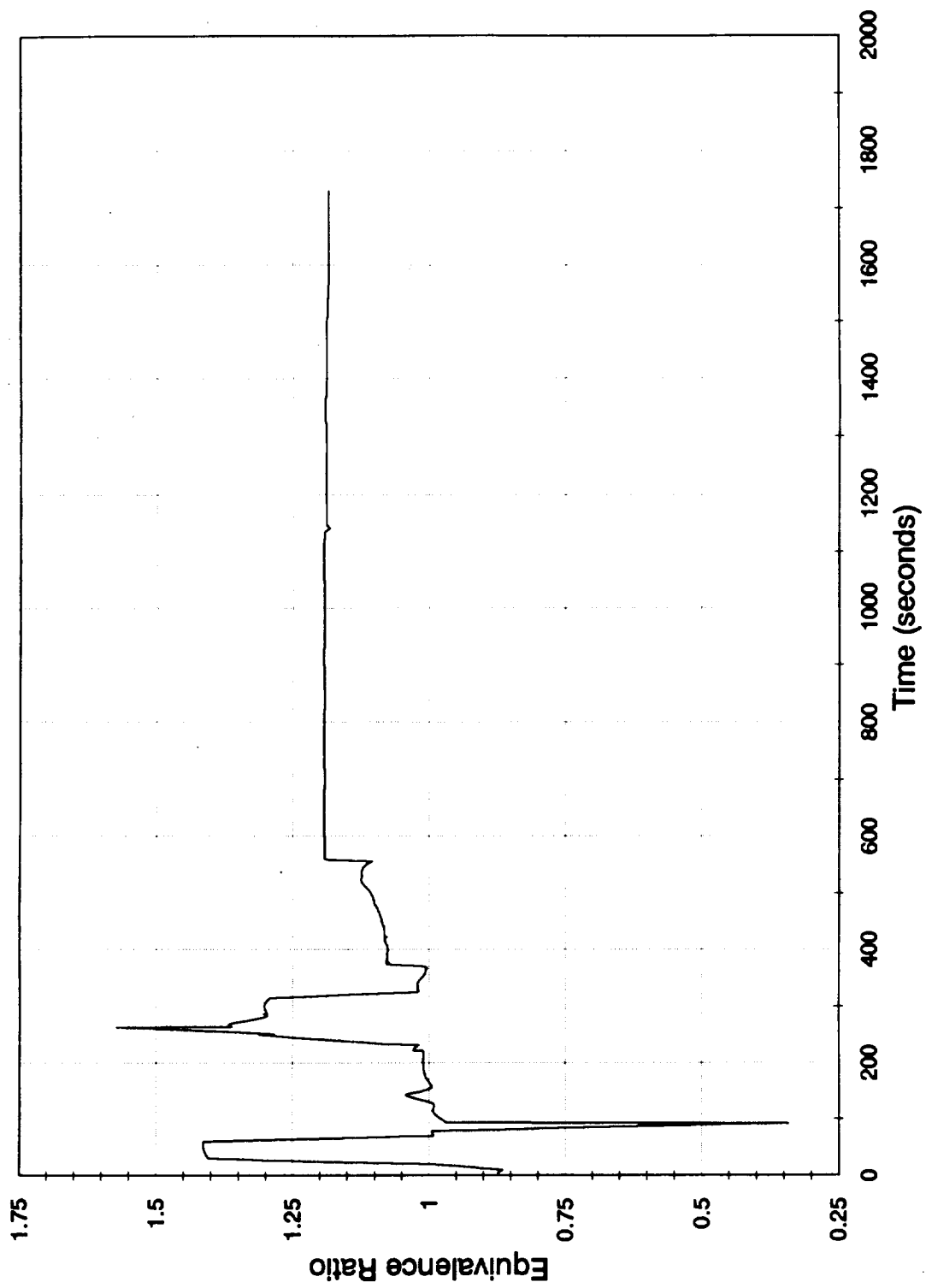


Figure V-9. Demonstration Case - Equivalence Ratio vs Time

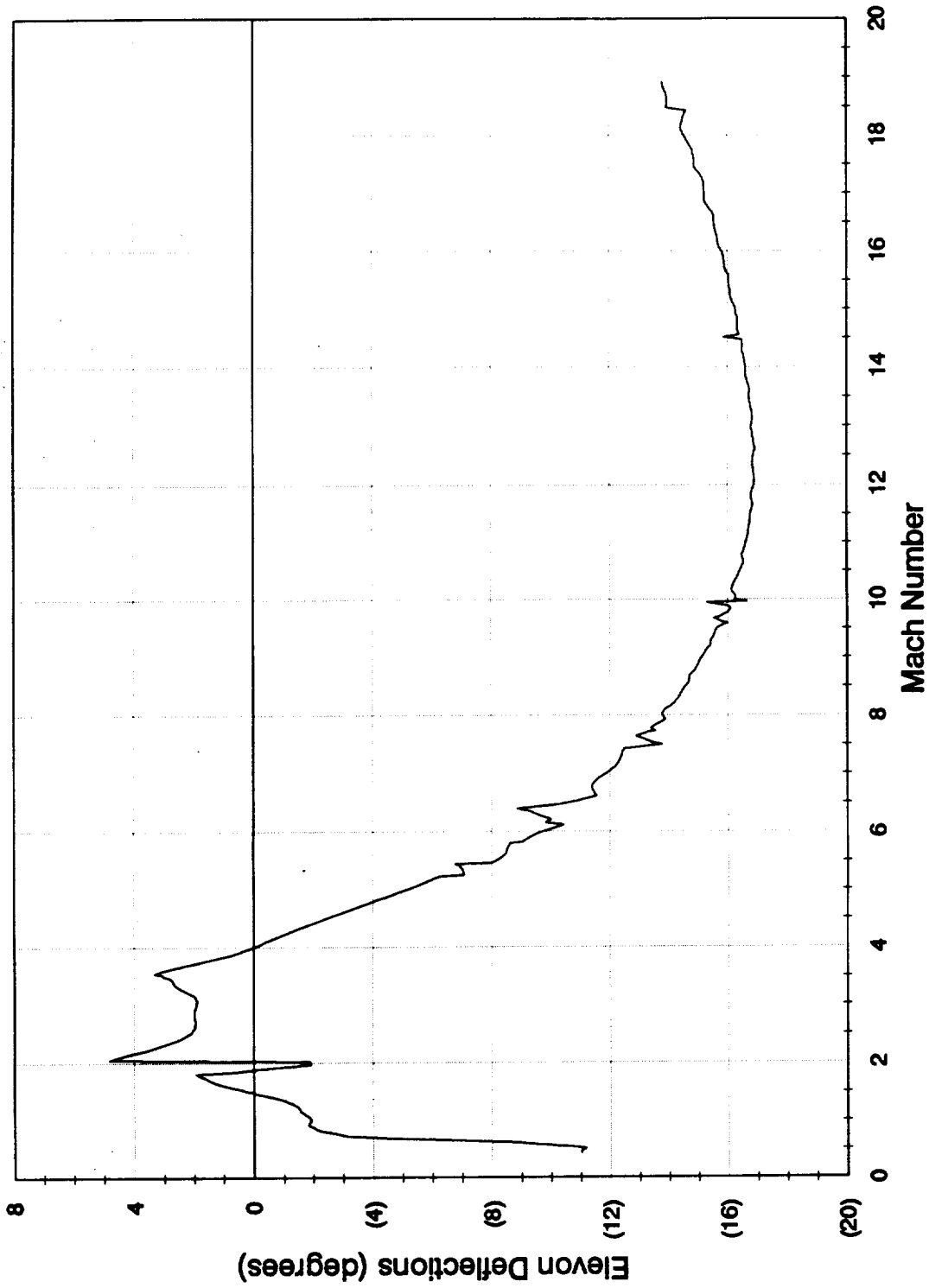


Figure V-10. Demonstration Case - Elevon Deflection vs Mach Number

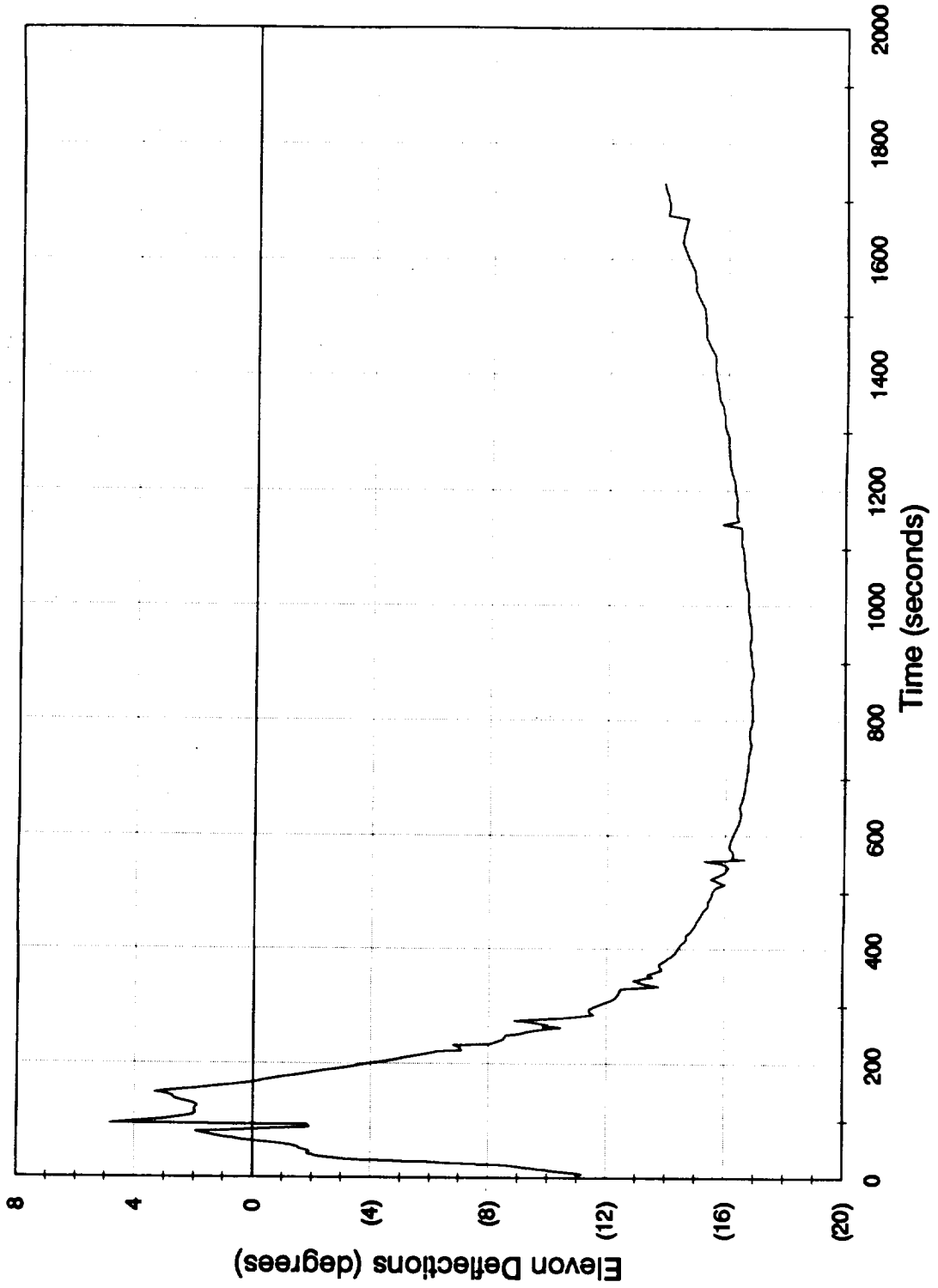


Figure V-11. Demonstration Case - Elevation Deflection vs Time

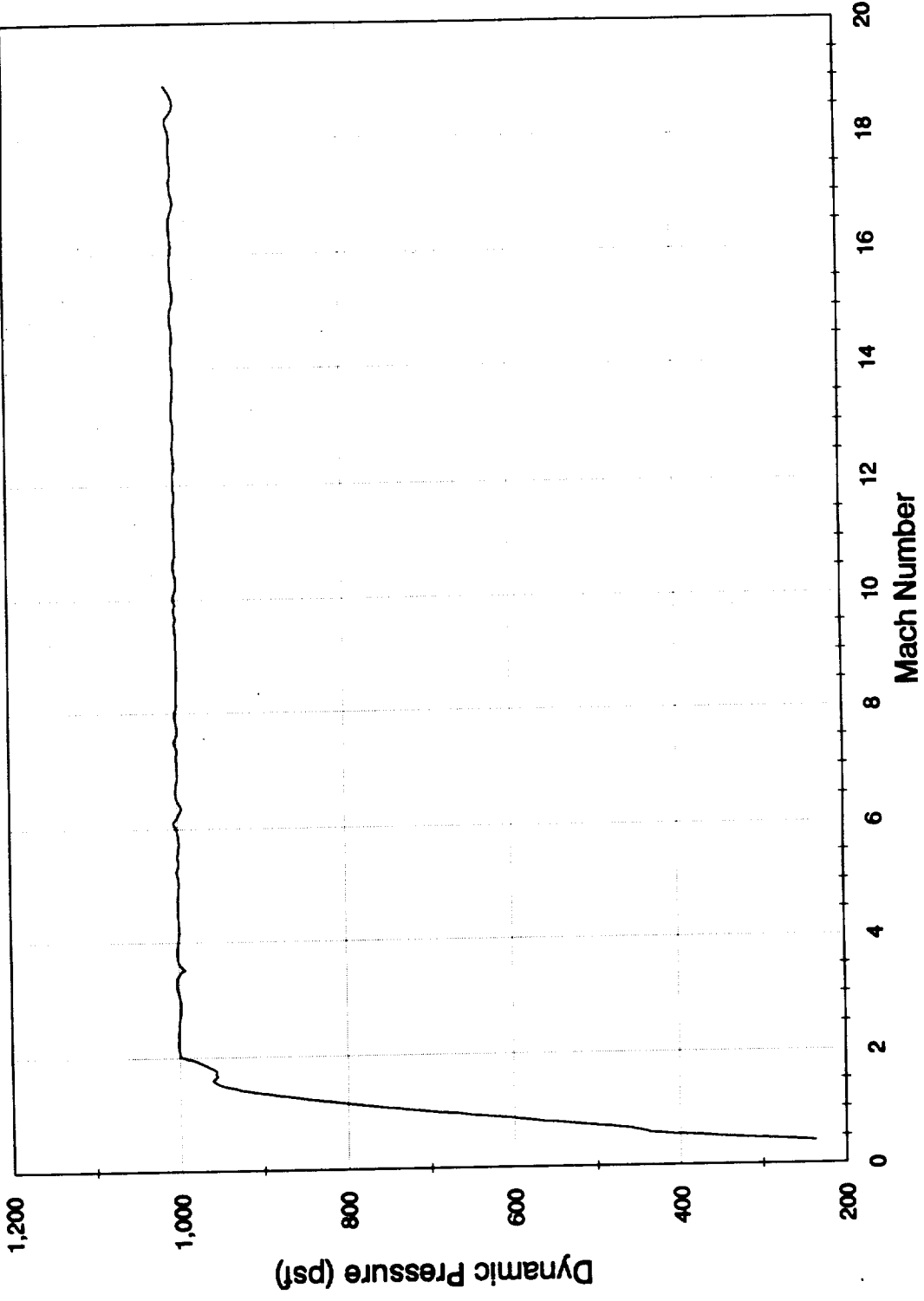


Figure V-12. Demonstration Case - Dynamic Pressure vs Mach Number

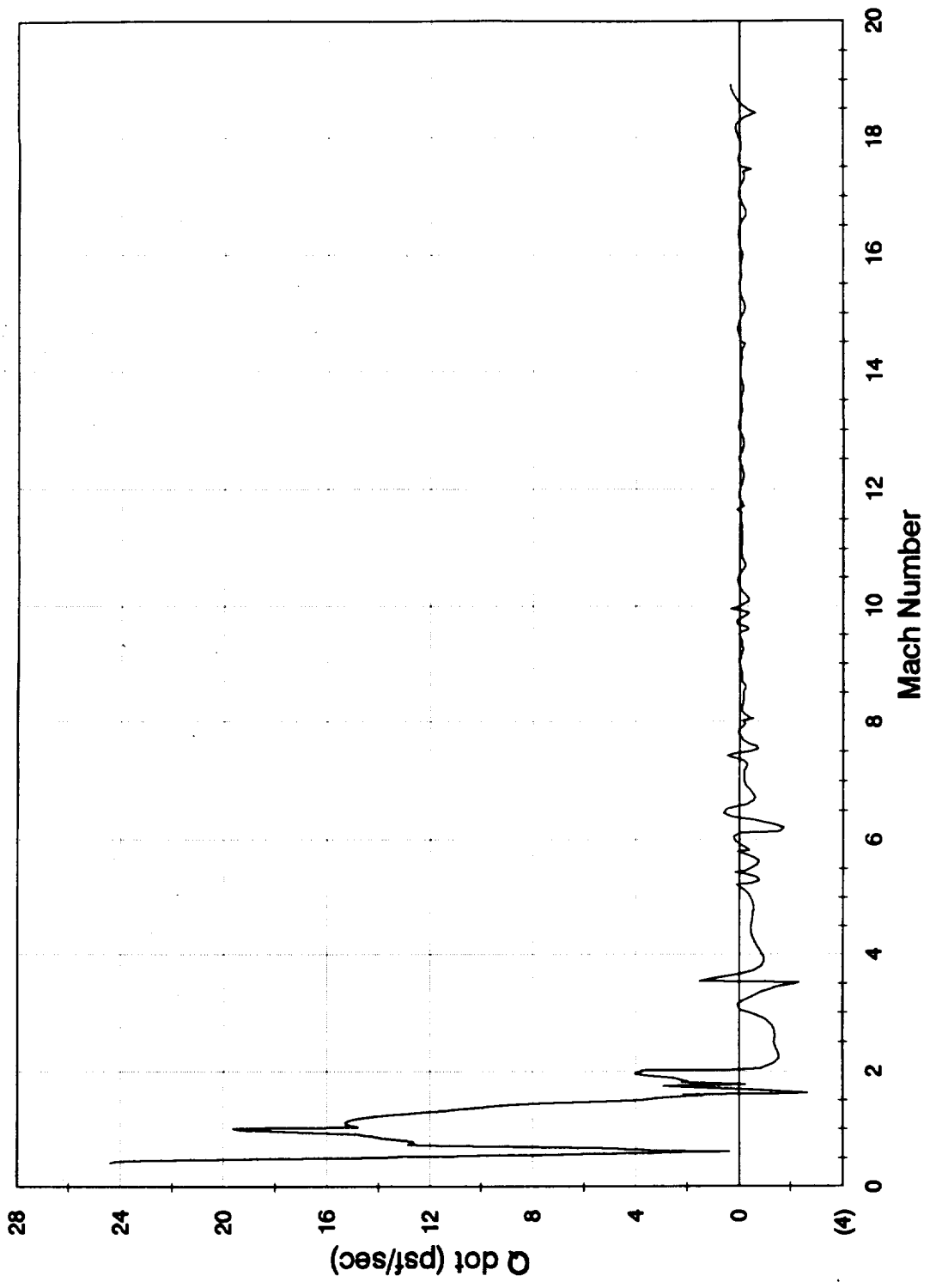


Figure V-13. Demonstration Case - Dynamic Pressure Derivative vs Mach Number

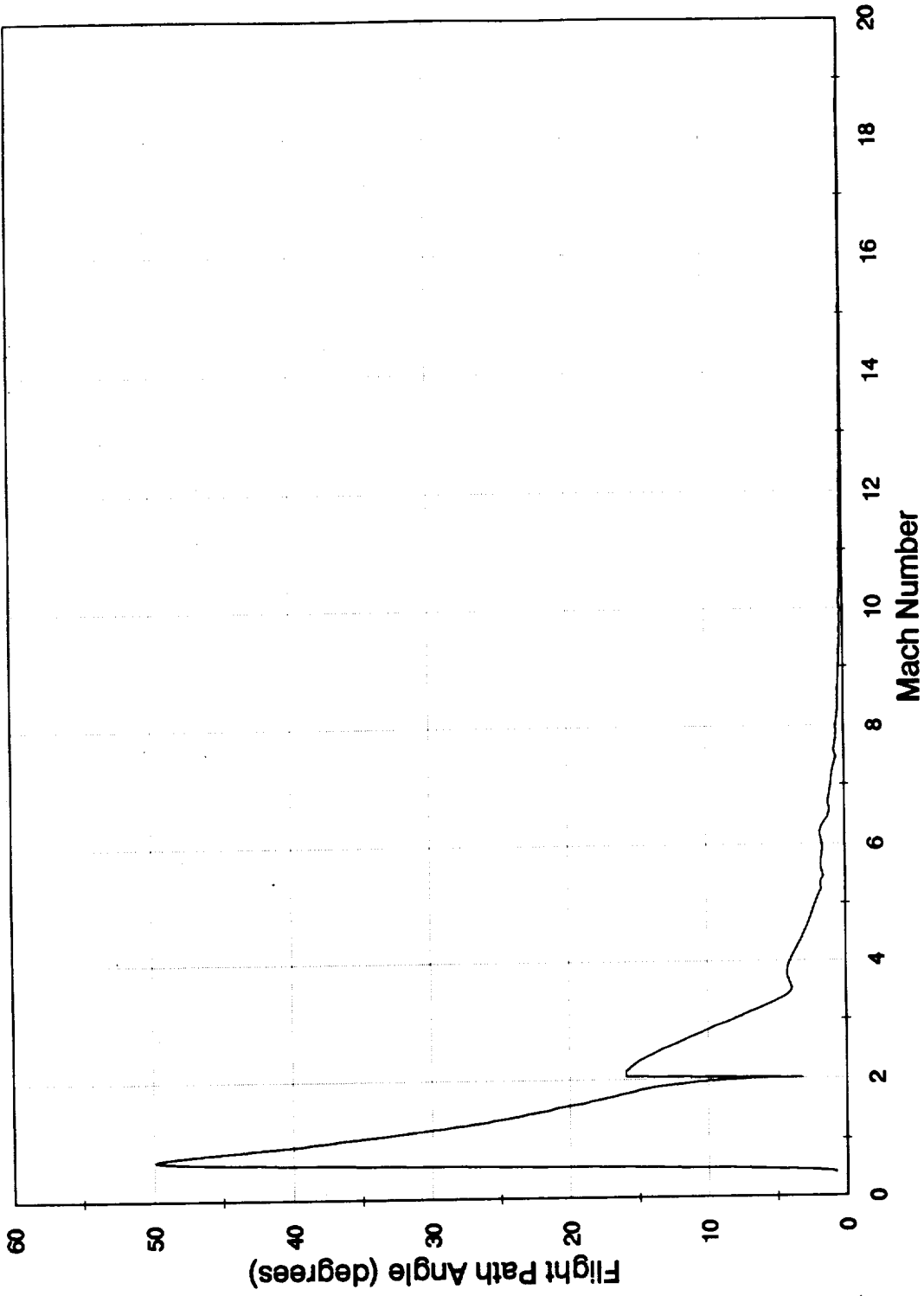


Figure V-14: Demonstration Case - Flight Path Angle vs Mach Number

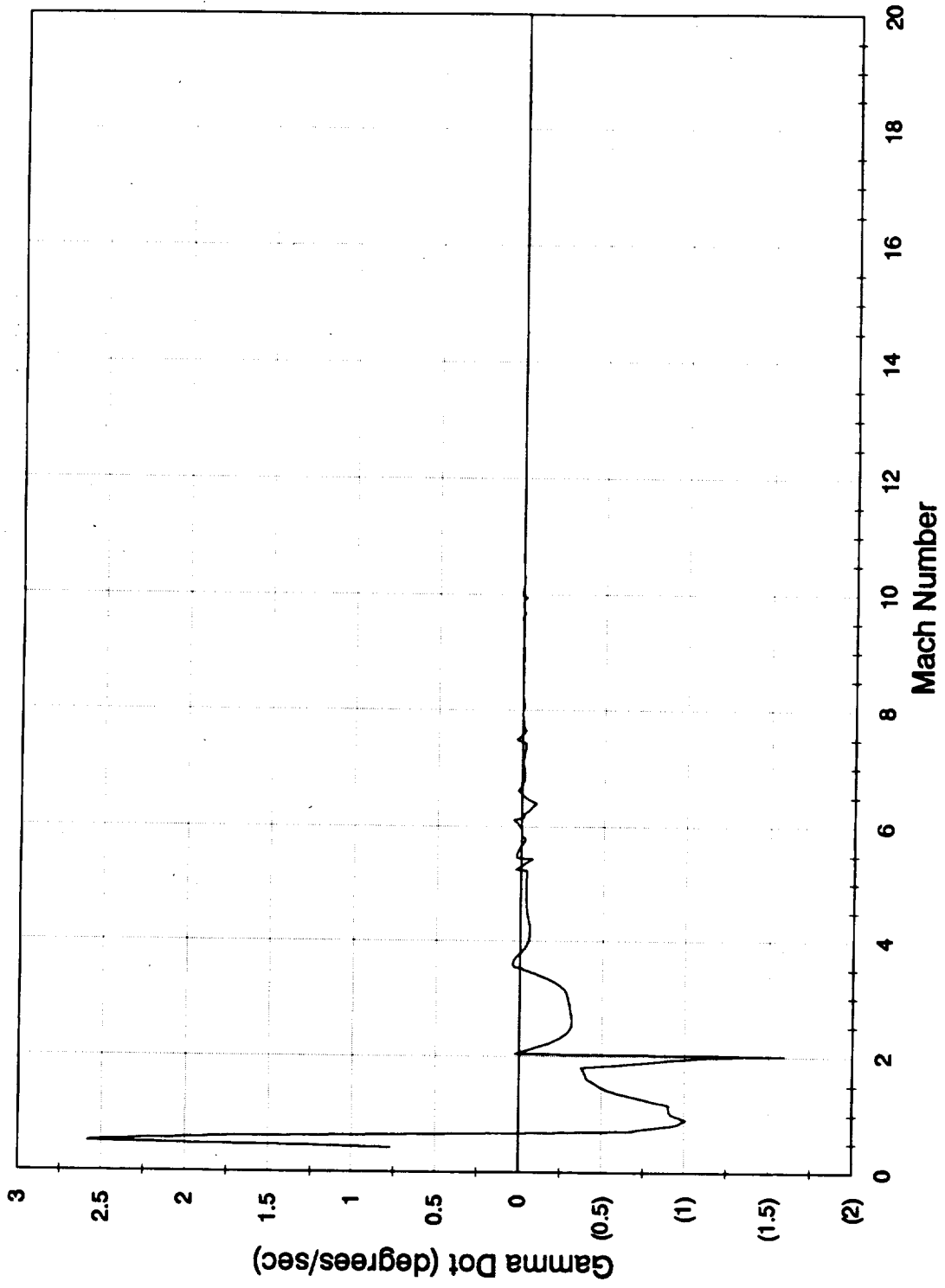


Figure V-15. Demonstration Case - Flight Path Derivative vs Mach Number

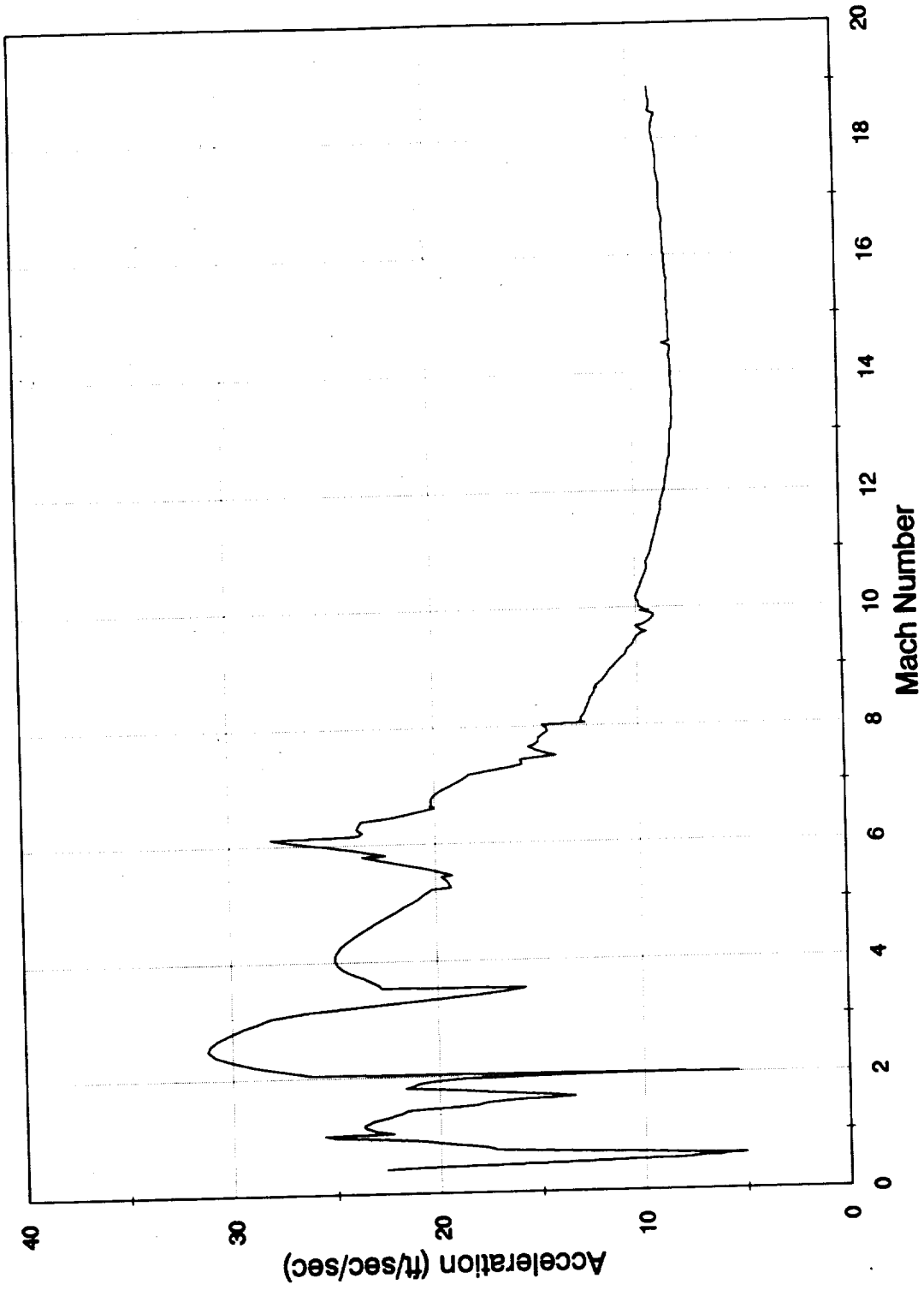


Figure V-16. Demonstration Case - Ground Relative Acceleration vs Mach Number

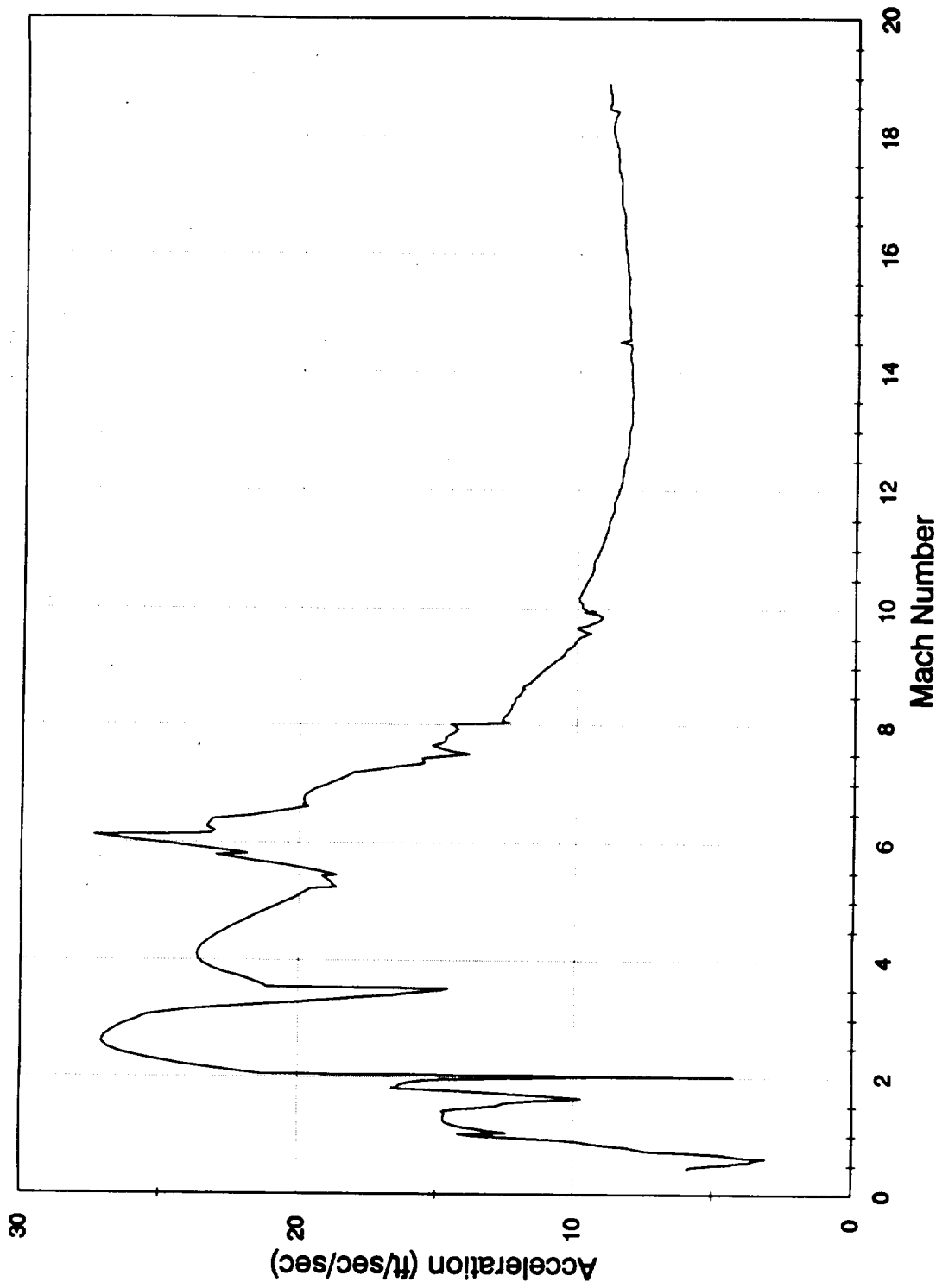


Figure V-17. Demonstration Case -Inertial Acceleration vs Mach Number

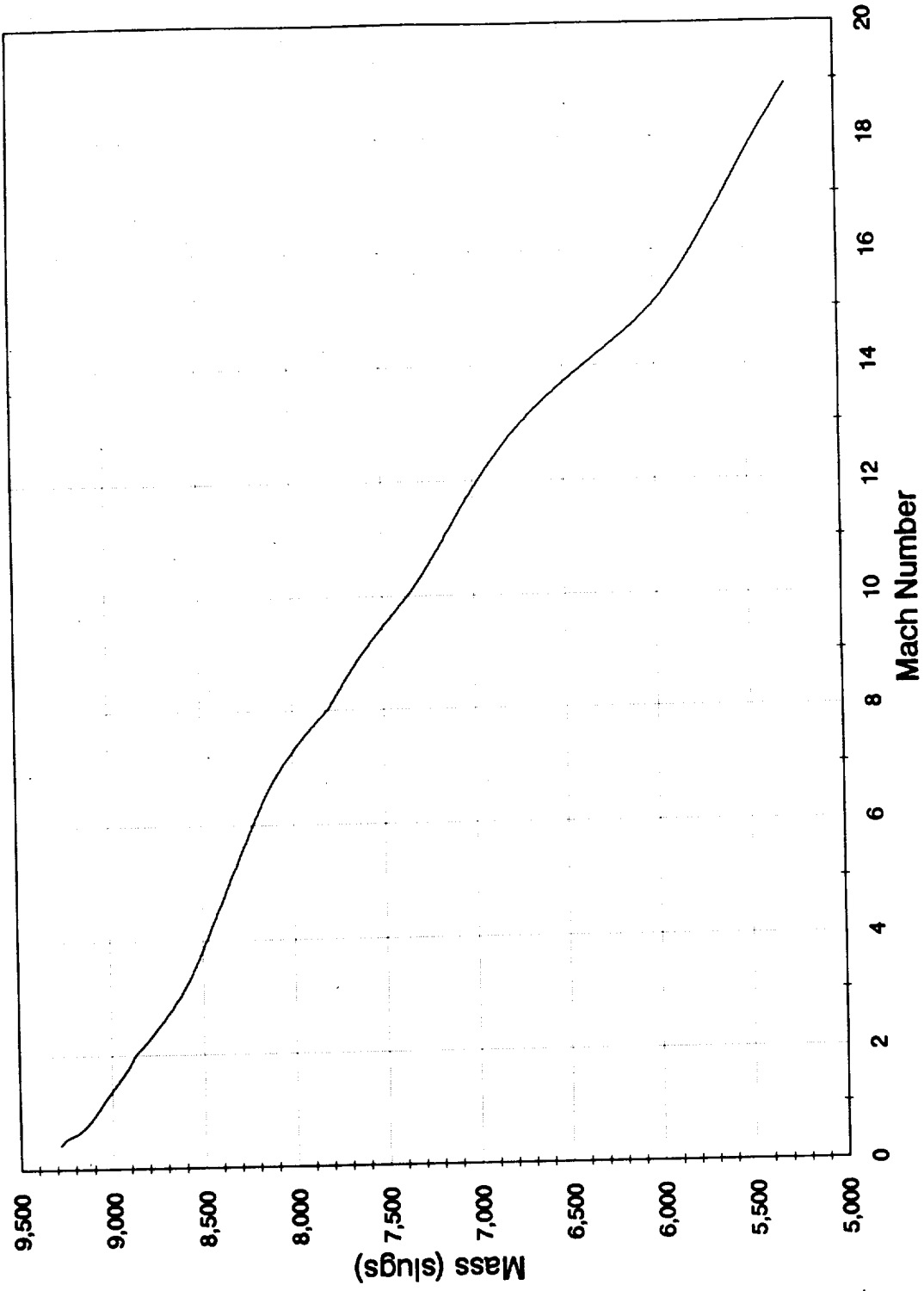


Figure V-18. Demonstration Case - Mass vs Mach Number

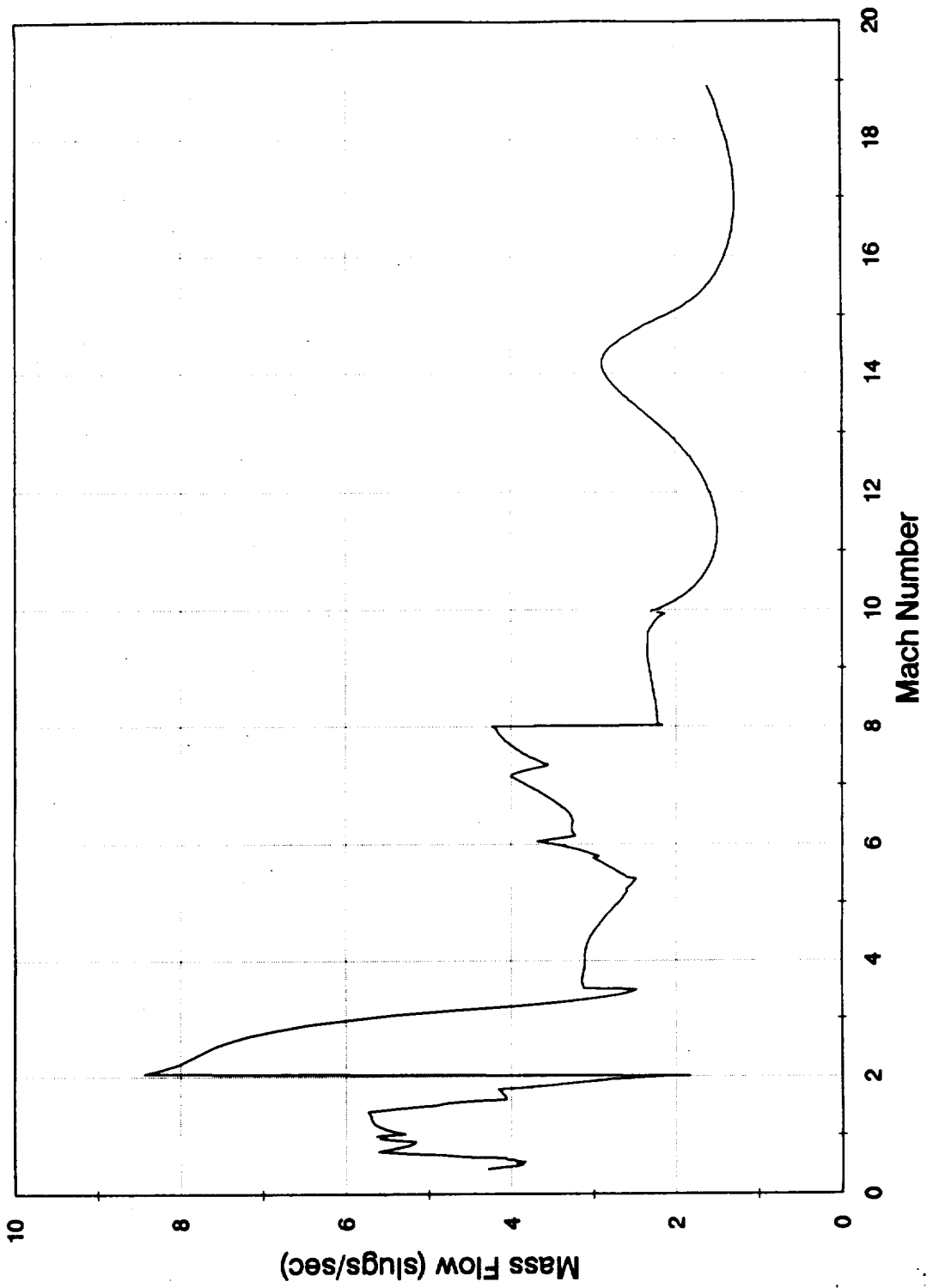


Figure V-19. Demonstration Case - Mass Flow vs Mach Number

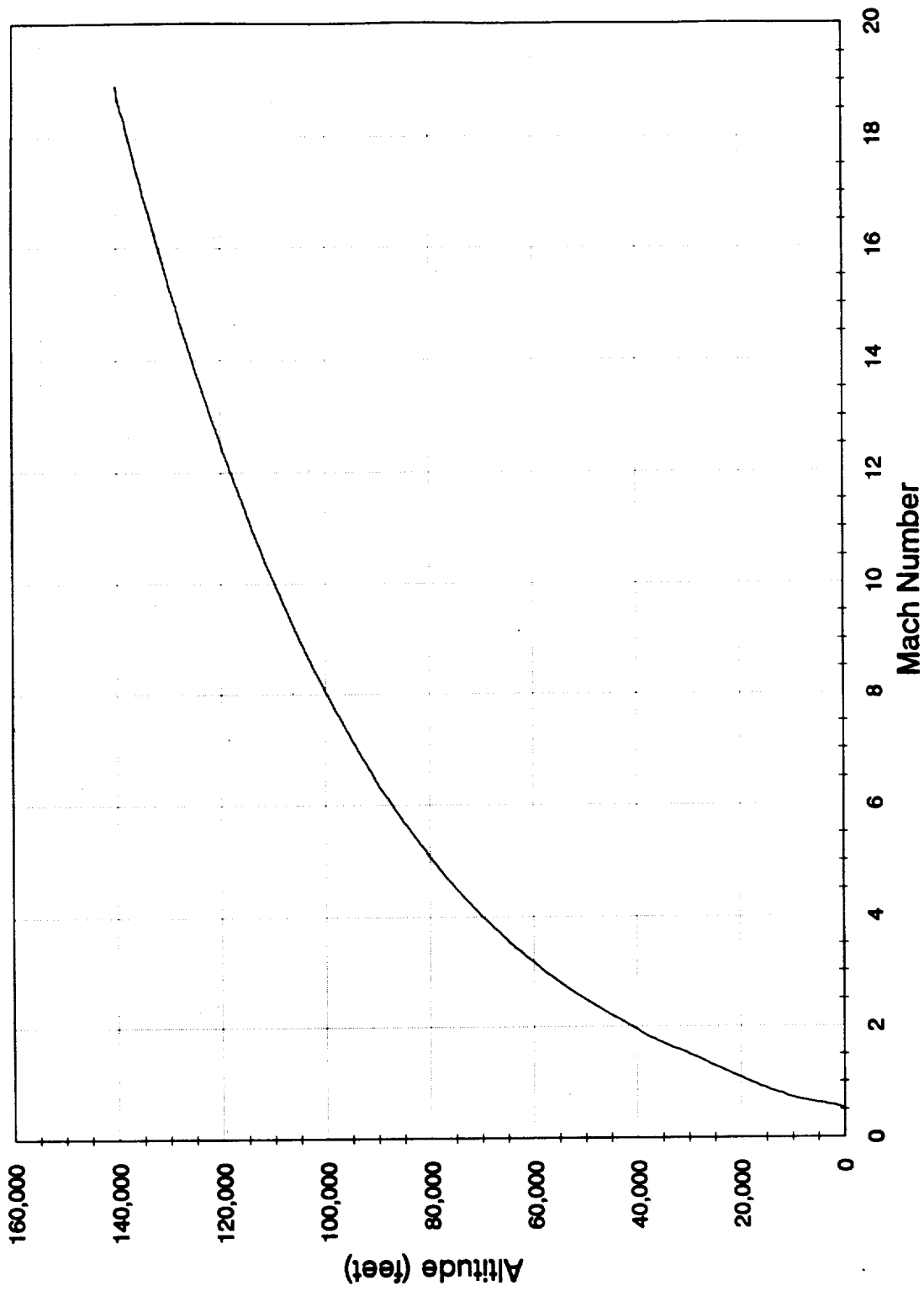


Figure V-20. Demonstration Case - Altitude vs Mach Number

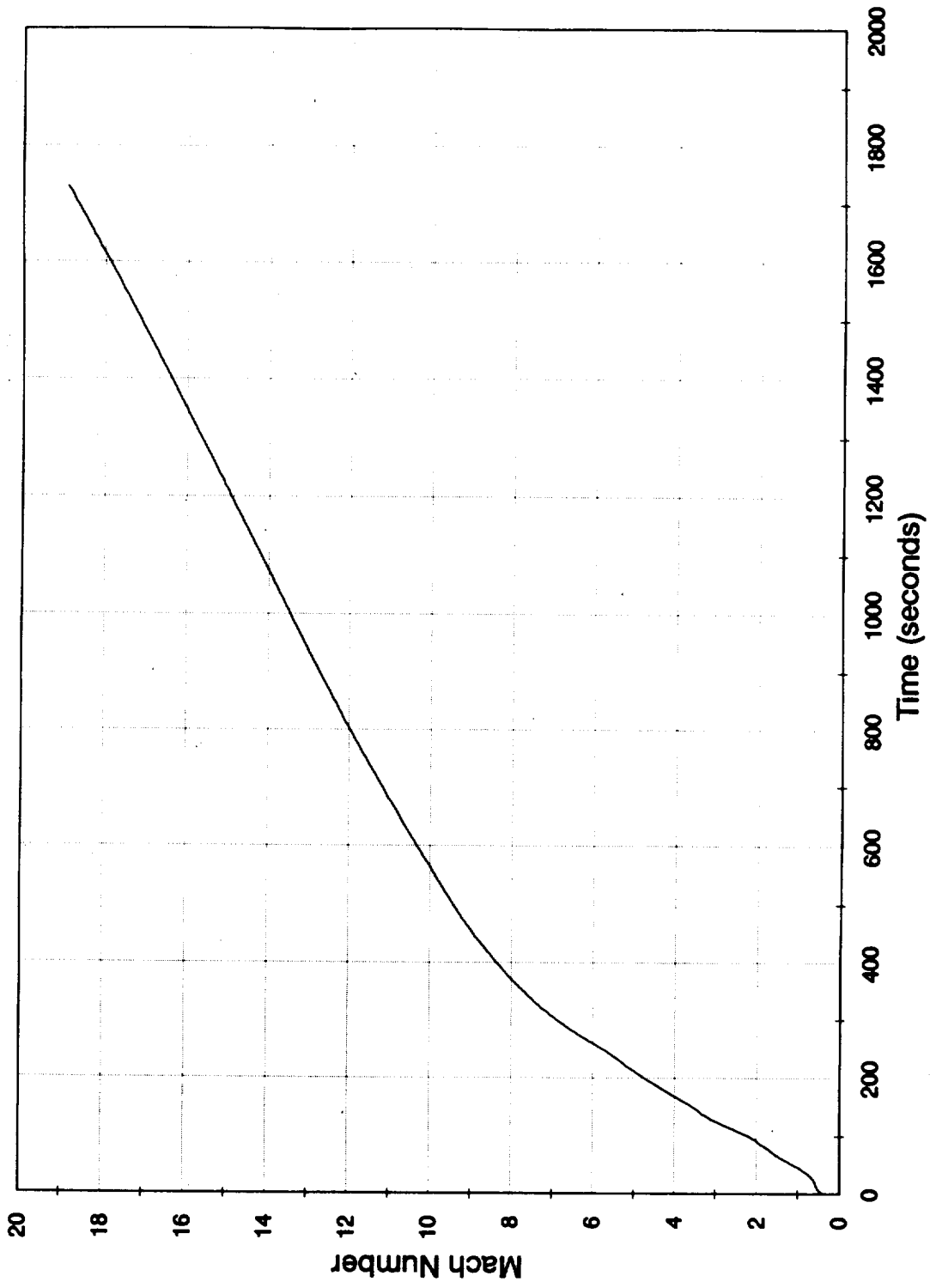


Figure V-21. Demonstration Case - Mach Number vs Time



# Report Documentation Page

|   |  |  |   |   |                  |
|---|--|--|---|---|------------------|
| 1. Report No.<br>NASA CR-187623   |  | 2. Government Accession No.                          |   | 3. Recipient's Catalog No.  |                  |
| 4. Title and Subtitle<br>Air Breathing Hypersonic Vehicle Guidance and Control Studies; An Intergated Trajectory/Control Analysis Methodology: Phase I  |  |  |   | 5. Report Date<br>September 1991  |                  |
|   |  |  |   | 6. Performing Organization Code   |                  |
| 7. Author(s)<br>Philip D. Hattis and Harvey L. Malchow  |  |  |   | 8. Performing Organization Report No.   |                  |
|   |  |  |   | 10. Work Unit No.<br>505-64-40-01   |                  |
| 9. Performing Organization Name and Address<br>The Charles Stark Draper Laboratory, Inc.<br>555 Technology Square<br>Cambridge, MA 02139  |  |  |   | 11. Contract or Grant No.<br>NAS1-18565                                       |                  |
|   |  |  |   | 13. Type of Report and Period Covered<br>Contractor Report                    |                  |
| 12. Sponsoring Agency Name and Address<br>National Aeronautics and Space Administration<br>Langley Research Center<br>Hampton, VA 23665-5225  |  |  |   | 14. Sponsoring Agency Code  |                  |
|   |  |  |   | 15. Supplementary Notes<br><br>Langley Technical Monitor: John D. Shaughnessy |                  |
| 16. Abstract<br>A tool which generates optimal trajectory/control histories in an integrated manner is generically adapted to the treatment of single-stage-to-orbit air-breathing hypersonic vehicles. The methodology is implemented as a two point boundary value problem solution technique. Its use permits an assessment of an entire near-minimum-fuel trajectory and desired control strategy from takeoff to orbit while satisfying physically derived inequality constraints and while achieving efficient propulsive mode phasing. A simpler analysis strategy that partitions the trajectory into several boundary condition matched segments is also included to construct preliminary trajectory and control history representations with less computational burden than is required for the overall flight profile assessment. A demonstration was accomplished using a tabulated example (winged-cone accelerator) vehicle model that is combined with a newly developed multidimensional cubic spline data smoothing routine. A constrained near-fuel-optimal trajectory, imposing a dynamic pressure limit of 1000 psf, was developed from horizontal takeoff to 20,000 ft/sec relative air speed while aiming for a polar orbit. Previously unspecified propulsive discontinuities were located. Flight regimes demanding rapid attitude changes were identified, dictating control effector and closed-loop controller authority was ascertained after evaluating effector use for vehicle trim. Also, inadequacies in vehicle model representations and specific subsystem models with insufficient fidelity were determined based on unusual control characteristics and/or excessive sensitivity to uncertainty. |  |  |   |   |                  |
| 17. Key Words (Suggested by Author(s))<br>constrained trajectories      optimal trajectories<br>cubic splines                    propulsive mode phasing<br>generic air-breathing hypersonic      guidance and control<br>integrated analysis                    single-stage-to-orbit (SSTO)<br><u>near-minimum-fuel trajectories</u>  |  |  | 18. Distribution Statement<br><br>Unclassified - Unlimited<br><br>Subject Category - 08 |   |                  |
| 19. Security Classif. (of this report)<br>Unclassified  |  | 20. Security Classif. (of this page)<br>Unclassified |   | 21. No. of pages<br>88  | 22. Price<br>A05 |